Johannes Gutenberg-Universität Mainz

Fachbereich 09 – Chemie, Pharmazie und Geowissenschaften

Thesis submitted for the degree of

Master of Science

Synthesis of DNA Origami-Polymer Conjugates

by

Katharina Eigen

Subject of Study: Biomedical Chemistry

1st Reviewer: Prof. Dr. Tanja Weil
2nd Reviewer: Prof. Dr. Andreas Walther

Mainz, September 2022

Synthesis of DNA Origami-Polymer Conjugates

Master Thesis at the Johannes Gutenberg-Universität Mainz

by Katharina Eigen

1st Reviewer: Prof. Dr. Tanja Weil

2nd Reviewer: Prof. Dr. Andreas Walther
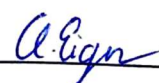
Submission date: 26 September 2022

This Master thesis was written between March and September 2022 at the Max-Planck Institute for Polymer Research under the supervision of Prof. Tanja Weil. The second review was contributed by Prof. Andreas Walther.

Hereby, I, Katharine Eigen, matriculation number 2732730, declare, that I have written this master's thesis independently and that I have not used any written or electronic sources nor other aids than those indicated. I have marked all statements that have been taken verbatim or in spirit from other writings.

Hiermit versichere ich, Katharina Eigen, Matrikelnummer: 2732730, dass ich meine Masterarbeit selbstständig verfasst und keine anderen als die angegebenen schriftlichen und elektronischen Quellen sowie andere Hilfsmittel benutzt habe. Alle Ausführungen, die anderen Schriften wörtlich oder sinngemäß entnommen wurden, habe ich kenntlich gemacht.

Mainz, 26.09.2022
_____
Ort, Datum

_____
Katharina Eigen

Acknowledgments

Firstly, and foremost, I would like to thank Prof. Tanja Weil for offering me the opportunity to join her group for my master thesis during the past months.

In addition, I would like to thank Prof. Walther for providing further review of my thesis.

Furthermore, I would like to express my thanks to Dr. David Ng for his great support during my thesis, being always available to answer questions and to contribute to the development of further ideas. Additionally, many thanks for the confocal measurements.

Moreover, a special thanks to Nico Alleva, my Ph.D. mentor in this time, who collaborated in the results in this thesis. Therefore, parts of the presented results will also coexist in Nico's PhD thesis.

Supplementary, I would like to thank all other group members of the AK Weil, who helped me during my research time and were always open for the discussion of variant topics. Special thanks at this point to Yong Ren and Jeena Thekkeyil for measuring TEM, as well to Darijan Schüler for his support with the ÄKTA purification. Besides the scientific exchange, I really enjoyed the time I spend with the group members, tasting lots of international culinary specialities and doing sports together.

Finally, I would like to thank my boyfriend, my family, and my friends, who accompanied me during this time.

Abstract

DNA nanotechnology enables the precise organisation of functional moieties on nanometre scale through hybridization of extended staple DNA of DNA origami and DNA-hybrid materials. This programmability offers much potential for the application in material science and nanomedicine. In this work, the high predictability of folded DNA, so called DNA origami, was used for the template-guided organisation of DNA-polymer conjugates. Following the crosslinking of the polymer chains on the origami surface, DNA-template degradation gave access to nanometre-sized polymer particles of predetermined controlled shapes. These well-defined structures cannot be produced by conventional self-assembly methods of amphiphilic block copolymers.

Furthermore, high biocompatibility and nanoscale control make DNA origami a suitable tool for biomedical application. Here, the limited cellular uptake of "naked" origami structures was overcome DNA origami coating with three different polymer systems.

Kurzfassung

Die DNA-Nanotechnologie ermöglicht die präzise Organisation funktioneller Einheiten auf Nanometerebene durch Hybridisierung von verlängerten DNA-staple Strängen auf der Origami-Oberfläche und DNA-Hybridmaterialien. Diese Programmierbarkeit bietet großes Potenzial für die Anwendung in den Materialwissenschaften und der Nanomedizin. In dieser Arbeit wurde die hohe Vorhersagbarkeit gefalteter DNA, so genannter DNA-Origami, für die Template-Organisation von DNA-Polymerkonjugaten genutzt. Durch den, an die Vernetzung der Polymerketten auf der Origami Oberfläche anschließenden, DNA-Template-Abbau wurde die kontrollierte Synthese von Polymerpartikeln im Nanometerbereich ermöglicht, deren Strukturen nicht mittels herkömmlicher Selbstassemblierungsmethoden von amphiphilen Blockcopolymeren hergestellt zugänglich sind.

Darüber hinaus sind DNA-Origami aufgrund ihrer hohen Biokompatibilität und der Kontrollierbarkeit im Nanobereich geeignet für die biomedizinische Anwendungen. Durch die Funktionalisierung der Origamioberfläche mit drei verschiedenen Polymersystemen konnte die begrenzte Zellaufnahme von DNA-Origami verbessert werden.

Abbreviations

Compounds and methods

A	Adenine
ADH	Adipic acide dihydrazide
AFM	Atomic force microscopy
C	Cytosine
CTA1	4-Cyano-4-(phenylcarbonothioylthio)pentanoic acid N-succinimidyl ester
CTA2	2-(Dodecylthiocarbonothioylthio)-2-methylpropionic acid N-succinimidyl ester
CTA	Chain transfer agent
DAAM	Diacetonacrylamide
DMA	*N,N'*-Dimethylacrylamide
DMF	Dimethylformamide
DOSY-NMR	Diffusion-ordered NMR spectroscopy
G	Guanine
GPC	Gel permeation chromatography
HEA	2-Hydroxyethyl acrylate
HRP	horseradish peroxidase
LCST	Lower critical solution temperature
NIPAM	*N*-isopropylacrylamide
NMR	Nuclear magnetic resonance spectroscopy
NHS	*N*-Hydroxysuccinimid
OEGMA	Oligo(ethylene glycol) methyl ether methacrylate
ODN	Oligonucleotide
PEGMEMA	Poly(ethyleneglycol)methylethermethcrylate
PEG	Polyethylene glycol
PMMA	Poly(methyl methacrylate)
RAFT	Reversible addition–fragmentation chain-transfer
RDRP	Reversible-deactivation radical polymerization
ROP	Ring-opening cationic polymerization

ssDNA	Single-stranded DNA
SNA	Spherical nucleic acid
T	Thymine
TEM	Transmission electron microscopy

Formula symbol

Eq.	Equivalents
DNA^c	Complementary DNA
Cf.	Cross-reference
Đ	Dispersity
M_w	Molecular weight
T_m	Melting temperature T_m

Content

List of Figures

List of Tables

1 Introduction

This chapter offers a brief introduction in the scientific background of polymer chemistry and structural DNA nanotechnology, showing DNA as a functional tool to accurately predict structures using the genetic code. The advantages of various hybrid materials are presented, whereby the combination of DNA and polymers are of major importance. The synthesis, properties and different applications of DNA-polymer conjugates and DNA origami-polymer materials are presented, demonstrating the great potential of this hybrid class.

1.1 The programmability of Deoxyribonucleic Acid

The genetic information in nature is encoded in the diversity and arrangement of nucleotides in the deoxyribonucleic acid (DNA). This storage of information enables life via replication and the synthesis of proteins, whose importance is expounded in the "central dogma" of biology.

DNA is a polymer composed of four nucleotides, which contains nitrogenous bases adenine (A), thymine (T), guanine (G), cytosine (C), a deoxyribose and a phosphate group, which conditions the high genetic diversity. The Watson-Crick base pairing leads to the formation of a right-handed double helix structure consisting out of two anti-parallel single-stranded DNA (ssDNA) strands which are complementary to each other.[1]

Due to its unique properties in terms of programmability and self-recognition, DNA gained increasing interest in the synthetic world, opening a new, promising research field. The so-called "structural DNA nanotechnology" was first proposed in 1982 by Seeman[2], enabling the formation of precise nano scaled structures with limitless geometries. This progress was possible because of developments in the automated DNA synthesis.[3] The variability of sequences and the amount of oligonucleotides (ODN) offered the possibility to design higher-ordered motifs like Y-shaped DNA[4], Holliday junctions[5], G-quadruplexes[6] and DNA origami[7] (cf. **Figure 1**).
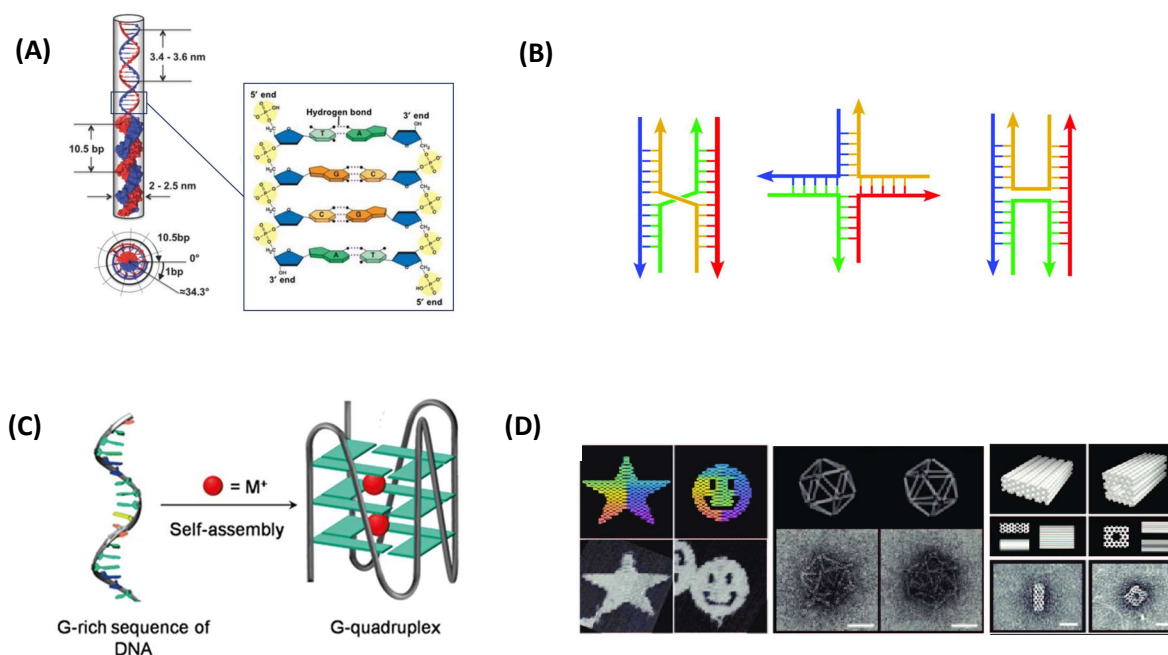
Figure 1: Examples and background of structural DNA nanotechnology. The structure of DNA double-helix and Watson-Crick base pairing (taken from [1]), (B) Four-stranded DNA Holliday junctions in the parallel stacked-X, open-X and antiparallel stacked-X configuration (taken from [8]), (C) Self-assembly of Guanine-rich sequences to two-dimensional G-quadruplex (taken from [6]), (D) First designed DNA origami structures visualized by AFM measurement (taken from [7],[9]).

1.1.1 DNA Origami

In DNA nanotechnology, mainly two approaches are used to design DNA-based structures. The multistranded approach uses ODN, whose self-assembly leads to the formation of tile structures. Larger structures are formed by the assembly of tile structures through hybridization of the sticky ends.[10] However, this strategy has many disadvantages such as the requirement of an exact stoichiometry, the purification of ODNs and assembly-products, a high proportion of misfolding and a limited access to structures.[7]

These limitations could be circumvented, when Rothemund[7] revolutionized the field of DNA-nanotechnology in 2006 by introducing the use of scaffolded-based DNA origami technique. A long ssDNA (scaffold DNA) is folded in a predetermined shape with the help of short ssDNA, called staple strands. The high performance of this new technique can be explained with the use of a long scaffold strand, resulting in an entropic advantage.[11] Since an excess of staples is used, hybridization with the common scaffold leads to the correct initial arrangement of the scaffold. This favours the continuous correct arrangement of the remaining staple strands, meaning most of the misfolding during the annealing process is corrected immediately. Its robust character, the good availability of well-defined nanostructures with artificial shapes and the addressable surface makes DNA origami a

promising tool in material science and nanomedicine.[12] The structural diversity encompasses tiles[13], tubes[14] and honey-comblike[9] structures. The original design technique and the first shapes designed by Rothemund[7] are demonstrated in **Figure 2**.
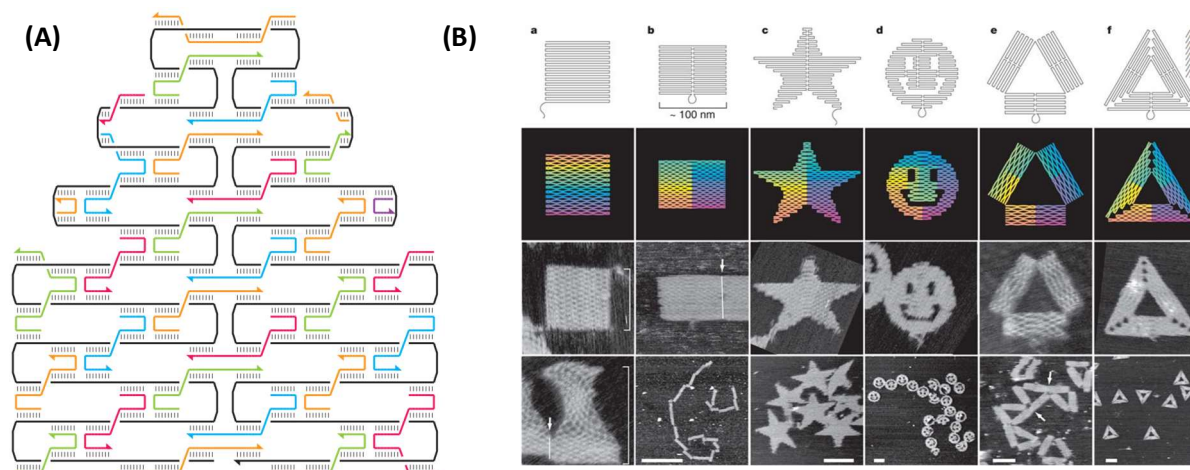
Figure 2: The original DNA origami design technique and shapes of Rothemund[7]. Guided by multiple staples strands (coloured) the scaffold DNA (black) is folded into the desired shape (taken from [7]). (B) Designs of 2D DNA origami structures and their atomic force microscopy (AFM) images (taken from [7]).

The synthesis of 2D DNA origami structures such as rectangular shapes, stars, or triangles as well as the synthesis of three-dimensional structures ascribe to one fundamental rule. Based on the B-type DNA, a periodic array of crossovers (1.5 helical turns) connects every helix within the structure to two neighbouring helices. With the support of computer programs, the necessary set of staple strands can be calculated for the design of the desired structures.[7] Within the 3D DNA origami, antiparallel helices are additionally interconnected resulting in a high package density and rigidity. Therefore, 3D DNA origami show greater resistance to mechanical stress in comparison to 2D DNA origami structures.[9]

A major objective in structural DNA nanotechnology is to mimic biological functions, which often requires nanometre-scaled shapes and the exact placement of active groups on the structure. Due to the self-recognition properties and the high structural diversity of DNA, DNA nanotechnology is a powerful tool to mimic natural systems. This field of research includes the design of DNA-based systems, which can control catalytic reactions, enhance drug delivery or can be used to study diseases.[15] There are many examples in literature, which already verified the mimicry of for example protein nucleators, enzyme reactions or plasma membranes.[15] For instance, in 2012 Langecker *et al*.[16] published a paper on the design of a honey comp lattice structure with cholesterol modified ssDNA. Due to the funnel-shaped structure and the introduction of hydrophobic cholesterol

elements, this system functioned as a transmembrane channel for lipid bilayers (cf. **Figure 3 (A)**). Apart from the advantage of self-assembly and addressability of origami nanostructures, a further field of interest is the development of dynamic nanostructures. The design of nanomotors and actuators, remind to the directional transport in living cells. This new system includes either the incorporation of biomolecules or can act directly as a motor.
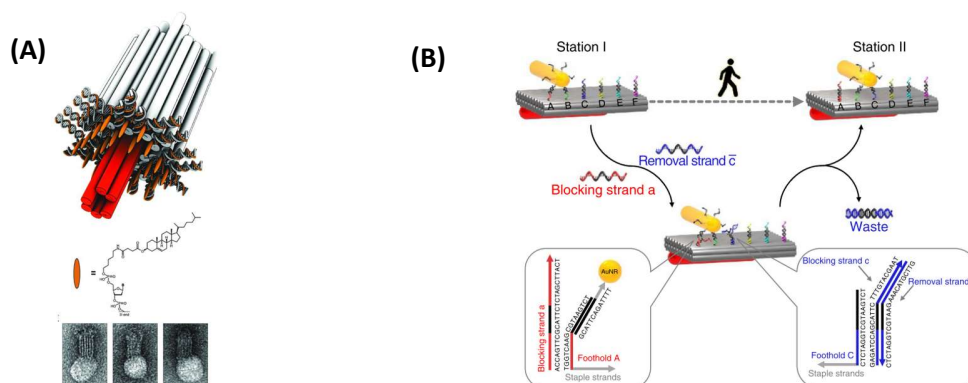
Figure 3: Mimicry of biological functions. (A) Mimicry of a transmembrane channel by the use of a cholesterol-modified honey comb lattice structure (taken from [16]), (B) Prominent example for dynamic nanostructures, where strand-displacement effects the movement of gold nanorods on the origami surface (taken from [17]).

A series of dynamic systems were demonstrated, which base on the natural phenomena of strand displacement. One of several examples of strand displacement was used by the working group of Gu *et al*.[18], who designed a DNA-walker system. These molecular robots were installed onto a DNA origami surface, where a DNA-walker travelled along a predetermined direction and can react to external stimuli. Recently, a further example of movement on 2D or 3D DNA origami through strand displacement was developed. The authors used a gold nanorod with discrete strands, which dynamically binds to immobilized plasmonic stators on the origami route. Along this predetermined track, such walker system shows nanometre accuracy (cf. **Figure 3** (B)).[17]

1.1.2 Limitations of DNA

In the last decades, many systems, encompassing the above-mentioned intriguing and dynamic structures, have been developed. Although, these nanostructures have demonstrated the power and uniqueness of DNA origami, biomedical applications are still challenging due to several environmental requirements.

The melting temperature T_m of DNA origami depends on the length of the DNA and on the specific nucleotide sequence (ratio of stronger C-G to weaker A-T base paring). Above this melting temperature the DNA denatures, which describes a process of unwinding of double helices or for origami structures a dissociation of scaffold DNA and staple strands. A typical origami structure shows a melting temperature between 50 and 65 degrees Celsius.[19]

The most challenging obstacles of the application of DNA nanotechnology in a physiological environment is to exploit the manifold advantages of DNA origami structures while overcoming the many limitations, simultaneously. The advantages include the highly biocompatibility[20], the design of diverse shapes and the possibility to decorate the origami surface with a plethora of biomolecules, dyes, or drugs. On the contrary, low yields, high costs of DNA and the performance of larger scales limit the biomedical usage. Apart from that, the stabilization of DNA structures in physiological environment and the enhancement of the cellular uptake gained increasing interest in this research field. On top, DNA origami could induce severe inflammatory response, making a medical usage problematic.[21]

All biomedical applications require the integrity of DNA origami structures. Therefore, investments in specific conditions to increase the stability becomes more important. Due to the highly ionic character of DNA, synthesis and further reactions are limited to aqueous medium containing Ca^{2+}/Mg^{2+} (10-20 mM).[22] Binding of these bivalent cations to the negatively charged phosphate backbone, effects DNA double-helices stabilization by compensating the electrostatic repulsion between neighbouring DNA strands. In contrast, biological mediums like blood serum have a much lower Ca^{2+}/Mg^{2+} concentrations, making a use in physiological medium challenging.[23] DNA-degrading nucleases, like DNase I, are found in all biological compartments within the cells of the human body. DNase I catalyse the hydrolysis of DNA phosphodiester bond, which connects two adjacent nucleotides leads to the destruction of DNA structure.[24]

Although DNA shows high biocompatibility, an inflammatory immune response could be initiated. Perrault and Shih[21] incubated plain DNA origami with mice splenocytes and monitored primarily the levels of interleukin 6 and 12 (IL-6/12). They observed a high increase of cytokine production,

indicating an inflammatory immune response. To overcome this barrier, the same authors used lipid or protein coated DNA origami, which reduced IL-6 to a negligible level.

Besides the limited stability of DNA, cellular uptake of negatively charged DNA origami is reduced due to repulsive forces with negative cellular membranes.[25]

The creation of hybrid materials through the decoration of DNA origami with different structures is the most common way to tackle poor translocation rates, possible immunogenicity, and low stability. The conjugation of hydrophobic molecules (lipids)[26], proteins[27] and polymers[28],[25] to the DNA origami surface can circumvent these limitations. This new class of hybrid materials will be explained more in detail in subsection 1.3.1, where it's advantages and disadvantages will be faced.

1.2 RAFT polymerization

This chapter provides an insight into controlled living radical polymerisation methods, with a focus on RAFT polymerisation, which provides access to the controlled synthesis of polymers.

1.2.1 Controlled living radical polymerization

Controlled living radical polymerisation combines the advantages of radical polymerization and living polymerisation. The major virtue of radical polymerization is that the reaction can be performed under relatively undemanding conditions, which offers a great advantage in comparison to e.g. ionic polymerisation.[29] In contrast, anionic living radical polymerization paved the way to more narrow molecular weight distribution and a higher control over the composition of polymer structures. If this system is not external terminated by impurities, no termination step occurs formally. However, the reaction must be performed under inert conditions and impurities have to be circumvented.[30]

To circumvent the uncontrolled properties of radical polymerization, the living character of anionic polymerization can be mimicked by the development of a new reaction type: the degenerative chain transfer. The introduction of a fast dynamic equilibrium between so-called "dormant-species" and propagating radicals gives all chains the same probability to grow, which leads to the formation of homogenous structures. The combination of the living polymerization character and the radical polymerization in reversible-deactivation radical polymerization (RDRP) produces several benefits. For instance, polymers with lower molar dispersity, predictable molar mass and high end group fidelity can be synthesized.[31],[32] RDRP is based on a dynamic equilibrium between the reactive growing chain and the corresponding dormant species.

The most frequently used polymerization methods of RDRP are *Reversible addition–fragmentation chain-transfer* (RAFT polymerization) and *Atom-transfer radical polymerization* (ATRP). Within the RDRP, it further differentiated between activation/deactivation and degenerative chain transfer. ATRP thereby represents an example for reversible activation/ deactivation. The use of the transition metal such as copper results in the preferential presence of dormant species, which leads to a reduction of active chains in the system. The reaction occurs between alkyl halogenides and transition metals via oxidative insertion, which enables the propagation of growing polymer chains.[32] In contrast RAFT polymerization is a prominent example for degenerative chain transfer.[31] In degenerative chain transfer, no change of total number of reactive species during the transfer process occurs.[32]

1.2.2 RAFT polymerization

Reversible addition–fragmentation chain-transfer (RAFT) is one of the most versatile and effective polymerization methods, which represents a prominent method of reversible degenerative chain transfer. It was published in more than 10000 papers and over 1000 patent families in the last decades.[33]

RAFT is one of several polymerizations methods, whose living character is given due to the degenerative transfer of the growing polymer chain. Beside from the initiator, which acts as the radical source, RAFT makes use of a chain-transfer agent (CTA). A fast equilibrium between growing chains and CTA, ensures the same probability for all chains to grow at a given time.[31] **Figure 4** shows the proposed RAFT mechanism, which usually starts by thermal or light-induced decomposition of the initiator (e.g. AIBN). This step generates two homogenous radicals followed by the initiation of polymerization. The presence of CTA converts the growing chains into an intermediate radical, which fragments rapidly to a new propagating species.[34] This new formed radical (R·) can provide chain growth, while the new macro-CTA is formed at once. This "degenerative" mechanism describes the similarity between starting reactant (CTA) and product (macro CTA) in terms of reactivity. The high end-group integrity enables a further chain growth, so the polymer topology can be controlled.[35]
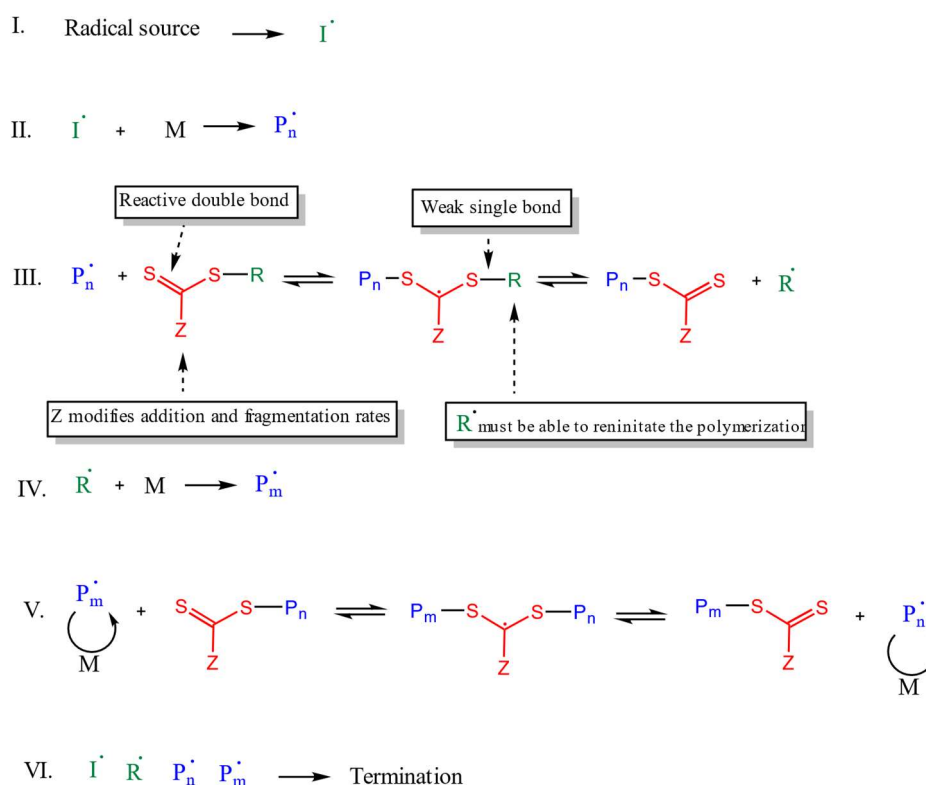
Figure 4: Proposed mechanism of Reversible Addition-Fragmentation Chain Transfer Polymerization. The mechanism was adapted from [32] and [34].

The various reactivity of monomers require different CTA classes to stabilize the intermediate radical in an appropriate way.[31] Typically, there are four different classes of CTAs, which differ in the group next to the C=S bond. These four classes are: dithioesters, trithiocarbonates, xanthates and dithiocarbamates. Trithiocarbonates are usually applied for the polymerization of acrylic monomers. In contrast, dithioester enable a high control over less activated methacrylate monomers.[36] The most common chain-transfer agents are dithio-compounds, whereby the functional group "Z" affects the stability of the thiocarbon double-bond and the intermediate radical.[33] The stabilization of the R leaving group affects the location of the equilibrium (III., V.) and therefore influence the polymerization.

The end-group chemistry of RAFT-polymers, polymerized via thiocarbonylthio-CTAs, is an important issue. Firstly, a reactive thiocarbonylthio group is necessary for block copolymer synthesis. This required further chain growth, which may be prevented by the instability of this group. Secondly, the reactive end group must be removed after polymerisation due to its inherent reactivity. Besides the disadvantages, end-group chemistry offers the possibility to introduce new functional groups that can be used for further reactions. For example, nucleophiles or an excess of the initiator AIBN can be applied, which leads to radical termination of the growing polymer chain.[36]

RAFT polymerisation enables the controlled synthesis of polymers characterised by a narrow molecular weight distribution, a defined molar mass and predeterminable end groups. This method enables the formation of a wide variety of structures, including block copolymers, stars or hyperbranched polymers.[31],[36] A major advantage of RAFT compared to ATRP is the high tolerance of different monomers. In comparison to ATRP, which relies on the use of transition metals, not subsequently purification is necessary. This simplifies primarily the implementation for biomedical use.[31] The versatility, the good controllability and the low demands make RAFT a suitable method to synthesize a wide range of polymers.

1.3 DNA Polymer Hybrid materials

The formation of artificial DNA biomolecule hybrid materials offer a solution from DNA limitations (cf. 1.1.2) such as an enhanced cellular-uptake, solubility, biodistribution or improved stability.[37] These DNA-biomolecule hybrid materials encompass inorganic and organic compounds such as DNA-protein[27], DNA-peptide[38] or DNA-lipid[26] structures, which are well investigated. In comparison, the application of DNA-polymer hybrid materials was deferred. One reason is the highly ionic character of DNA, which makes the reaction in aqueous environment more complicated, while hydrophobic polymers and monomers require organic solvents to guarantee high solubility.[39] Furthermore the synthesis of DNA-polymer conjugates were aggravated since the availability of DNA was limited. With the development of the automated solid-phase synthesis of DNA, accessibility and costs of DNA were improved.[40] Despite the difficulties, DNA-polymer conjugates exhibit great potential, which is presented in this section.

DNA-Polymer hybrid materials can be categorized through noncovalent and covalent interactions, which lead to the formation of 1D/2D or 3D structures, like DNA origami. In the following, the explanation will be restricted to the formation of covalent DNA-polymer conjugates, whose synthesis and application will be introduced in this thesis.

Covalent DNA-Polymer Conjugates

The synthesis of covalent hybrid materials encompasses three different methods: *grafting to*, *grafting from* and *grafting through*, which utilize the controlled-living polymerizations methods described in chapter 1.2. The three methods are schematically illustrated in **Figure 5**. Each of these approaches has various advantages and disadvantages, which are briefly presented below.

The *grafting from* approach (**Figure 5 (A)**) uses a covalent DNA-bond initiator, wherefrom polymerization occurs *in situ*. This polymerization method is limited by the instability of used initiator. Therefore, mild conditions are required. To handle the DNA, the system is typically restricted to low reaction volumes. To circumvent uncontrolled termination of polymerization, special degassing techniques are necessary.[41] These high reaction standards restrict the monomer scope. So far, *grafting from* method was established for RAFT and ATRP polymerization. The *grafting to* methods provides an alternative method to circumvent these limitations.[42]

The grafting to approach (**Figure 5 (B)**) uses presynthesized end-functionalized polymers and mostly 5' or 3'-modified DNA, which are conjugated in a following step. Therefore, both molecules can be

characterized prior to the conjugation reaction.[43] Due the independent synthesis of both compounds, a wide range of monomers and different solvents can be used for polymer synthesis. Furthermore, the performance in larger scales enables a better control over the polymerization. In contrast to the *grafting from* method, steric hindrance of large polymer chains may shield the reactive handle and reduce the conversion of coupling-reaction.[42]
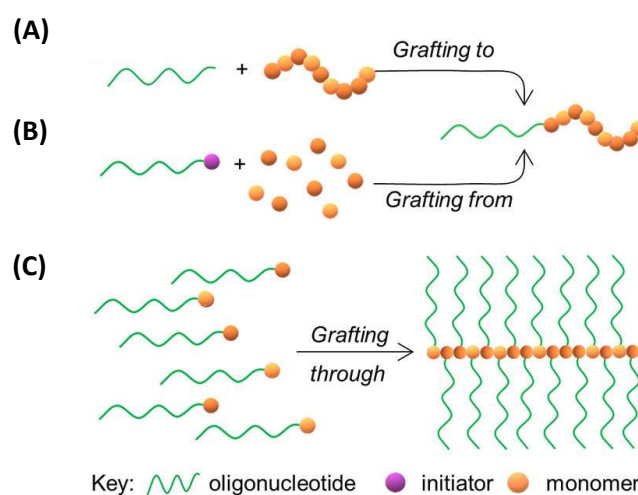
Figure 5: Schematic illustration of *grafting -to*, *-from* and *-through* approach. (A) *Grafting to*-polymer synthesis occurs prior to the conjugation reaction, (B) Grafting from-in situ polymerization from polymer bond initiator, (C) Grafting through-ODN conjugated monomers with polymerizable groups (taken from [44]).

The conjugation synthesis can be performed using two different strategies: i) solid-phase functionalization (phosphoramidite synthesis) and (ii) solution coupled functionalization. Due to several drawbacks of solid-phase functionalization like a low yield, a limited availability of functional groups and the necessity of purification after the modification of DNA, solution-based ODN-polymer synthesis offers a promising alternative method. [45]

A popular strategy for solution-based ODN-Polymer synthesis includes the conjugation reaction of amine-modified ODN with NHS-modified targets. This method was investigated for different functionalized polymers like PGLA-NHS[46] or pNIPAM-NHS[47]. A further possibility to synthesize conjugates encompasses the use of alkyne end-modified DNA and azide-functionalized polymers (Huisgen [1+3] dipolar-cycloaddition). Moreover, Michael addition offers an alternative way for the synthesis of this hybrid materials. In this approach acrylate-functionalized polymers and thiol-modified ODN act as Michael acceptors and Michael donors, respectively.[48]

For the grafting through approach (**Figure 5 (C)**), ODN functionalized monomers with polymerizable groups create copolymers with a linear backbone and defined side chains, giving access to brush and hyperbranched structures.[49]

Categorization of DNA-Polymer conjugates

DNA-Polymer conjugates are very tunable structures due to the accessibility of different monomers, switchable block-lengths and -ratios. They are commonly categorized in two classes: purely hydrophilic and amphiphilic hybrid materials.

The use of hydrophilic polymers gained crucial importance for the synthesis of DNA-based hydrogels, which are applied in drug delivery systems.[50],[43] Recently, it has been discovered that short ODN, which shows three-dimensional structures, can bind to biomolecules in a precise manner. These so called aptamers behaviour is comparable to the highly specific antigen-antibody binding.[51] Polyethylene glycol (PEG) is a common tool for the enhancement of biodistribution and biocompatibility. The development of PEG-aptamer hybrid materials has already proven itself in glaucoma treatment.[18]

The conjugation of hydrophobic polymers to DNA is more challenging due to phase separation, as already described in the previous chapter. To enable a successful conjugation, water-organic solvent mixtures or protected DNA must be applied.[52] These block-copolymers exhibit amphiphilic features, where phase-separation drives the self-assembly in aqueous environment into various structures. The formation of micellar-like structures with hydrophobic polymer core and hydrophilic DNA-shell, facilitates a further possibility of functionalization of this nanostructure.[53]

Functionalities of DNA-polymer conjugates

To sum up this chapter, an overview of possible functionalities of primarily amphiphilic DNA-polymer conjugates is shown in **Figure 6**, where DNA-polymer conjugates are subclassified in three categories: i) functionalities based on polymers, ii) functionalities based on DNA and iii) synergistic functionalities.
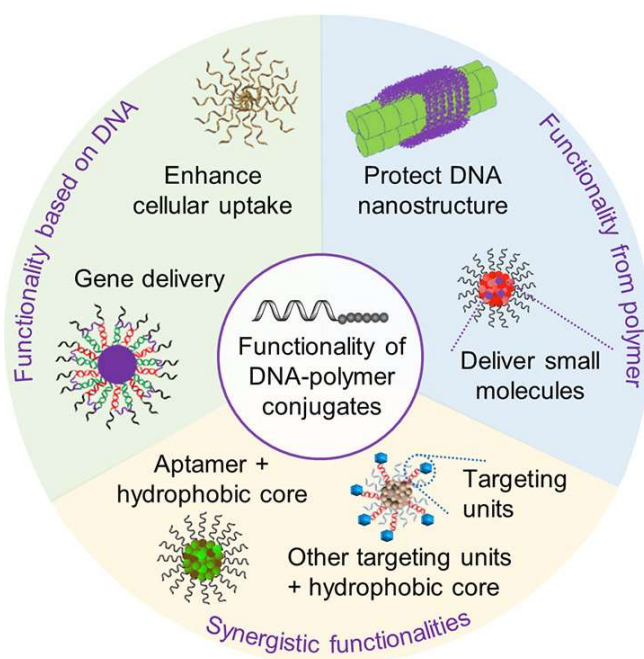
Figure 6: Categorization of functional DNA-polymer conjugates. Schematic illustration was taken from Whitfield *et al*.[44].

Several DNA-polymer conjugates, which mostly consist out of hydrophobic polymers like p(NIPAM)[54], PS[55] or PCL[55], have been published. Their self-assembly behaviour to micellar structures enables the transport of small molecules inside their core, with the additional possibility to functionalize the outer DNA-shell for cell targeting. Moreover, polymers stabilize and protect DNA-structures from degradation, making them possible for biomedical application is possible.

Self-recognition properties of DNA can be used for gene delivery, which was successfully demonstrated by Zhang *et al*.[56] who synthesized a siRNA cross-linked hydrogel. Besides from cargo transport, the nucleic acid shell of spherical nucleic acids (SNAs) shows an effective cellular uptake.[55]

The combination of the properties of DNA and polymers enables versatile application. In addition to the functionalization of ssDNA, three-dimensionally folded DNA, DNA origami, can also be coated with polymers. This topic is presented in section 1.3.2.

1.3.1 DNA Origami hybrid materials

Beside from the synthesis of DNA-polymer conjugates, DNA Origami hybrid materials enable a breakthrough in nanometre-scaled organisation of molecules. For instance, this molecular precision is used for distance-dependent molecular interaction studies such as multilayer enzyme cascades[57], controllable energy transfer[58] or templated synthesis of nanopatterned polymeric nanostructures.[59],[60],[61]

The most important methods to introduce functionalities to the DNA origami surface use extended staple strands, serving as sticky ends, which could function as attachment points for complementary, functionalized DNA (**Figure 7 (A)**).[15] A further modification of staple DNA strands includes the introduce of small functional groups by solid-supported DNA synthesis, including e.g. amines, alkynes, thiols, azides, maleimides or fluorophores (**Figure 7 (B)**).[15] Non-covalent interactions can occur e.g via biotin-streptavidin or aptamer-protein (thrombin[62] or trypsin[63]) binding, where ODN are functionalized either with biotin or aptamers (**Figure 7 (C)**). Another method uses Guanine-extended DNA, which forms secondary structures, called G-quadruplex **(Figure 7 (D)**). They consist out of four guanine bases, stabilized by Hoogsten-type hydrogen bonds. This system can catalyse hydrogen peroxide-mediated oxidation.[64],[65] This method is explained more in detail in subsection 1.3.2.
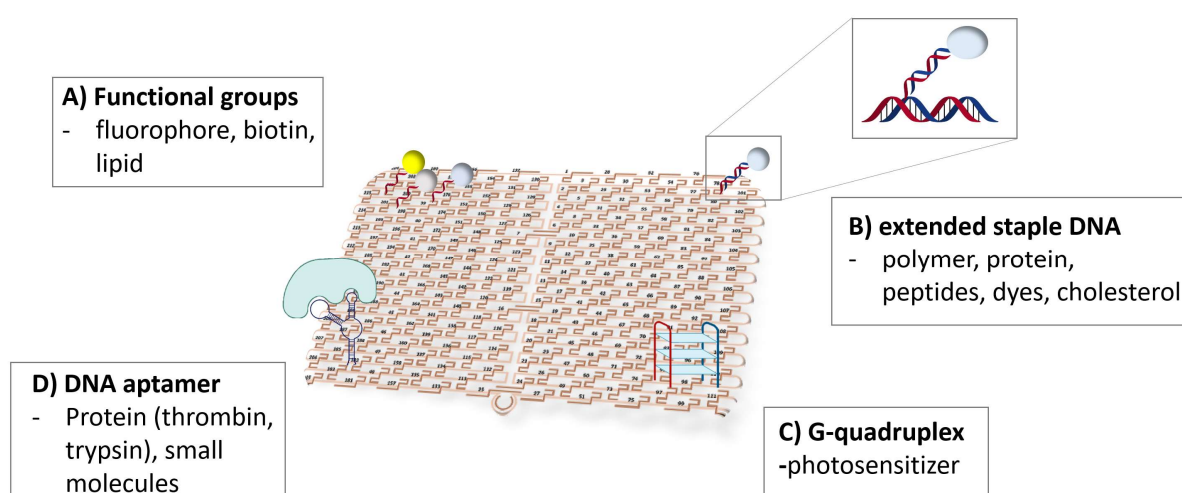
Figure 7: Schematic illustration of the introduction of functionalities to DNA origami surface. The image was adapted from [66].

1.3.2 DNA Origami polymer patterning

Patterning of DNA origami surface enables the transfer of structural information from DNA to different polymers by hybridization of complementary DNA-polymer conjugates to the origami surface. This templated bottom-up synthesis of nanostructures enables the formation of smaller, more precise constructs, whose sizes and shapes can be highly controlled. Due to the introduction of different extended staple DNAs, not only defined positions can be addressed but also several functionalities like different polymers or fluorophores can be introduced at once. The number of sticky sequences determinates the density of polymers on the origami surface, which influences the stability substantially. [28]

Besides from the use of the DNA template, the choice of the polymer can engineer the properties of DNA origami-polymer hybrid materials due to the large variety of polymers encompassing hydrophobic, hydrophilic or stimuli responsive polymers.[67] Analogously, to the synthesis of DNA-polymer hybrid structures mentioned in section 1.3, there are two fundamental strategies to differentiate between DNA origami polymer hybrid material syntheses: *grafting onto* and *grafting from*. For *grafting to* the preformed DNA polymer conjugates, either DNA-polymer brushed or terminal-modified conjugates, can hybridize to their complementary sticky handles on DNA origami surface. Steric hindrance of polymer chains makes a high patterning-density challenging, whereas for *grafting from* approach this limitation is negligible. Polymerization occurs from immobilized ODN bound initator on DNA origami surface, determining defined positions of the polymer chains.[42],[68]

A prominent example was published by Krissanaprasit[69] *et al*., who described a programmed switching of a single-molecule conjugated polymer (**Figure 8 (A)**). Therefore, a DNA-polymer brush was located on the DNA origami surface by hybridization of single-stranded handles to sticky sequences on the DNA origami. This DNA-polymer brush could be aligned in three different positions: in a straight line, left-turned or right-turned. These orientations could be tuned via a strand displacement, whose different orientations were visualized by atomic force microscopy and Förster resonance energy transfer.

The polymerization from DNA origami surface was successfully demonstrated for ATRP, with tailored properties and higher grafting density.[70] For example, the synthesis of grafted nanostructures with polymerization of poly(ethyleneglycol)methylethermethcrylate (PEGMEMA) was executed. PEGMEMA was selected because of its good biocompatibility and wide applications in bionanotechnology.[71] After the crosslinking, the templated-guided nanostructure was released into the solution, through degradation of DNA origami.[42]

A further *grafting from* strategy was presented by Wang[72] and his co-workers. G-quadruplexes act as DNAzymes on the origami surface of triangular structures. The addition of cofactor hemin and hydrogen peroxide leads to a horseradish peroxidase (HRP)-like system, which catalyses the formation of polyaniline. The G4/hemin polymerization method was adapted by Yu *et al.*[73] to polymerize dopamine under acid conditions (**Figure 8 (B)**). The highly crosslinkable nature of dopamine, therefore often named "supramolecular clue", leads to the formation of rigid, stabile
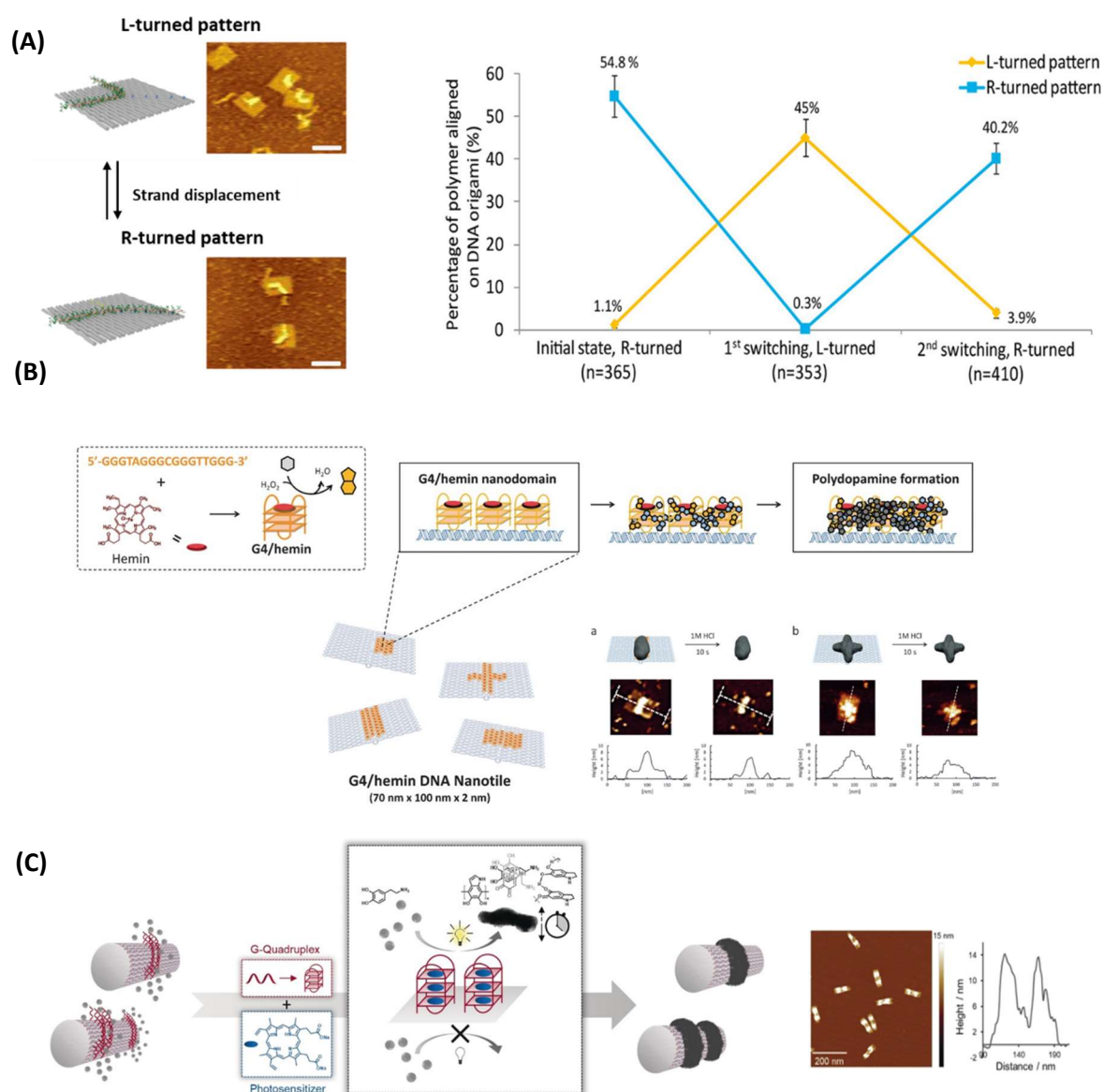
Figure 8: Examples for the patterning of DNA origami surfaces. (A) Nanomechanical switching of a single-polymer chain on DNA origami surface based on toehold-mediated strand displacement. Left: AFM images of L-turned and R-turned pattern. Right: Percentage of aligned polymer on the DNA origami surface during the switching process (taken from [72]), (B) Controlled polymerization strategy of dopamine by installing confined DNAzyme domains on DNA origami surface. Right: AFM images of released nanostructures after 1M HCl degradation of DNA templates. (taken from [73]), (C) Photoinduced polymerization of dopamine on 3D origami tubes (taken from [60].)

nanostructures, which were intact even after the liberation from the DNA template. Furthermore, the system was optimized by switching to the photoinduced system, where the photosensitizer protoporphyrin IX initiates the multistep oxidation of dopamine after the irradiation (**Figure 8 (C)**).[60]

While these achievements have proven their potential for the synthesis of well-defined nanostructures with nanometre-scaled resolution, the number of publications in this field of DNA origami-hybrid materials is still low.[44] Limited characterization techniques, mostly based on AFM measurement, steric hindrance, or solubility issues due to the different behaviour of polymer and DNA in the same solvent, make this topic challenging. Furthermore, DNA availability is still rather limited due to its high costs. This leads to small-scale procedures, which prevent an industrial application. Especially the *grafting from* approach is limited to imaging techniques like AFM or Transmission electron microscopy (TEM), because a characterization of polymers prior to the conjugation reaction cannot be achieved.

Therefore, the synthesis method *grafting to,* which was recently published for decoration of several DNA origami structures, offers an alternative approach. This method could widen the range of applicable polymers and therefore the accessibility of DNA origami polymer hybrid materials due the more independent conjugate synthesis.[59]

2 Objectives

In this section the main objectives of this thesis will be given. Based on synthesized DNA-polymer conjugates, three topics will be investigated. Firstly, the DNA origami template-guided design of polymer nanoparticles and secondly the examination of the potential of polymer nanopatterned DNA origami for cellular uptake. As a supplemental topic, the synthesis of DNA multiblock copolymers is also provided. The objectives of this thesis are summarized in a scheme.
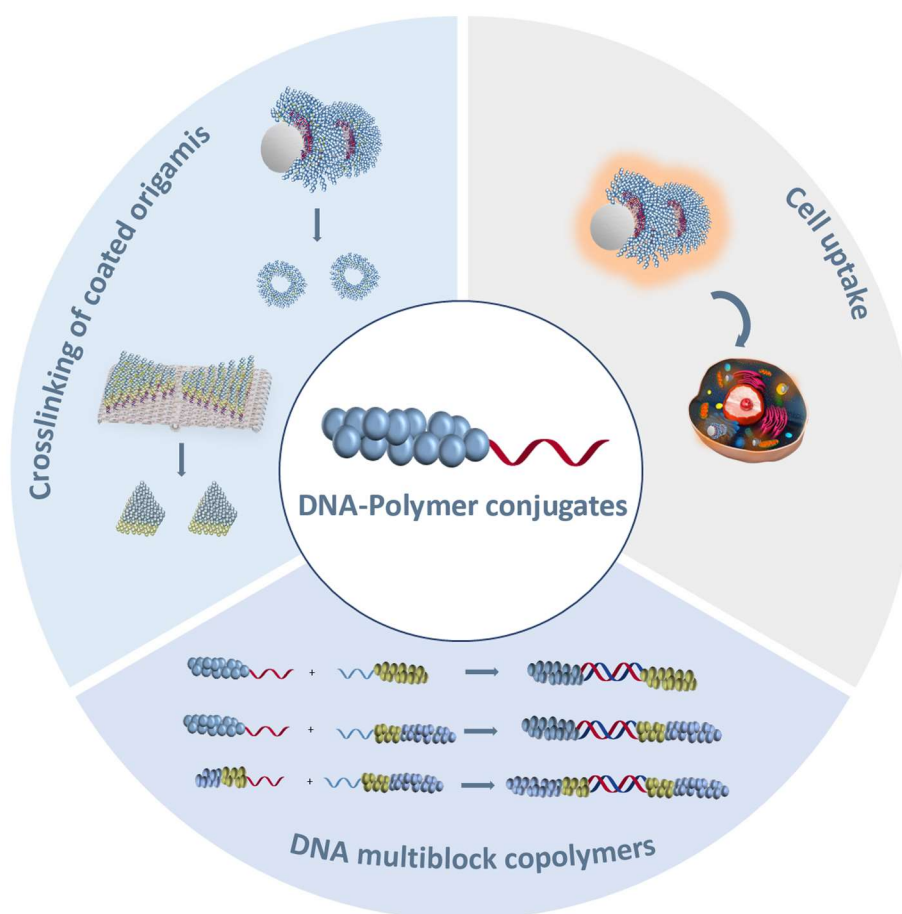
Figure 9: Overview of applications of DNA-polymer conjugates in this work. ▨ Nano-scaled structures generated by coating of DNA origami with DNA-p(DAAM-*b*-DMA) conjugates, followed by the crosslinking of polymer chains on the origami surface and the origami template-degradation. ▨ Cell uptake studies of fluorescence labelled, and polymer coated DNA origami tubes. ▨ Synthesis of DNA multiblock copolymers through sequence-hybridization of DNA-polymer conjugates.

DNA-polymer conjugates

RAFT polymerization, a controlled living radical polymerization, has great potential to create defined structures in terms of composition, length and adjusting the properties by post-modification. The high control over the molecular weight distribution, the unpretentious conditions and the versatile end group chemistry of RAFT polymerization are further advantages.[32] Thus, this approach is chosen for this project to create a wide range of polymers exhibiting differences in hydrophobicity, block length and ratio.

These NHS-functionalized polymers can react with amine-modified ssDNA via the *grafting to* approach to from various DNA-polymer conjugates. Subsequently, the chromatographic purification using *Fast Protein Liquid Chromatography* (FPLC) is to be implemented. This approach might offer an advantageous way to purify DNA-polymer conjugates from remaining polymer and ssDNA compared to the spin filtration method used until recently. These purified conjugates shall serve as base structures for the formation of 2D- and 3D-DNA-polymer hybrid materials.

Crosslinking of coated DNA origami

In literature, the diverse properties of block copolymers were used to form self-assembled structures such as micelles or polymersomes, whose applications are of crucial importance in biomedicine.[74] However, since these amphiphilic structures hardly offer a controllable self-assembly process, the enhanced precision and predictability of nanostructure formation is advantageous. In contrast, in nature a wide variety of unique and well-defined biomolecules such as peptides, proteins or DNA can be found, of which DNA shows incomparable programmability and self-recognition properties. Thus, mimicking and using DNA to design DNA-hybrid materials acquired a good reputation in the last decades. [50],[55] For that reason, different DNA-polymer hybrid materials using the various advantages of DNA shall be investigated in this work.

In DNA nanotechnology, two- and three-dimensional folded DNA origami offer a new dimension in templated organisation of polymer functionalities by introducing polymer chains to the surface of the DNA origami in a highly predictable way.[28],[73] By functionalizing the origami surface with radical initiators, polymerization can occur directly on the origami surface.[73] However, this method requires stringent conditions, which are circumvented in this work using the *grafting onto* approach.[43] The preformed DNA-polymer conjugates are introduced to the origami surface at designated positions by hybridization to complementary sticky sequences. In the scope of this thesis, rectangular- and tube-formed DNA origami are used as templates for the synthesis of nanometre-scaled polymer particles.

For this intention, the origami structures are nanopatterned with DNA-p(DAAM-*b*-DMA)-conjugates, whose p(DAAM) units can be crosslinked, followed by the degradation of the DNA-template. The thereby released nanoparticles possess predictable, well-defined structures, which cannot be obtained using conventional methods like the self-assembly of amphiphilic block copolymers. Conventional methods only lead to the formation of spherical structures, whereas in this work the DNA origami templated design allows the formation of polymer triangles.

Cellular uptake of patterned DNA origami structures

So far, the application of origami structures in biomedicine is challenging due to their low stability in physiological environments and the electrostatic repulsion between both the negatively charged DNA origami structure and the cell membrane. This leads to the degradation of the DNA origami structures and hinders the cellular uptake, respectively.[23],[24] To reduce these limitations of cellular penetration, DNA origami structures are protected by a polymer coat. With regard to Winterwerber *et al.*[25], who investigated the cellular uptake of poly norepinephrine coated DNA origami tubes, in this thesis three different homopolymer patterned DNA origami tubes are tested to their cell-internalization. The results of this cell uptake experiments can probably be used for the development of *in vivo* drug delivery vehicles for cancer therapy.[75]

DNA multiblock copolymers

In this thesis, another possible application of DNA-polymer conjugates came to attention: the synthesis of multiblock copolymers. Multiblock copolymer synthesis using conventional polymerization methods suffer from a low sequence selectivity, monodispersity and programmability.[76] By utilizing the self-assembly properties of complementary DNA-polymer conjugates, the limitations of conventional block copolymerization methods are circumvented. This way, multiblock copolymers are synthesized in a combinatorial manner, encompassing the formation of triblock, tetrablock or pentablock copolymers.

3 Results

The reaction of polymers and DNA results in a completely new hybrid material that combines the advantages of both substance classes. In the present work the self-recognition properties of DNA are used for the following three different applications. Induced by the sequence hybridization of two complementary DNA-polymer conjugates larger multiblock copolymers are formed. Furthermore, DNA-polymer conjugates are used for surface patterning of 2D/3D DNA origami structures, which allows the exact positioning of functional moieties with nanometre resolution. Finally, nanopatterned structures are tested regarding their cellular uptake capability.

3.1 Covalent DNA-polymer conjugates

The combination of chemical properties of both polymer and DNA leads to a new substance class, which compromises new properties like enhanced stability, solubility and biodistribution.[37]

Covalently bound DNA-polymer conjugates can be synthesized via *grafting to*. Therefore, preformed polymers can be linked to the DNA in a further step. This method offers several advantages like the use of different solvents or monomers. Additionally, it facilitates the fully characterization of the polymer prior to conjugation reaction and an easier scalability.[44] *Grafting to* allows access to a wide diversity of DNA-polymer conjugates, whose synthesis can involve hydrophobic or hydrophilic homopolymers as well as block copolymers.

3.1.1 Synthesis of polymers via RAFT-polymerization

Reversible addition-fragmentation chain transfer (RAFT), a living polymerization method, offers many advantages like a narrow molar dispersity, high end-group fidelity and the capacity for continued chain growth which makes block copolymer systems accessible.[32] In addition, a wide range of monomers can be used, allowing the synthesis of diverse polymers with a wide range of properties. A fast equilibrium between growing chains and a chain transfer agent CTA, ensures the same probability for all chains to grow at a given time.[31]

The CTA selection depends on the monomer system. RAFT polymerization with methacrylates was performed using 4-Cyano-4-(phenylcarbonothioylthio)pentanoic acid N-succinimidyl ester (CTA 1). The homopolymer and diblock copolymer synthesis of acrylates and acrylamides was carried out using 2-(Dodecylthiocarbonothioylthio)-2-methylpropionic acid N-succinimidyl ester (CTA 2). To

enable the chain start, the initiator azobisisobutyronitrile (AIBN) was necessary, which serves as a radical source. The reaction was carried out at 55-70 °C, resulting in the decomposition of AIBN, which leads to the formation of two reactive 2-cyanoprop-2-yl radicals under the release of nitrogen (r=$\frac{AIBN}{CTA}$ = 2). The reactions were performed in dimethylformamide (DMF) or 1,4-Dioxane. To prevent the termination of the chain transfer, the reaction mixture was purged with argon to remove oxygen from the solution. The reactive thiocarbonyl group was removed with a high access of AIBN (>50 eq) at 80°C.

Within this thesis, different homopolymers and one block copolymer were synthesized, which were used for the formation of DNA-polymer conjugates (subsection 3.1.2). The used monomers have distinguished properties to investigate. All of them are biocompatible and water-soluble which enables the subsequent reaction with modified DNA (cf. 3.1.2). Synthesized polymers differ in their hydrophobicity and therefore influence their behaviour in aqueous solvents.

Following monomers were utilized for the synthesis of both homo polymers and block copolymers, whose general synthesis is shown in **Figure 10** and **Figure 11**.
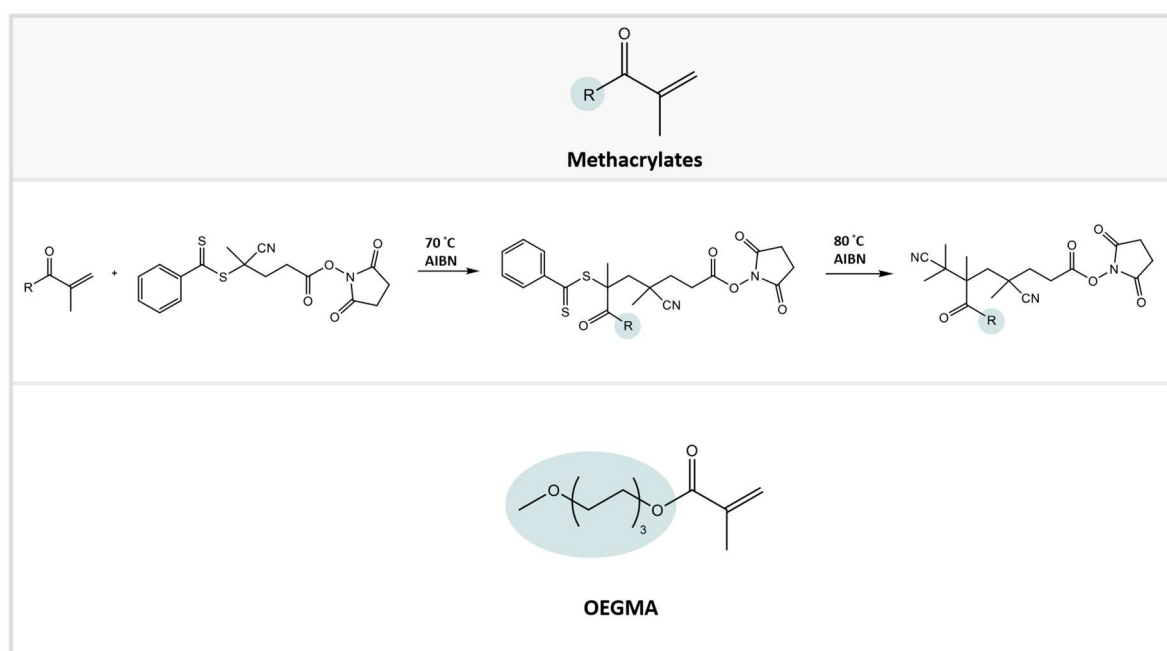
Figure 10: *Generalized equation of polymethacrylates synthesis.* The reaction was carried out at 70 °C using 4-Cyano-4-(phenylcarbonothioylthio)pentanoic acid N-succinimidyl ester (CTA 1) and azobisisobutyronitrile (AIBN). An excess of AIBN enabled to remove the CTA group. Oligo(ethylene glycol) methyl ether methacrylate) (OEGMA) was polymerized under these conditions.

Poly(oligo(ethylene glycol) methyl ether methacrylate) (p(OEGMA)), whose structure is demonstrated in **Figure 10**, was used because of its non-toxic and non-immunogenic properties.

P(OEGMA) shows in comparison to other used monomers characteristic brush like structure with hydrophilic oligo(ethylene glycol) side chains.[77]

The generalized synthesis of polyacrylamides and polyacrylates is displayed in **Figure 11**.
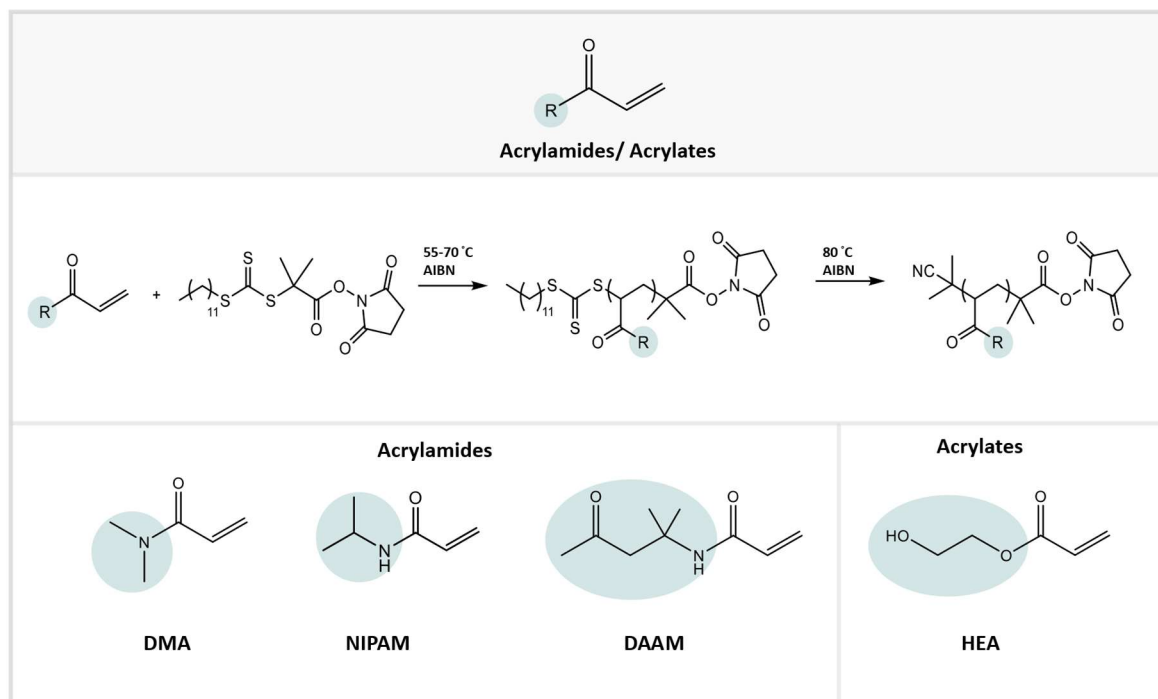
Figure 11: General synthesis of polyacrylamides and polyacrylates. 2-(Dodecylthiocarbonothioylthio)-2-methylpropionic acid *N*-succinimidyl ester (CTA 2) was used as a chain transfer agent. The reaction was performed at 55-70 °C, the product was precipitated in ether and the CTA group was removed by an excess of AIBN. *N,N'*-dimethylacrylamide (DMA), 2- Hydroxyethyl acrylate (HEA), *N*-isopropylacrylamide (NIPAM) and Diacetonacrylamide (DAAM) were polymerized under these conditions.

Poly(2-hydroxyethyl acrylate) (p(HEA)) is an even more hydrophilic polymer then p(OEGMA) due to the formation of hydrogen-bond by its hydroxyl group.[78]

Poly(*N,N'*-dimethylacrylamide) (p(DMA)) exhibits hydrophilic properties as well. Its thermo- and pH responsive properties make it an interesting tool for the design of block copolymers. At low pH-level, protonation of p(DMA) side chains effectuates water-solubility, whereas in basic or neutral environment p(DMA) exhibits a high water solubility due to the formation of hydrogen-bonds.[79]

A further used polymer is Poly(*N*-isopropylacrylamide) (p(NIPAM)). P(NIPAM) is a hydrophobic, thermoresponsive polymer, whose lower critical solution temperature (LCST) is close to the human body temperature (32-33 °C). Therefore, at room temperature it shows a solid state, while transforming into gel state under physiological conditions.[80]

The synthesized homopolymers were characterized by DMF-gel permeation chromatography (GPC) with Poly(methyl methacrylate) (PMMA) as an intramolecular standard (cf. **Figure 12**).
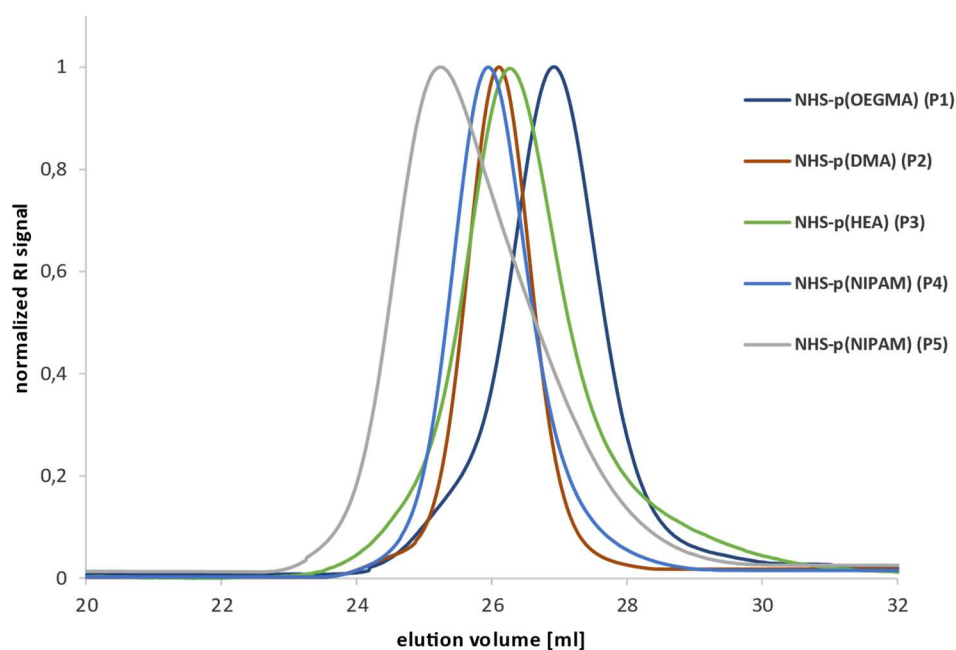
Figure 12: DMF-GPC results of synthesized NHS-homopolymers using RAFT-polymerization. DMF-GPC traces of NHS-p(OEGMA), -p(DMA), p(HEA) and -p(NIPAM) using PMMA intramolecular standard.

The GPC-traces show the results of five different homopolymer syntheses. In **Figure 12** the normalized RI signals are plotted against the elution volume in ml. All homopolymers show narrow, monomodal curves, which indicates a controlled synthesis via RAFT polymerization. The results of GPC measurement are listed in **Table 1**, where the molecular weight (M_w), the dispersity (Đ) and the calculated repeat units ($\overline{X_n}$) of the homopolymers are listed, respectively.

Table 1: Determined DMF-GPC data of homopolymer systems. Molecular weights (Mw), calculated repeat units ($\overline{X_n}$) and dispersity (Đ) of the polymers.

Homopolymer		M_w [g/mol]	$\overline{X_n}$	Đ
NHS-p(OEGMA)	P1	18696	61	1.10
NHS-p(DMA)	P2	22125	220	1.08
NHS-p(HEA)	P3	22149	130	1.32
NHS-p(NIPAM)	P4	25745	225	1.12
NHS-p(NIPAM)	P5	30840	270	1.25

Furthermore, the measurement of the product ^{1}H-NMR shows the successful synthesis of the different polymers. **Figure 13** demonstrate an example of the NMR measurement of p(OEGMA).
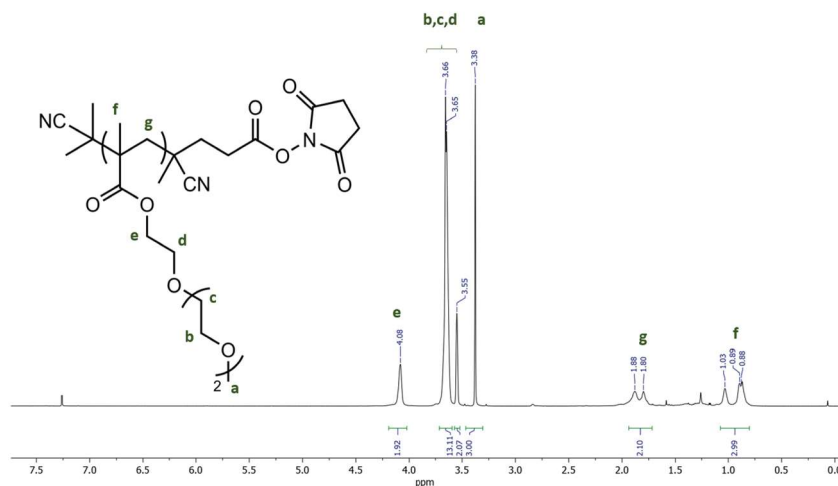
Figure 13: Product ^{1}H-NMR (700 Hz, CDCl$_3$) of p(OEGMA).

Normalization on the terminal methoxy group (3H, δ= 3.39 ppm, **a**) enables the assignment of protons of the repeat unit, which are marked in green letters. Since no aromatic signals are detected, a successful CTA removal can be assumed. Additionally, to confirm that only one diffusing species is present, a ^{1}H-Diffusion-Ordered Spectroscopy-NMR (^{1}H-DOSY-NMR) was measured.
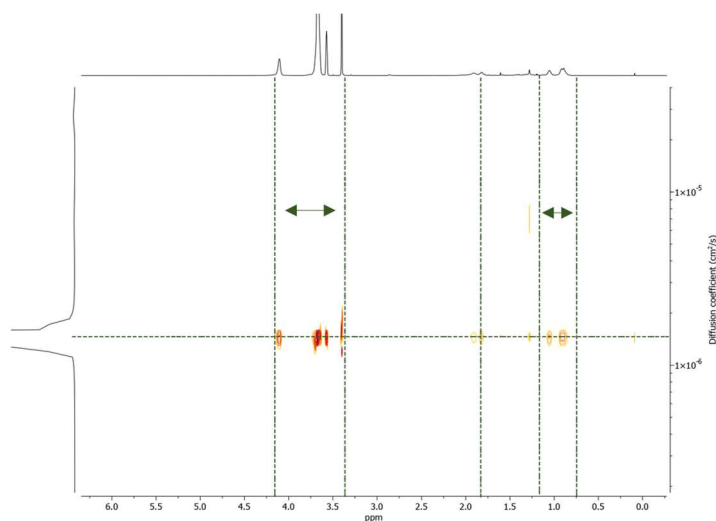
Figure 14: ^{1}H-DOSY-NMR of p(OEGMA).

^{1}H-DOSY-NMR confirms the presence of only one diffusing species. The NMR spectra of the other homopolymers can be found in the Appendix A.

NHS-p(DAAM-*b*-DMA) synthesis

Additionally, to the homopolymer synthesis, the NHS-p(DAAM-*b*-DMA) block copolymer was synthesized (**Figure 15**).
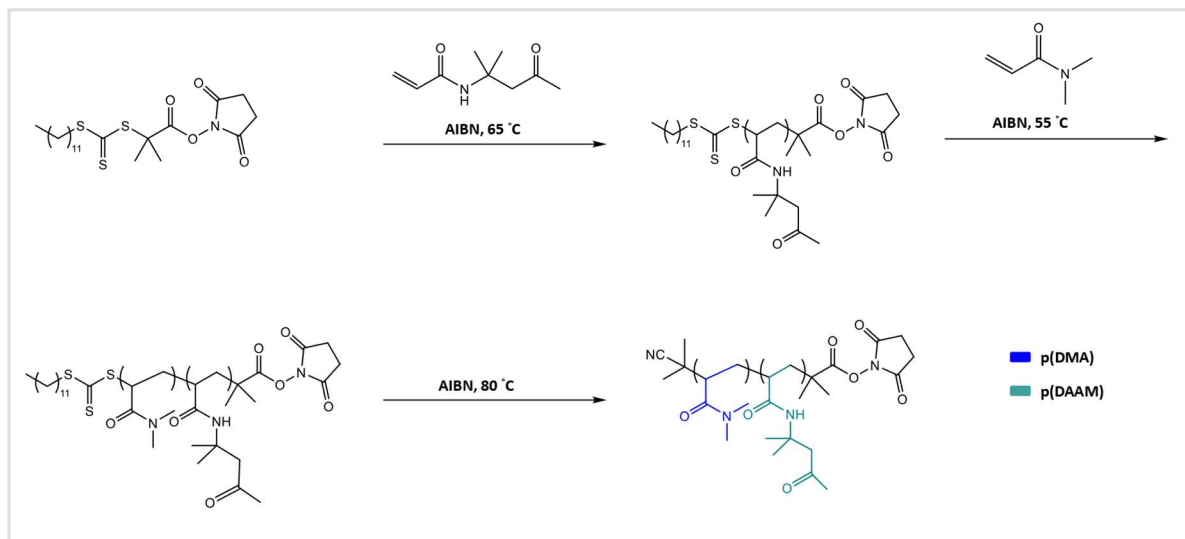
Figure 15: Overview of NHS-p(DAAM-*b*-DMA) synthesis. The first block was synthesized using CTA 2, AIBN and diacetonacrylamide (DAAM). The addition of AIBN and *N,N'*-dimethylacrylamide (DMA) leads to the synthesis of the block copolymer, whose reactive end group was removed by an excess of AIBN.

P(DMA) was selected because of its high water solubility, which allows the reaction with DNA in one system. This DNA-polymer hybrid material synthesis is discussed in subsection 3.1.2.

Poly(diacetonacrylamide) (p(DAAM)) was chosen as the second block, because it allows the possibility of a subsequent crosslinking reaction. This property was indispensable for the DNA origami template-guided nanoparticle synthesis, which is presented in section 3.2. In contrast to the very hydrophilic p(DMA), p(DAAM) exhibits more hydrophobic properties, which leads to the formation of an amphiphilic block copolymer. Due to the tunable block- length and ratios, hydrophobicity as well as the number of crosslinkable carbonyl groups can be adjusted. In this scope, three different NHS-p(DAAM-*b*-DMA) block copolymers were used for further DNA-functionalization (cf. subsection 3.1.2).

It was observed that precipitation of the homopolymer leads to partial removal of the CTA end-group, which reduces further polymerization of the second block. Thus, without precipitation and isolation of the p(DAAM) homopolymer system, the formation of the second block was performed.

For the calculation of the 2nd block, 90 % of monomer conversion was assumed, based on experiences of previous NHS-p(DAAM-*b*-DMA)-syntheses under the same conditions. **Figure 16** shows the results of the NHS-p(DAAM-*b*-DMA) block copolymer GPC measurement.
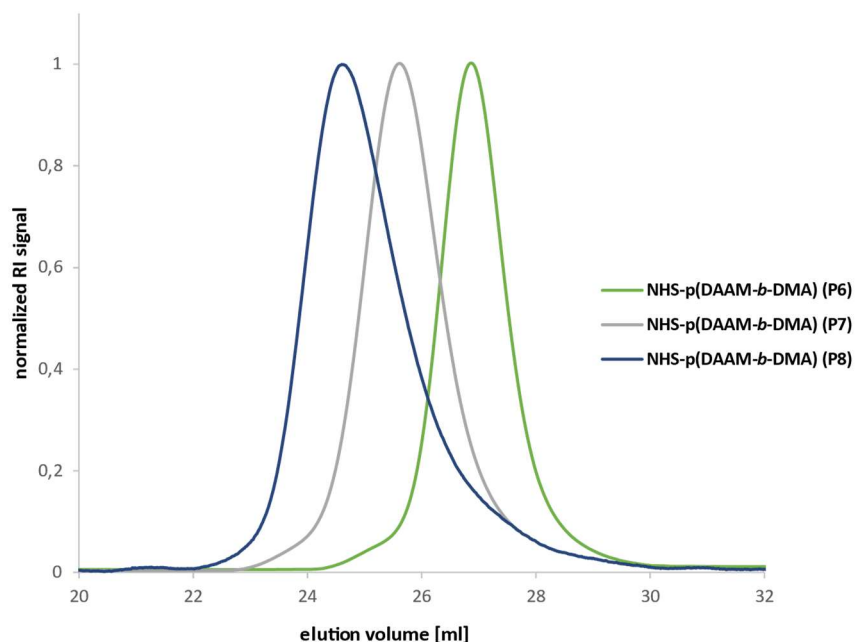
Figure 16: GPC results of NHS-p(DAAM-*b*-DMA) block copolymers. DMF-GPC traces of three block copolymer systems, which differ in their block- lengths and -ratios. PMMA was used as the intramolecular standard.

All traces show a narrow, monomodal course of the curve. In accordance with the lowest elution volume, P8 exhibits the highest molecular weight. The determined results of the block copolymer GPC measurement are summarized in **Table 2**.

Table 2: Determined DMF-GPC data of block copolymer systems. Molecular weights (Mw), calculated repeat units ($\overline{X_n}$) and dispersity (Đ) of the polymers.

Homopolymer		M_w [g/mol]	$\overline{X_n}$	Đ
NHS-p(DAAM-*b*-DMA)	P6	17917	30 (DAAM) 127 (DMA)	1.13
NHS-p(DAAM-*b*-DMA)	P7	26014	42 (DAAM) 188 (DMA)	1.20
NHS-p(DAAM-*b*-DMA)	P8	40704	31 (DAAM) 355 (DMA)	1.19

Apart from the polymer length, the three block copolymers also differ in their block ratio. P6 and P7 exhibit a very high hydrophilicity with a p(DMA)/p(DAAM) content of 42 % and 45 %, respectively. P8 shows a higher hydrophobicity with a p(DMA)/p(DAAM) ratio of 12 %, which influences both the superstructures formation and the accessible crosslinkable p(DAAM) groups for the in section 3.2 introduced topic.

Despite from GPC measurement, ^{1}H-NMR of NHS-p(DAAM) homopolymer and NHS-p(DAAM-*b*-DMA) block copolymer are shown in **Figure 17**.
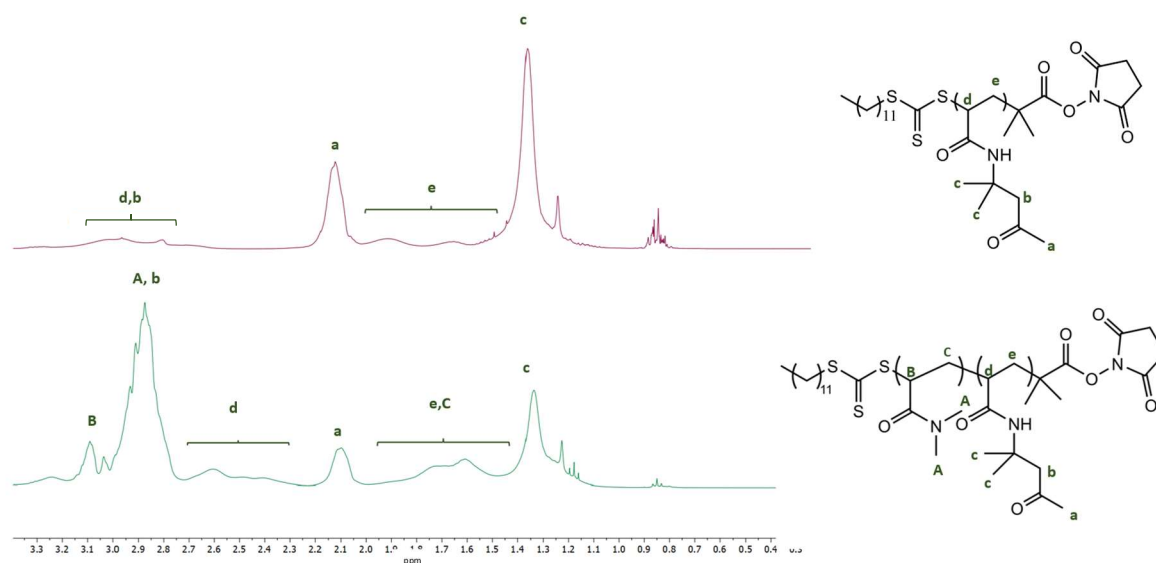
Figure 17: Stacked ^{1}H-NMR (400 Hz, CDCl$_3$) of NHS-p(DAAM) and NHS-p(DAAM-*b*-DMA) (P6).

The intensive peaks A and b, suggest a successfully synthesis of the second block. Since the signals of the final group are superimposed by those of the repeating units, it is not possible to calculate the number of repeat units via end-group analysis.

RAFT polymerization enabled the synthesis of different homopolymer and block copolymer systems with narrow molecular distributions. Polymer system P2, P7 and P8, which were used for further experiments, have not been synthesized in the scope of this work but allowed a wider range of polymers to be available. Due to the versatile properties, the ideal conditions for the formation of various DNA-polymer hybrid materials were given, which is presented in subsection 3.1.2.

3.1.2 DNA-polymer conjugate synthesis

The synthesis of polymers is a very well-established method and provides many opportunities to vary properties of the polymer in terms of hydrophobicity, block length and functional groups. As described in subsection 3.1.1, the polymers properties can be well adjusted, particularly through RAFT polymerization. The intended use of DNA can be extended by the combination with polymers because it enables to adjust their functionality and influence the stability of DNA.

One of three possible methods for synthesizing DNA-polymer conjugates is the *grafting to* approach. This method encompasses the conjugation reaction of presynthesized polymers and terminal functionalized ODN.[44] This solution-based approach results in an amphiphilic or purely hydrophilic diblock product, whose properties can be predetermined by the two reactants.

The performance of the conjugation reaction in one system is aggravated by the different solubilities. The ionic character of DNA restricts the conjugation reaction to more polar solvents, which limits the system to hydrophilic monomers and polymers. Otherwise, phase separation of both reactants due to the different behaviour in the present solvent can reduce the yield of the conjugation reaction.

The coupling of NHS-activated polymers with amine-modified ODN is one of the most established methods for DNA-polymer conjugation. This reaction was carried out in a DMF/H_2O mixture with the addition of steric hindered base *N,N'*-Diisopropylethylamine (DIPEA), which is commonly use in amide coupling.[81] The reaction is schematically illustrated in **Figure 18**.
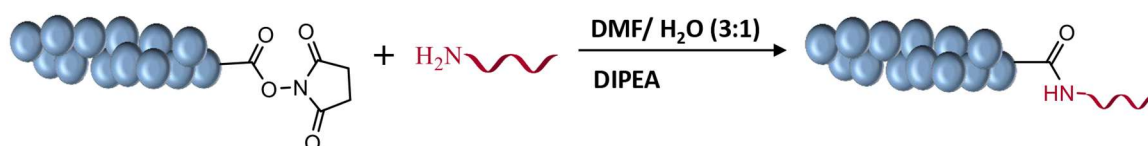
Figure 18: Amide coupling of NHS-activated polymer and amine-modified ODN. To ensure solubility of ODN and polymer the reaction was performed in DMF/H_2O (3:1) mixture.

This method offers an efficient way to synthesis DNA-polymer conjugates in solution. Due to the good solubility of the polymers and the DNA in the reaction mixture, aggregation of both is prevented. Therefore, the reactive functionalities are highly accessible, and a high conversion can be achieved. Moreover, commercially available DNA and common organic solvents can be used. The bioconjugation reaction of the NHS-functionalized polymers was performed with the 5'amino

oligonucleotide (complementary sticky A (StA^c; 5'-NH$_2$-TTTTCTCTACCACCTACTA-3', sticky A (StA: 5'-NH$_2$-TTTTAGTAGGTGGTAGAG-3'). To ensure a higher conversion of expensive ssDNA, a 50-equivalent excess of NHS-functionalized polymers was used. Synthesized DNA-polymer conjugates and the respective abbreviations are listed in **Table 3**. To determine the conversion of coupling reaction, a 15 % native PAGE gel was prepared. **Figure 18** shows the DNA-polymer conjugates of all homopolymers (C1^c-C3^c) and block copolymers (C4^c-C6^c).
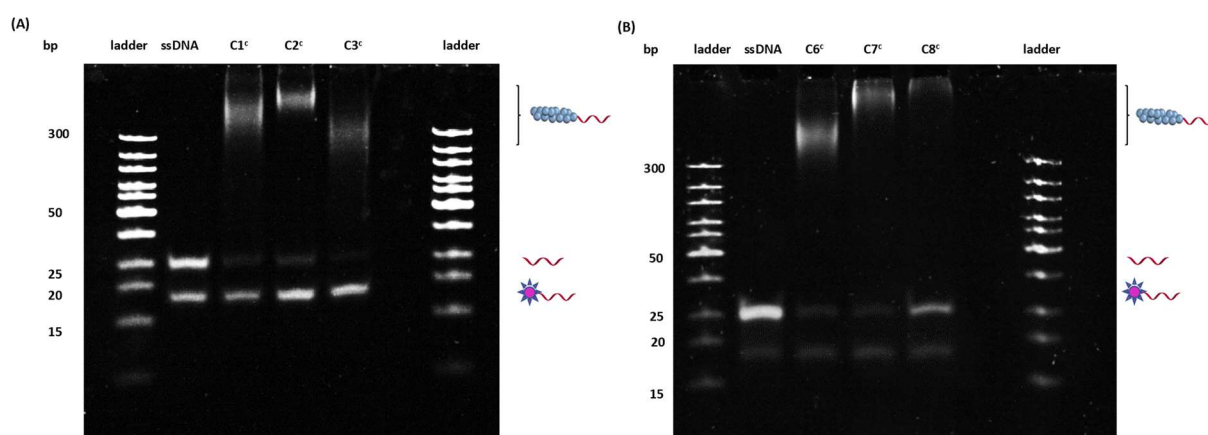
Figure 19 : Native PAGE gel (15 %) of conjugation reaction products. (A) PAGE gel of DNA-homopolymer conjugates C1^c-C3^c. (B) PAGE gel of DNA-block copolymer conjugates C6^c-C8^c. All samples were stained with SYBR gold. Lane 1 and 7 contain the ladder (GeneRuler^{TM} Ultra Low Range DNA Ladder (Thermofisher)). Lane 2 shows the 5'amino oligonucleotide^c (ssDNA) and lane 3-5 show the conjugates (C1^c-C3^c/ C4^c-C6^c) with an excess of Rh6G-DNA, respectively.

Amine-modified ssDNA was applied as a reference, which was used to calculate the yield of the coupling reaction. To ensure that the same amount of DNA was applied, an additional excess (2 eq) of complementary rhodamine DNA (Rh6G-DNA) was added to all samples. A comparison of the band intensities of ssDNA (lane 2, 300 bp) and unreacted ssDNA of the conjugation reaction (lane 3-5) allows to calculate the conversion this reaction. The software *ImageJ* was used to integrate the bands of the PAGE gel. The calculated conversions are summarized in **Table 3**.

Table 3: Calculated conversions of the conjugation reaction. Ratio of ssDNA-integrals from lane 2 to remaining ssDNA after conjugation in lane 3-5. The evaluation of PAGE gel was performed using the software *ImageJ*.

DNA-polymer conjugate	DNA-p(OEGMA)	DNA-p(DMA)	DNA-p(HEA)	DNA-p(DAAM$_{30}$-*b*-DMA$_{127}$)	DNA-p(DAAM$_{42}$-*b*-DMA$_{188}$)	DNA-p(DAAM$_{31}$-*b*-DMA$_{355}$)
Abbreviation	C1[c]	C2[c]	C3[c]	C6[c]	C7[c]	C8[c]
Conversion [%]	86	78	94	91	93	65

The DNA-polymer conjugates of homopolymers C1[c]-C3[c] show comparable yields due to similar molecular weight (18.000 -22.000 g/mol). A comparison of the conversions of DNA-p(DAAM-*b*-DMA) conjugates (C6[c]-C8[c]) show a block length dependence. Conjugate C8[c,] which possess a higher molecular weight, exhibit a much lower conversion. It can be assumed that a larger DAAM block results in lower water solubility and therefore leads to the formation of superstructures. Thus, the reaction of ssDNA is affected, which results in a higher ssDNA-band intensity in lane 5 of C8[c].

To enable a high conversion of DNA-polymer conjugate synthesis (65-95 %) in a DMF-water mixture of 3:1, a polymer excess is required, which simplifies the subsequent purification of polymer and DNA.

3.1.3 Purification of DNA-polymer conjugates

One of the main limitations of the *grafting to* approach is the subsequent purification of the DNA-polymer conjugate. To ensure higher conversion of the conjugation reaction, an excess of polymer is required, making a purification from remaining polymer and unreacted ssDNA necessary. One possibility to remove unreacted ssDNA is to spinfilter (20k MWCO spinfilter) the reaction solution with nuclease free water to a minimum of six times (1 h, 4000 rpm, 5 ml H$_2$O).

Remains of polymer can be removed via spin filtration (Amicon Ultra-0.5 mL Centrifugal Filters MWCO 100K) after the annealing of DNA-polymer conjugate to the DNA origami surface. The higher molecular weight and amphiphilic character of block copolymers, especially conjugate C8[c], leads to the formation of supramolecular structures, which prevent the complete removal of polymer via spin filtration.

To fully purify all DNA-polymer conjugates from polymer and ssDNA, *Fast Protein Liquid Chromatography* (FPLC) purification was established, which was performed with ÄKTA[pure]. Purification of conjugates is achieved by using the anion exchange column Capto™ HiRes Q 5/50, which allows the binding of the negatively charged DNA-species. Milli Q water was applied as an

eluent, which guarantees the solubility of the polymer, the conjugates and the ssDNA. The DNA species could be eluted using 2M NaCl after binding to the column and the removal of uncharged species. Both the net charge and the size or shielding effects of the charges have a significant influence on the elution volume. Since the DNA and conjugates differ primarily in their size, separation via anion exchange chromatography was enabled.

DNA-p(DMA) conjugate (C2[c]) was chosen as the model system to demonstrate purification of polymer and ssDNA. In **Figure 20** the absorption maximum of DNA at 260 nm was plotted against the elution volume in ml to compare the elution volumes of polymer, amine-modified ssDNA and conjugate.
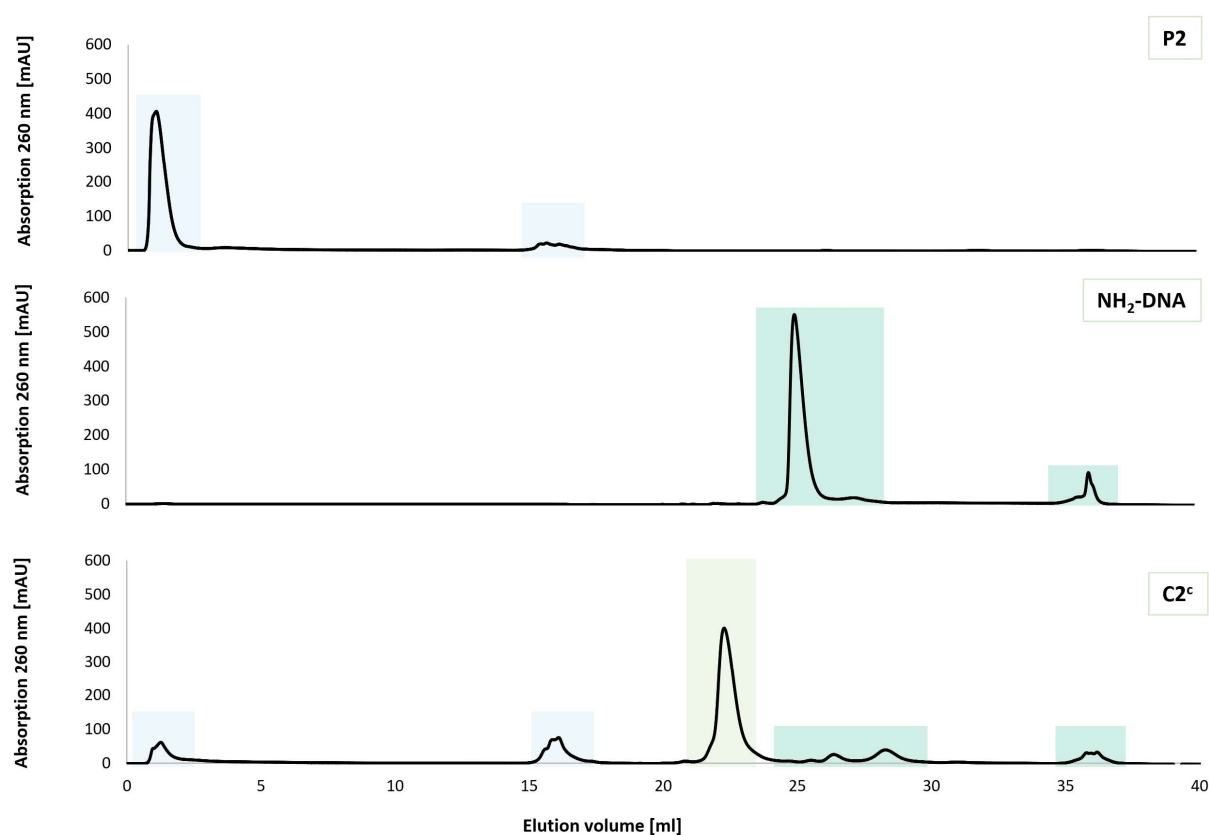
Figure 20: Elution diagrams of ÄKTA[pure] purification. Same concentrations of P2 p(DMA), amine-modified ssDNA and DNA-p(DMA)-conjugate (C2[c]) were applied on the column and eluted using the same gradient to compare the respective elution volumes.

To create a comparable result, the injection concentration of DNA and polymer correspond to the DNA-polymer conjugation approach. Due to the spin filtration of C2[c] prior to the ÄKTA purification, the ssDNA was already partly removed from the solution, which causes a lower intensity of the NH$_2$-DNA peak. The light green peak with an elution volume of 22 ml can be clearly assigned to the conjugate.

To confirm these results, a 15 % native PAGE gel (**Figure 21**) of a similar measurement as illustrated in **Figure 20** was performed.
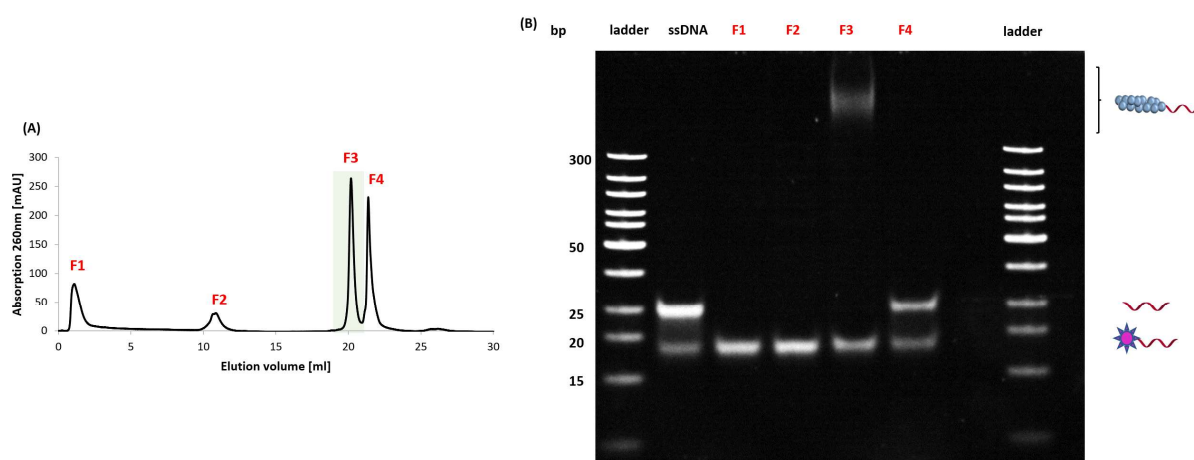
Figure 21: Analysis of ÄKTA-fractions via 15 % PAGE gel of C2^c purification. (A) ÄKTA purification of DNA-p(DMA) conjugate (C2^c). The collected fractions, indicated with F1-F4, are applied to the gel. (B) PAGE gel of collected fractions. Complementary rhodamine DNA was used for hybridization. Ladder: GeneRuler^{TM} Ultra Low Range DNA Ladder (Thermofisher). Lane 2 shows the 5'amino oligonucleotide^c (ssDNA) and lane 3-6 show the fractions (F1-F4) of ÄKTA^{pure} purification with an excess of Rh6G-DNA, respectively. The samples were stained with SYBR Gold.

The corresponding fractions (F), attributable to a signal at 260 nm, were combined and applied to the gel. A comparison of F3 (lane 5) and ssDNA (lane 2) shows a shift to a higher molecular weight, which confirms the synthesis of the DNA-p(DMA) conjugate. Since lane 5 shows no band with similar migration behaviour as the ssDNA in lane 2, a successful purification of this conjugate can be assumed. The F4 fraction show the same running behaviour as ssDNA (lane 2). Accordingly, this lane shows unreacted ssDNA from the conjugation approach. Therefore, ÄKTA purification allows a fully removal of unreacted ssDNA.

To prove the successful removal of polymer from the reaction solution, a GPC was measured. This molecular weight of this conjugate was determined to be M_w= 26378 g/mol (M_w(theor.) = 28673 g/mol), which is slightly slower than the expected molecular weight.

Furthermore, two alternative purification methods were examined. Firstly, it was investigated whether a complete removal of the polymer can be achieved with a lower NaCl elution concentration (2 % of 2M). The target of this procedure was to prevent the polymer from eluting simultaneously with the conjugate as the ion concentration increased. However, the results did not show any differences to the former approach. Secondly, it was tested whether washing the column with ethanol (10 CV) followed by putting the system back to water, can remove the polymer from the

column due to an enhanced solubility. This purification method was first established for DNA-p(DMA) (C2^c) purification, whose results are shown in **Figure 22**.
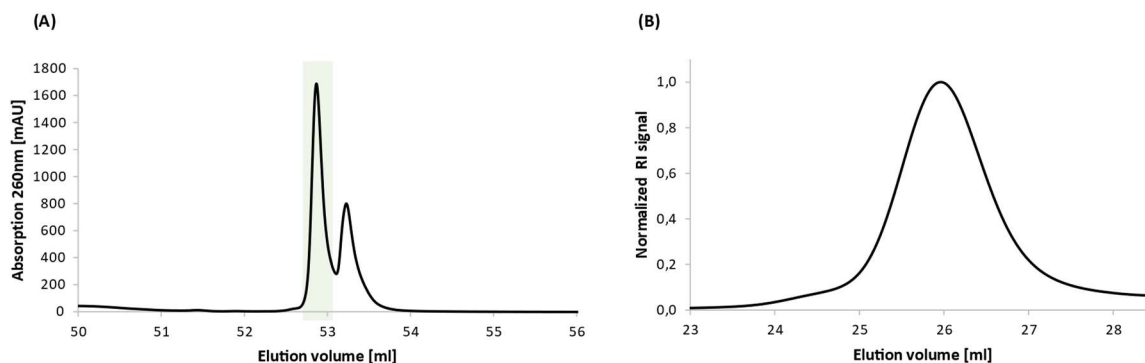
Figure 22: ÄKTA^{pure} purification of DNA-p(DMA) C2^c conjugate. (A) Elution diagram of C7^c via washing with EtOH. (B) DMF-GPC of isolated green marked C7^c.

The DMF-GPC measurement shows a monomodal distribution with a determined molecular weight of M_w= 26378 g/mol (M_w(theor.)= 28673 g/mol) for the purification of DNA-p(DMA) conjugate (C2^c).

DNA-(DAAM-*b*-DMA)-conjugate (C7^c) purification was performed under the same conditions (cf. Appendix C). GPC measurement determined a molecular weight of of M_w= 2101 g/mol, which deviates from theoretical molecular weight (M_w (theor.) = 32926 g/mol). The deviation from theoretical molecular weight can be explained with differences in diffusion behaviour of DNA because of both a deviating charge and hydrodynamic radius in comparison to the polymer.

In accordance with the different elution behaviour of polymer and conjugate, shown in **Figure 20** and the monomodal course of the curve (**Figure 22**), a complete polymer-removal can be assumed. The complete purification of ssDNA was demonstrated using page gel, which was demonstrated in **Figure 21**.

3.1.4 Synthesis of DNA multiblock copolymers

Due to the well controllable structures and tailorable chains, polymers offer adjustable properties, which are determined by the nature of monomer, the respective block lengths and ratios. These factors influence the self-assembly behaviour of amphiphilic polymers and the emergence of various shapes such as spherical, lamellar or micelle-like structures.

However, a high number of blocks in block copolymers, leads to a lack sequence selectivity, monodispersity and programmability.[76] These restrictions can be circumvented using preformed conjugates, whose final properties are only established after the sequence hybridization with the complementary DNA-polymer conjugate. Using this method, multiblock copolymers can be synthesized in a combinatorial manner, encompassing the formation of triblock-, tetrablock or pentablock copolymers. The design of more controllable and predictable multiblock copolymers facilitate the formation of ordered multidimensional arranged DNA-polymer structures.

The equimolar hybridization of DNA-polymer conjugates via a temperature program (37 °C for 1 h and cooled to 30 °C) lead to the formation of multiblock copolymers. **Figure 23** shows a schematic illustration of the synthesized polymers, which were produced via sequence hybridization. In addition, multi block copolymer synthesis was proven by PAGE gel analysis.

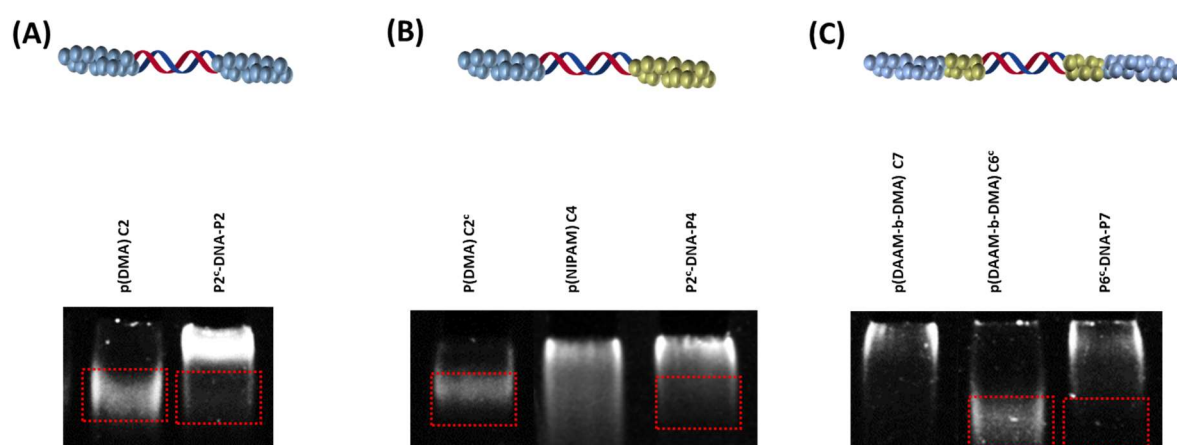**Figure 23: Cut-outs of 10 % PAGE-Gel of DNA multiblock copolymers.** (A) DNA-p(DMA) (C2) and triblock copolymer p(DMA)-DNA-p(DMA) (P2c-DNA-P2), (B) p(DMA) (C2c), DNA-p(NIPAM) (C4) and triblock copolymer p(DMA)-DNA-p(NIPAM) (P2c-DNA-P4), (C) p(DAAM-*b*-DMA) (C7), p(DAAM-*b*-DMA) (C6c) and pentablock copolymer p(DAAM-*b*-DMA)-DNA-p(DAAM-*b*-DMA) (P6c-DNA-P7). All samples were stained with SYBR gold.

Figure 23 (A) shows the formation of p(DMA)-DNA-p(DMA) triblock copolymer, which consist out of two hydrophilic polymer and one hydrophilic DNA blocks. Since no band with similar running behaviour to conjugate C2[c] can be detected in the block copolymer lane, a high hybridisation rate can be assumed. In **Figure 23 (B)** p(DMA)-DNA-p(NIPAM) the triblock copolymer formations is illustrated. A comparison of migration behaviour of p(NIPAM)-conjugate (C4) and P2[c]-DNA-P4 does not allow any statement about the product development. However, the absence of a band with the same running behaviour as p(DMA) (C2[c]) after the synthesis of P2[c]-DNA-P4, suggests the formation of the block copolymer. Due to the p(NIPAM)-block a more hydrophobic segment is introduced, creating an amphiphilic system. **Figure 23 (C)** shows the successful synthesis of a pentablock, whose synthesis is proven by the absence of a p(DAAM-*b*-DMA)-DNA (C6[c]). P6[c]-DNA-P7 does not make a significant migration shift in this page gel compared to C7 (26014 g/mol), whose polymer owns a higher molecular weight than C6[c] (17917 g/mol).

The synthesis of diverse multiblock copolymers through sequence hybridization of DNA-polymer conjugates was proven by using a PAGE gel. Apart from that, there are still several drawbacks to consider. Due to the small proportion of DNA in the total molecule, the migration behaviour differs only slightly. This hinders a band-comparison of reactant and multiblock copolymer. Furthermore, a quantitative statement about the hybridisation is challenging, as the bands are relatively broad, which makes integration for quantification difficult. In addition, it must be guaranteed that the same amount of DNA is applied to the gel.

The preparative simplicity, structural diversity and programmability of this method offers some advantages over conventional methods. Furthermore, it provides much potential for follow-up studies regarding the application for the synthesis of hydrogel structures[50],[43] or the analyse of their self-assembly behaviour.

3.2 DNA origami templated design of polymer nanostructures

The use of DNA origami templates enables the synthesis of diverse nanometre-scaled polymer structures. Therefore, in the first subsection tube and rectangular DNA origami structures are introduced, whose stability was tested under the required conditions for subsequent nanoparticle synthesis. Two different DNA origami structures were coated with purified DNA-p(DAAM-*b*-DMA) conjugates from subsection 3.1.2, whose p(DAAM)-crosslinking guarantee a rigid patterning. The following degradation of DNA-template results in the release of the nanoparticles while preserving the structure. This method was investigated by Yu *et al.*[73] for a similar system.

3.2.1 DNA origami structures

In this thesis, two different types of DNA origami structures were used for patterning with DNA-polymer conjugates: DNA origami tubes and DNA origami rectangles with two sticky triangles. DNA origami tubes can be formed via 2D-DNA tiles using a scaffold DNA (M13mp18) and 216 staple DNA strands. 86 staple DNA strands were elongated by StA sequence (NH$_2$-TTTTCTCTACCACCTACTA). Thereafter, the 2D DNA-tile is folded to the 3D DNA origami tube. This was accomplished by applying extra folding DNA strands (20 DNA sequences, 32 nucleotides), which connect the two long, complementary edges of the DNA tile by hybridization. The folding was carried out with the help of a temperature program, which starts at 70 °C and cools down to 20 °C within two hours (0.5 °C/min to 35 °C, 1 °C/min to 20 °C). To prevent misfolding, an excess of folding DNA strands was used, which were removed by precipitation in polyethylene glycol afterwards.

In previous AFM measurements, it was observed that the coating of tube structures is preferable compared to rectangular structures. The larger distance of the sticky sequences on the curved tube surface reduces the sterically hindrance of the polymer chains amongst themselves and thus increases the hybridisation rate. Apart from this, three-dimensional origami structures showed a higher stability.[61] Because of these properties, the DNA origami tube was chosen as a template for polymer patterning.

In contrast, rectangular structures exhibit a closer proximity of sticky DNA sequences. This results in a higher closeness of adjacent polymer chains, which are designated to be linked together within this project. It was postulated that this crosslinking reaction might be preferable in the rectangular structures due to the greater spatial proximity. The used DNA origami structures within this thesis and their respective AFM images are illustrated in **Figure 24 (A)** and **(B)**.
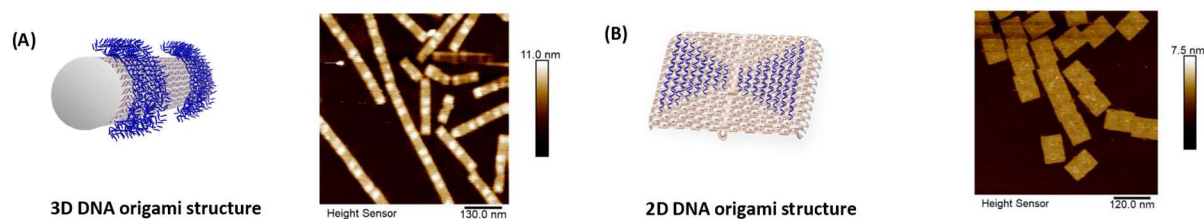
Figure 24: Schematic illustration and AFM images of used DNA origami structures. (A) 3-dimensional DNA origami tube and (B) 2-dimensional DNA origami rectangles with two StA triangles were used for nanopatterning.

3.2.2 Investigation of reaction conditions

The coating of DNA origami was performed with NHS-p(DAAM-*b*-DMA) block copolymer. P(DAAM) unit can react with the difunctional crosslinker adipic acid dihydrazide (ADH) under hydrazone formation. Acid catalysis greatly increases the crosslinking rate, which first requires the test of DNA origami stability under slightly acidic conditions.[82]

Double stranded DNA shows instability under extreme pH conditions. The hydrolysis of the phosphodiester backbone, DNA bases and glycosidic bonds leads to the degradation of DNA.[83] Thus, the DNA origami stability at pH=6, 5.5 and 5 was tested, which is required to ensure DNA origami integrity. The pH was adjusted by the addition of CH_3COOH/CH_3COONa buffer (1 M, pH= 4.7). The integrity of the origami structure was tested via atomic force microscopy (AFM) (cf. **Figure 25**).
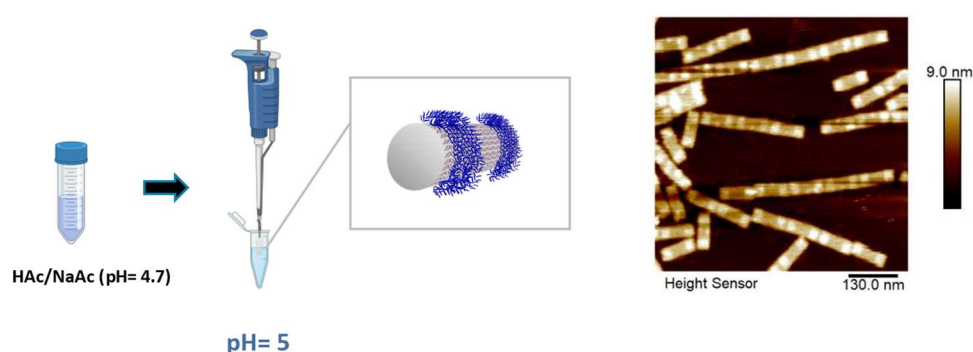

Figure 25: PH-stability test of DNA origami. AFM image of DNA origami tube at pH=5. The pH was adjusted using CH_3COOH/CH_3COONa buffer (1 M, pH= 4.7).

Since the origami structures were stable for several hours even at pH=5, the conditions for the crosslinking reaction of the coated origami were approved.

Furthermore, the crosslinking ability of the p(DAAM) unit was tested using pDAAM$_{115}$-*b*-DMA$_{50}$ (P9) block copolymer since proof on the origami level is very difficult. This polymer has a larger p(DAAM) block, which allowed to observe the disappearance of the carbonyl band via attenuated total reflectance Fourier-transform infrared spectroscopy (ATR-FTIR).

The compared IR spectra of the crosslinker ADH, the block copolymer (P9) and the crosslinked polymer are plotted in **Figure 26**. The crosslinked polymer samples were purified via spin filtration to ensure the removal of remaining of ADH.
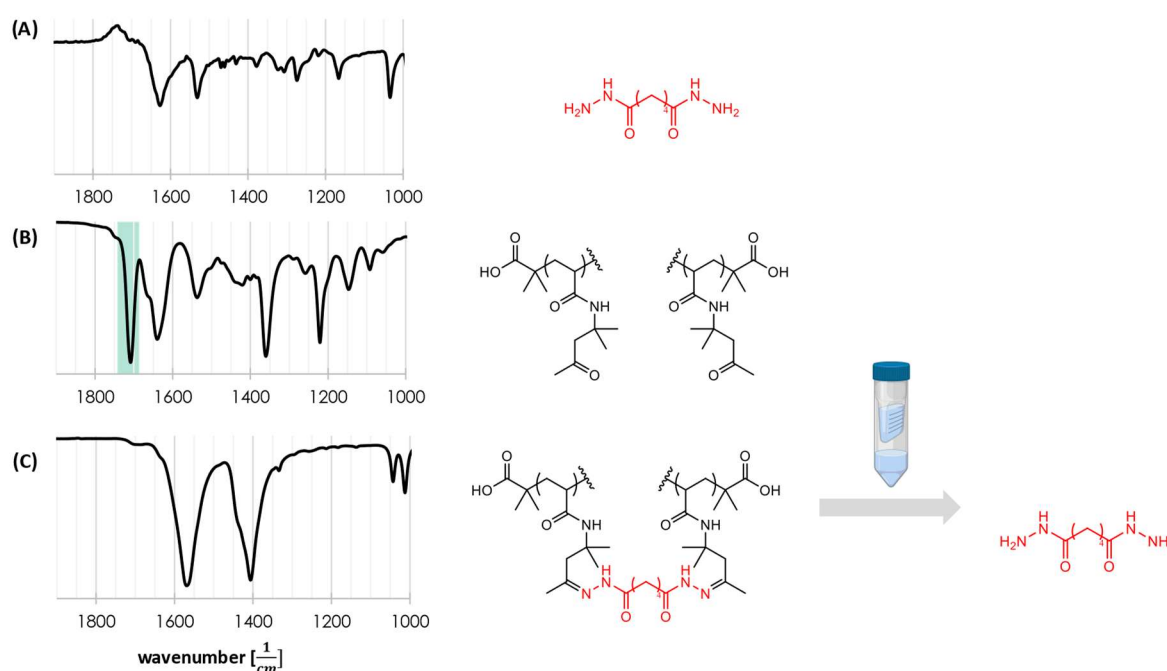
Figure 26: ATR-FTIR measurement to demonstrate the crosslinking ability of NHS-p(DAAM$_{115}$-b-DMA$_{50}$) block copolymer. (A) Spectrum of adipic acid dihydrazide (ADH), (B) NHS-p(DAAM$_{115}$-*b*-DMA$_{50}$) (P9), (C) ADH-purified crosslinked polymer.

The IR spectrum **Figure 26 (C)**, which represents the crosslinked block copolymer, shows a disappearance of the greenly marked carbonyl band of spectrum **Figure 26 (B)**. This indicates a successful hydrazone formation of carbonyl bands.

For the crosslinking reaction, the distance of adjacent polymer chains has a major impact. Therefore, it needs to be considered that the results from the FT-IR measurement can only be transferred to the actual system with a limited extent, since the distance and arrangement of the polymer chains differ in P9 and P7. The hydrophobicity and the block length influence the behaviour of both block copolymers, which effectuates the formation of different superstructures in solution. The higher hydrophobicity of NHS-p(DAAM$_{115}$-*b*-DMA$_{50}$) (P9) leads to the preferred micelles formation in

contrast to NHS-p(DAAM$_{42}$-*b*-DMA$_{188}$) (P7), which is more hydrophilicity. In micellar systems hydrophobic polymer chains show a higher proximity between themselves, favouring the crosslinking reaction.

However, the indirect ability of crosslinking for coated DNA origami was shown, which enables the template-guided synthesis of nanoparticles. Since the polymer chains on the origami surface are generally very close to each other, it was assumed that sufficient conditions for a crosslinking reaction were present.

3.2.3 DNA origami tube templated design of nanoparticles

Based on the results of the stability test (**Figure 25**) and the proof of crosslinking ability of p(DAAM-*b*-DMA) block copolymer (**Figure 26**), the coated DNA origami structures were set to be crosslinked at pH=5. Accordingly, the polymer structure forms a reinforced unit, which further increases the stability and guarantees the preservation of the nanostructure after the destruction of the template. **Figure 27** shows the individual steps of DNA origami tube templated design of polymer nanostructures.
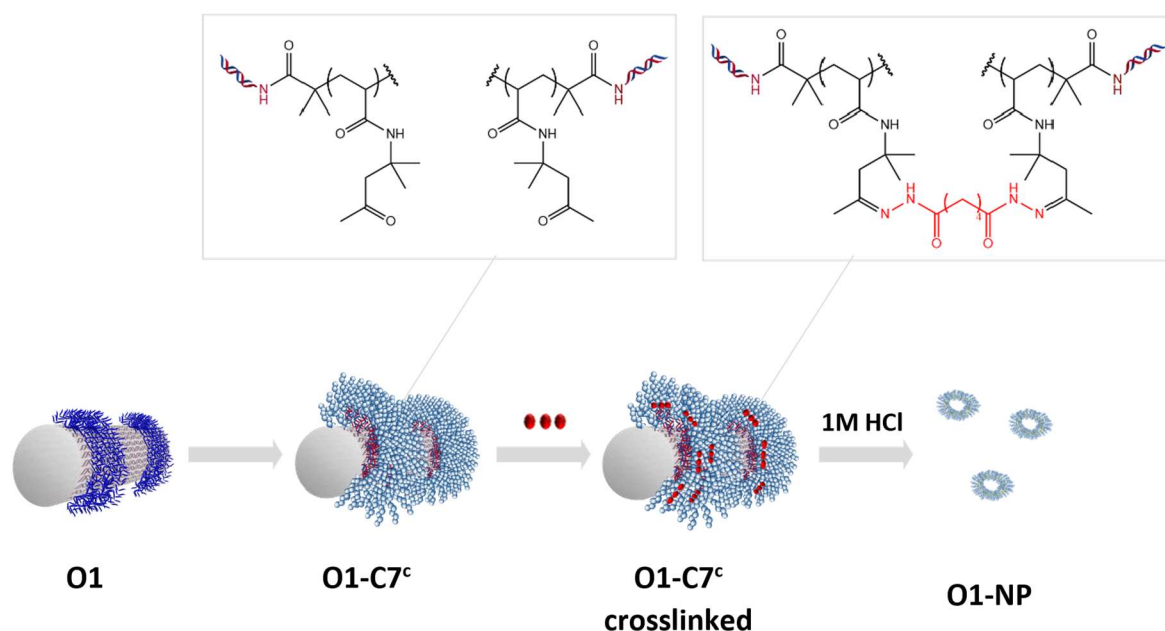
Figure 27 Schematic illustration of DNA origami tube templated design of nanostructures. O1: DNA origami tube with two StA areas, O1-C7^c: DNA origami tube coated with StA^c-p(DAAM-*b*-DMA) (C7^c), O1-C7^{c}crosslinked: at pH= 5 with ADH crosslinked coated DNA origami tube and O1-NP: generated nanoparticle after degradation of origami template via 1 M HCl.

Purified DNA polymer conjugates (C7^c) were used for patterning of the DNA origami structures. To ensure a high polymer density on the origami surface an excess of 50 eq. conjugate were used, which

were hybridized using a temperature program (37 °C/1h, cooled to 30 °C). Remaining conjugate was removed by spin filtration (MWCO 100K). Primarily, the single reaction steps were monitored via atomic force microscopy (AFM). This method enables the visualization of nanometre-scaled DNA structures through forces between the tip and the surfaces, which leads to the reflection of the cantilever. All measurements were carried out in the liquid state using PeakForce mode. The results of AFM measurement are visualized in **Figure 28**.

(A)
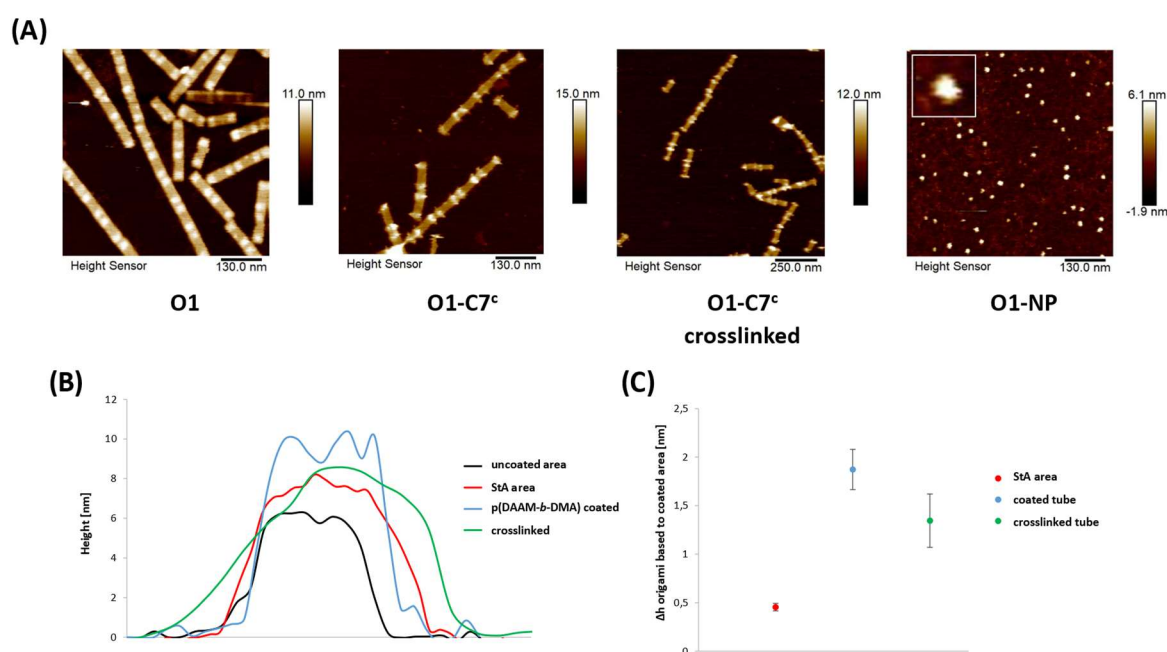

(B) **(C)**

Figure 28: DNA origami tube templated design of nanoparticles. (A) AFM images measured in 1xTAE/Mg buffer. O1: uncoated DNA origami tube, O1-C7^c: DNA-p(DAAM-b-DMA) (C7^c) coated origami, O1-C7^c crosslinked: ADH crosslinked coated origami, O1-NP: generated nanoparticles after the template degradation (B) height profiles of uncoated origami, StA-area, polymer coated, and crosslinked samples (C) averaged height difference between coated and uncoated areas on DNA origami surface. The respective standard deviations were calculated using three different origami structures.

The AFM image **Figure 28 (A)** of O1-C7^c shows light bands, whose edges are frayed in comparison to uncoated origami (O1). These light bands correspond to the StA area, whose structural change can be explained by coating with large DNA-polymer conjugates. The blue curve of the height profiles in **Figure 28 (B)** also indicates a successful coating due to an increased height, compared to the red curve of StA area. **Figure 28 (C)** confirms these results because the comparison of the averaged heights out of three different DNA origami shows an increase of height difference of 1.5 nm.

The coated DNA origami tubes were crosslinked with bifunctional adipic acid dihydrazide (ADH). The amount of crosslinker was calculated considering the number of sticky sequences on DNA origami surface and p(DAAM) repeat units. Since no prediction of hybridisation rate of conjugates and

extended sticky sequences on the origami surface is possible, a full coating was assumed for the calculation of ADH.

The AFM image of the crosslinked sample does not show an optical change of origami structure. The slight decrease in height after the crosslinking (**Figure *28* (B)**) may indicate a successful crosslinking reaction. However, the AFM does not provide a way to determine the true height of the origami structure, but rather represents the stability of the structure. It can be assumed that crosslinking of the polymer chains increases the stability of the polymer coating. Therefore, the deflection of the cantilever becomes more difficult, giving the appearance that the height of the structure decrease. To support this observation, the measurement should have been repeated. However, due to lack of time and complications with the AFM instrument, the measurement must be postponed.

After the crosslinking reaction, the DNA origami template was decomposed by the addition of 1 M HCl solution. In contrast to the expected "donut-like structures", the two-dimensional AFM image shows the homogenous formation of round, filled circles. These nanostructures show comparable height profiles, which could be a hint for the templated synthesis (cf. Appendix D). The absence of "donut-like structures" might be a result of a thermodynamically favoured collapse of the structure in solution due to the lack of inner stabilization. Because it cannot be ruled out that the DNA itself or remnants of the polymer, which may not have been completely removed, may form comparable structures, purification of conjugates were indispensable.

3.2.4 DNA origami rectangles templated design of nanoparticles

Thus, rectangular DNA origami structure with two triangles were chosen for new template-guided nanostructure formation (cf. **Figure 29**). The use of these origami for the templated design of polymer nanoparticles excludes a collapse of these structures.
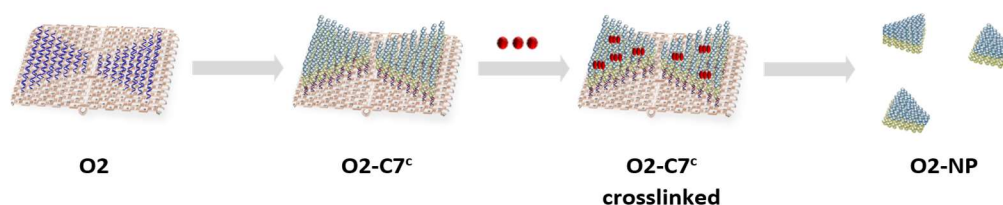

Figure 29: DNA origami templated design of rectangles. Coating of DNA origami rectangle with C7^c, crosslinking of polymer chains with ADH and degradation of DNA-template via 1 M HCl.

In an analogous way to DNA origami tube structures, coating, and crosslinking of rectangles were performed. It was assumed that the crosslinking reaction on DNA origami rectangle surface is

favoured due to the higher proximity of adjacent polymer chains of O2-C7^c. Furthermore, a structural collapse is excluded, why this system is more qualified to prove the method of templated nanostructure design. The results of AFM measurement of the respective step, as well the compared height profiles are demonstrated in **Figure 30**.
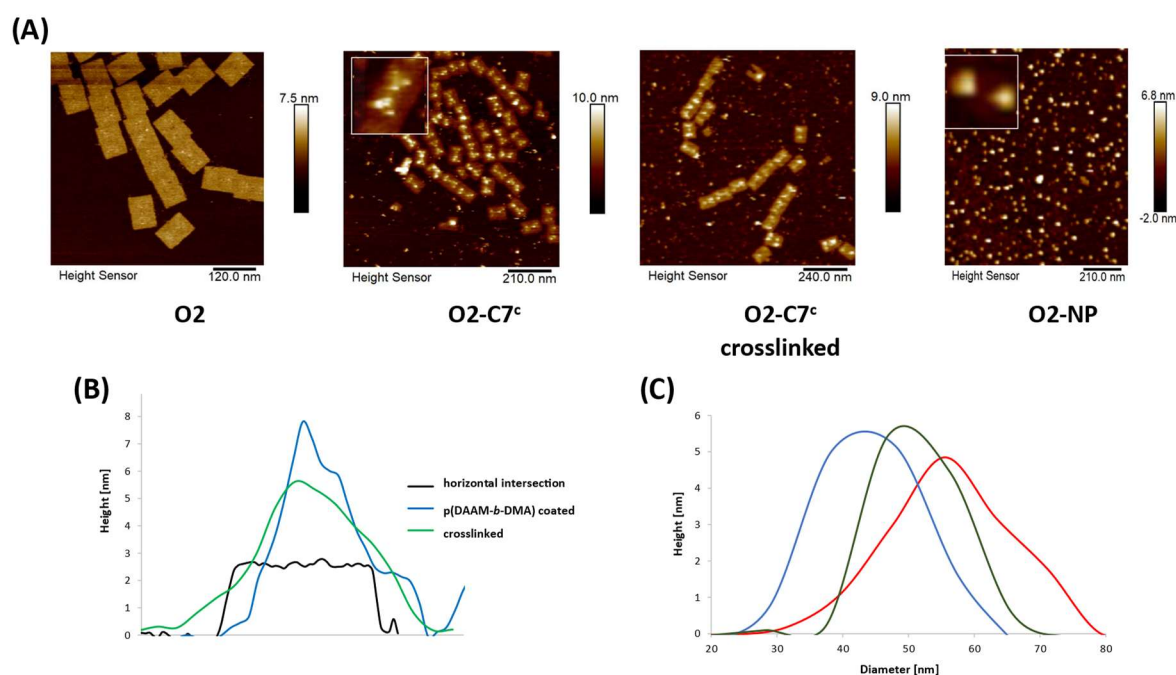

Figure 30*: DNA origami rectangle templated design of nanoparticles*. (A) AFM images measured in 1xTAE/Mg buffer. O2: uncoated DNA origami rectangle with two StA triangles, O2-C7^c: DNA-p(DAAM-*b*-DMA) (C7^c) coated origami, O2-C7^c crosslinked: ADH crosslinked coated origami, O2-NP: generated nanoparticles after the template degradation (B) height profiles of uncoated, polymer coated, and crosslinked sample (C) Comparison of height and diameter of generated triangles.

Bright triangles on the origami surface (O2-C7^c) in **Figure 30 (A)** indicates a successful coating, which can be confirmed by the height increase of 3-4 nm in **Figure 30 (B).** The black curve shows the horizontal intersection of the uncoated triangle, while the blue curve represents the patterned origami. Again, no optical structural change of the origami structures could be observed after the crosslinking of p(DAAM)-units on the surface. In addition, the height decrement after the crosslinking reaction of the origami structure in **Figure 30 (B)**, which is represented by the green curve, is ambiguous. O2-NP in **Figure 30** (**A)** show the AFM image after the addition of 1 M HCl. A closer look on the released nanostructures shows the formation of small homogenous triangles. In contrast to the tube guided template synthesis, random nanostructure formation by remains of the polymer or DNA is excluded.

3.3 Cellular uptake of coated DNA origami structures

Besides the synthesis of well-defined nanostructures, the application of stability enhanced DNA origami is of major interest. Still, biomedical applications are limited, because the presence of nucleases or the lower divalent cations concentration reduce the half-life in physiological environment.[23] Despite from stability issues, the negative charged phosphate backbone of DNA leads to electrostatic repulsion with the also negatively charged cell membrane, preventing cellular uptake.[25]

One possibility to ensure both enhanced cellular uptake and increased stability, is to shield the negative charged DNA origami by polymer coating. Winterwerber *et al.*[25] used photosensitive reaction centres to polymerize independently norepinephrine (NE) and dopamine (DA) at specific characteristic wavelengths. In subsequent cell uptake studies, pNE showed improved internalization.

In this thesis, the DNA origami tube (O3) was chosen for cell-uptake studies, due to the higher stability of 3D origami structures in comparison to tile structures.[25] The introduction of two StA areas on the origami surface allowed the precise annealing of complementary DNA-polymer conjugates. In between those two StA areas, the DNA origami tube (O3) possesses a further different single stranded DNA area (StE), which enabled the independent functionalization with the fluorescent rhodamine dye. Three DNA-homopolymer conjugates were used to compare the influence on cellular uptake: p(OEGMA) (O3-C1^c), p(DMA) (O3-C2^c) and p(HEA) (O3-C3^c), which are demonstrated in **Figure *31* (A)**.

Prior to the cell studies, TEM, AFM measurements as well as agarose gel electrophoresis were performed to test the integrity of the origami structures and the annealing of DNA-polymer conjugates to the surface (cf. **Figure 31**).
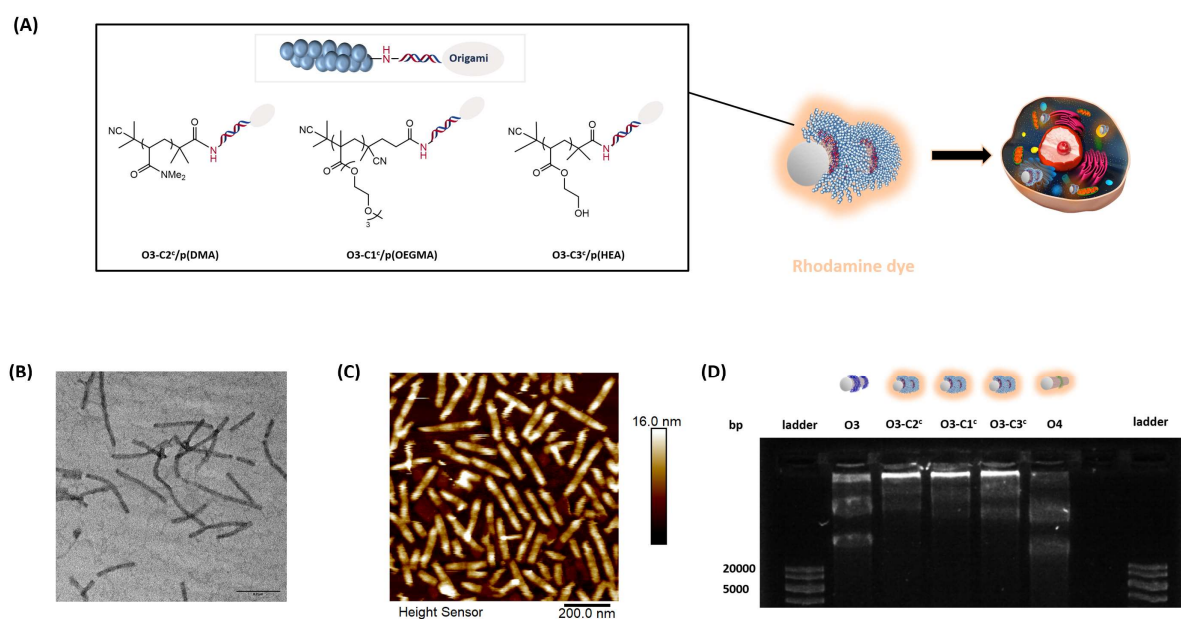
Figure 31: DNA-polymer conjugate and rhodamine dye coating of DNA origami tube (O3). (A) An overview of used DNA-polymer conjugates for the origami coating. (B) TEM image of p(DMA)/rhodamine coated tubes. Scale bar 200 nm. (C) AFM image of p(DMA) coated tubes. Scale bar 200 nm. (D) Monitoring of the uncoated, the coated DNA-origami tubes (O3-C1^c/C2^c/C3^c) and the control by 1% agarose gel, stained with SYBR Gold; Ladder: GeneRuler^{TM} 1kb DNA ladder (Thermofisher), O3: tube with two StA areas, O3-C2^c: rhodamine dye and p(DMA) coated tube, O3-C1^c: rhodamine dye and p(OEGMA) coated tube, O3-C3^c: rhodamine dye and p(HEA) coated tube, O4: tube only StE and rhodamine dye coated.

Figure 31 demonstrate the results of three different methods to test the integrity of DNA origami structures and the aspired nanopatterning. The TEM measurement (**Figure 31 (B)**) shows intact tube structures after the introduction of p(DMA) and fluorophore functionalities, yet it, does not allow a statement about successful nanopatterning. In return, a high increase, and a highlighting of StA areas in the AFM image of **Figure 31 (C)** confirm an annealing of DNA-polymer conjugates to the respective zones. The reduced migration behaviours of O3/C1^c-C3^c in comparison to O3 (uncoated origami) in **Figure 31 (D)** affirm an increased molecular weight due to the coating of the origami surface. To exclude cellular uptake of the uncoated origami, the negative control origami (O4) only exhibits a StE area for rhodamine labelling.

To verify the cellular uptake of respective coated DNA origami sample, confocal laser scanning microscopy was used. Therefore, MDA-MB-231 human breast cancer cells and origami samples were incubated together for 24 h (5000 cells/well). The rhodamine-labelled DNA origami were visualized with a white light laser at 550 nm. Using a DAPI channel (405 nm diode laser) NucleiBlue^{TM} Hoechst dye stained nuclei were visualized. The results of the cellular uptake studies are visualized in **Figure 32**.
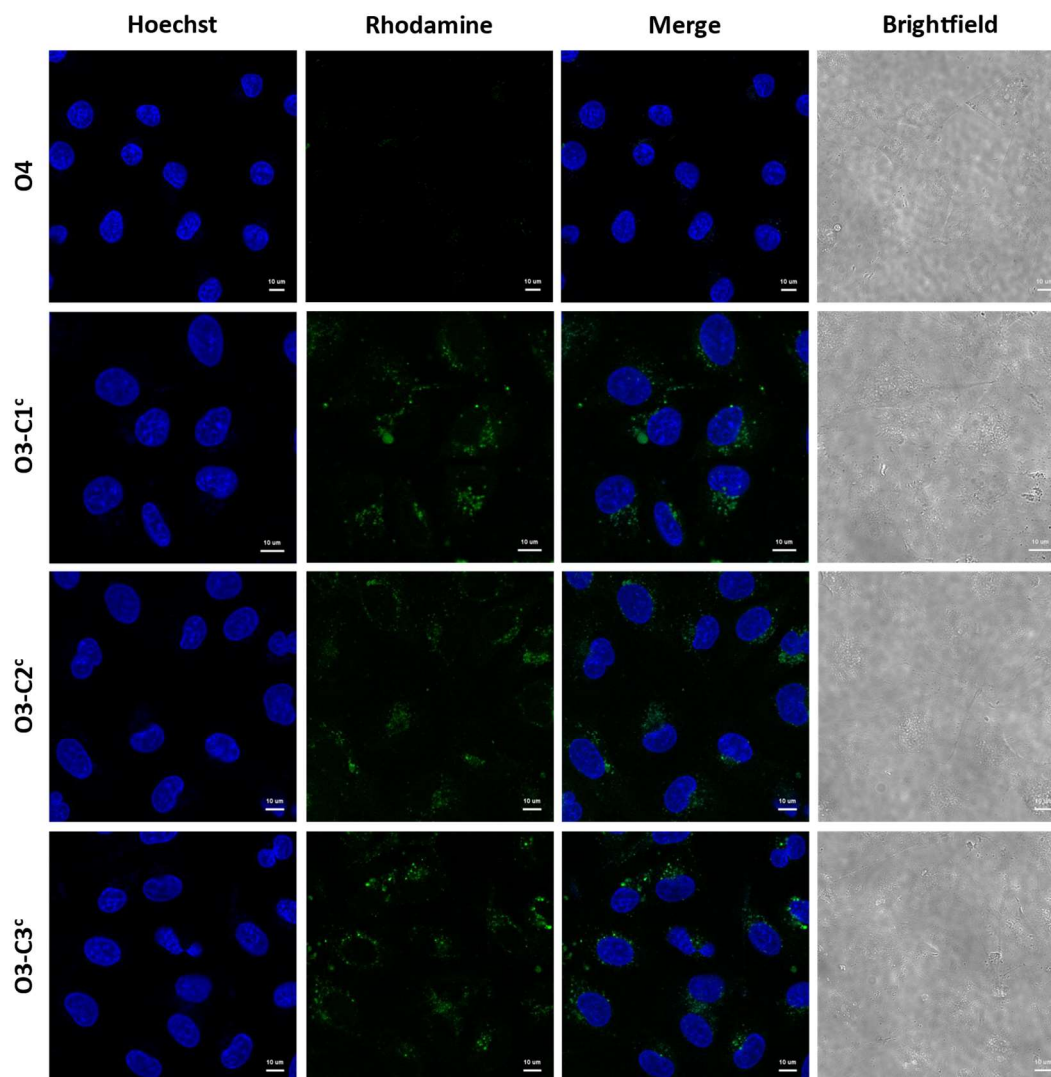
Figure 32: Internalization of polymer coated DNA origami tubes. Confocal laser scanning microscopy images of MDA-MB-231 cells treated for 24 h with rhodamine-labelled O4, O3-C1^c/C2^c/C3^c (white light, 550 nm). Nuclei were stained using NucleiBlue^{TM} Hoechst dye (DAPI channel, 405 nm). Scale bars = 10 μm. Images were processed with Icy Software.

The negative control (O4) of rhodamine-labelled samples does not show any signals of labelled DNA. This result confirms that neither uncoated DNA origami nor remaining labelled ssDNA were taken up by the cells. In contrast, the coated rhodamine-labelled DNA origami show significant higher fluorescent signals after cell internalization. The labelled materials accumulate around the NucleiBlue^{TM} stained nuclei and therefore indicate a successful uptake of coated DNA origami. In this experiment three different polymer-coated DNA origami O3-C1^c (p(OEGMA)), O3-C2^c (p(DMA)) and O3-C3^c (p(HEA)) have been tested. All three systems show comparable results in their cellular uptake, which allows the assumption that introduction of a protecting polymer shell could modulate membrane interactions that enables the cellular uptake.

4 Summary and Outlook

The present work deals with the synthesis of DNA-polymer conjugates, whose versatile applications were demonstrated in the three following projects:

1) DNA origami patterning with DNA-polymer conjugates for the template-guided design of nanometre-sized polymer particles,

2) cellular uptake experiments with homopolymer coated DNA origami tubes and,

3) the synthesis of multiblock copolymers via sequence hybridization of complementary DNA-polymer conjugates.

DNA polymer conjugates

NHS-p(HEA), NHS-p(OEGMA), NHS-p(NIPAM) and the block copolymer system NHS-p(DAAM-*b*-DMA) were synthesized successfully via RAFT polymerization. The obtained polymers were characterized by NMR and GPC-measurements, whereby synthesized polymers exhibit narrow molecular weight distributions (Đ =1.08-1.32), which indicated a controlled synthesis.

The subsequent DNA-polymer conjugate synthesis was performed via *grafting to* method using NHS-modified polymers and amine-modified ssDNA. This method gave access to a whole range of conjugates with different properties. These properties could be predefined by the choice of monomers, the polymer length, the number of blocks, and the modified DNA. It was demonstrated that an excess of polymer (50 eq) was required to achieve a high conversion (65-95 %) of DNA-polymer conjugation reaction in DMF/water mixture.

To avoid hybridization of unreacted DNA of the previous conjugation reaction and to obtain unambiguous results in the following electron microscopy measurements, the purification of remaining DNA and polymer residues was indispensable. Until recently, spin filtration was the common method to purify DNA-polymer systems. However, this method presents several disadvantages such as the clogging of filters, which results in high material costs and a reduced yield. Furthermore, spin filtration is incapable of purifying large block copolymer systems such as the p(DAAM-*b*-DMA) structures created in this project. This is due to the amphiphilic character, which

leads to superstructure formation. To still enable purification of DNA-p(DAAM-*b*-DMA) conjugates, the ÄKTA^pure purification was established. Subsequent analyse of collected fractions via PAGE-Gel and GPC measurement, indicated a successful purification.

The excess of polymer, which is necessary to enable a high conversion of ssDNA, complicates the essential purification. Thus, it would be desirable to reduce the required amount of polymer, which might be achieved by switching the system to a more effective azide-alkyne click reaction.[84] Starting from the different DNA-polymer conjugates, the special property of self-recognition of DNA was exploited to design 1D-, 2D- and 3D-structures, showing the potential of these hybrid materials.

Crosslinking of coated DNA origami

A key objective of DNA nanotechnology is the nanometre-scaled organization of functional moieties. Within this thesis, nanometre-sized polymer structures with precise shapes should be designed. Accordingly, two different DNA origami templates were nanopatterned with DNA-polymer conjugates. The use of rd staple DNA enabled the precise determination of the polymer chain positions on the origami surface. As a prove of the successful nanopatterning of origami architectures with DNA-p(DAAM-*b*-DMA) conjugates, an increased height of the origami structures was monitored via AFM measurements. To guarantee a stable scaffold of polymer around the origami, ADH was added as an external crosslinker to connect the p(DAAM)-units of adjacent polymer chains. Even though the AFM measurements gave hints for a successful crosslinking, this reaction could not be confirmed with certainty on the origami surface due to the limited significance level of AFM measurements. As a solution to fully prove the crosslinking reaction on the origami surface, a fluorescence-labelled crosslinker with the same functional groups as ADH, could be used to verify and quantify this reaction. Finally, the DNA-template was degraded to release polymeric structures into the solution.

As the first tested system, a DNA origami tube was chosen because of the lower steric hindrance of adjacent polymer chains on the origami surface. In contrast to the expected "donut-structure" formation after the template degradation, the liquid AFM measurement showed homogenous spherical structures. This led to the assumption that a structural collapse is thermodynamically preferred due to the lack of interior stabilization. To prove this hypothesis, the structure formation in less polar solvents needs to be investigated.

Apart from DNA origami tubes, 2D rectangular structures were used for nanopatterning, whose coating leads to the formation of two triangles due to the accordingly elongated staple DNA.

Crosslinking and degradation of this DNA-template showed the formation of nanometre-scaled triangles. This confirms the desired crosslinking reaction since the nanometre-scaled triangles would not persist without a successful crosslinking reaction. The thereby released nanoparticles possess predictable, well-defined structures, which are not accessible using conventional self-assembly methods of amphiphilic block copolymers.

For the nanopatterning of these two different DNA origami structures, investigated during this thesis, the medium-sized block copolymer conjugate (C7^c) has been used. To analyse the impact of the molecular weight and hydrophobicity of polymer systems on the origami patterning and the nanoparticle size, other block copolymers can be applied. Therefore, two more DNA-block copolymer conjugates (C6^c and C8^c) fulfil these demands, which have been provided during this work. Furthermore, future studies might encompass the variety of origami templates. For example, a fully coated tube structure or alternative 2D templates could be applied to generate other polymer nanostructures.

Cellular uptake of patterned DNA origami structures

The synthesis of complex DNA origami structures and their precise functionalization offer the possibility of being used as a drug carrier system.[75] This application demands the cellular uptake of the origami structures, which is reduced by the instability and negative intrinsic charge of the DNA.[23],[24] A polymer coating of the DNA origami might circumvent these limitations. Therefore, three different coated homopolymer DNA origami tubes (p(OEGMA), p(DMA), p(HEA)) have been tested in cell experiments.

Rhodamine-labelled, coated DNA origami structures were visualized via confocal laser scanning microscopy. The increased cellular internalization of all three system allows the assumption that polymer coverage of negative charged DNA enables the transport through the membrane.

To verify the cellular uptake, co-localization studies using another fluorophore attached to the origami surface can be carried out. According to cell uptake studies of Winterwerber *et al*. [78], false positive results of cell surface-bound DNA can be excluded by DNAase I-treatment of the origami incubated cells. Thereby, only internalized origami structures are detected during confocal microscopy. To further increase the cellular uptake capacity as well as the stability of the polymer shell, ADH-crosslinked p(DAAM-*b*-DMA) origami are a promising approach to study.

DNA multiblock copolymers

In this thesis, another possible application for the synthesized DNA-polymer conjugates emerged. By combining two preformed DNA-polymer conjugates via sequence hybridization, multiblock copolymer of a predetermined structure could be obtained. Since many complementary DNA-polymer conjugates are available, a huge variety of multiblock copolymers can be achieved. Via PAGE gel, the formation of two different triblock copolymers (p(DMA)-DNA-p(DMA), p(DMA)-DNA-p(NIPAM)) and one pentablock system (p(DAAM-*b*-DMA)-DNA-p(DAAM-*b*-DMA)) was achieved. In future studies, the water-soluble systems can be tested regarding their DNA-hydrogel formation. Additionally, superstructure formation of amphiphilic systems can be visualized via TEM measurement.

Overall, the potential of DNA-polymer conjugates in creating predefined DNA origami template-guided nanostructures and multiblock copolymers could be proven. On top of that, the enhanced cellular uptake of coated DNA origami tubes was verified. In conclusion, DNA origami-polymer hybrids are a promising tool to tackle future challenges in nanomedicine. Because of the highly controllable structures, the small size, and the protective coating of these origami-hybrid materials they might be applied as drug-carrier systems. Further, DNA origami templated design of unparalleled polymer nanoparticles offers the possibility for an additional application in material science.

5 Experimental Part

5.1 Analytical Instruments and Methods

Reagents and solvents were purchased from commercials sources (Fisher Scientific, Roth, Thermofisher, Sigma Aldrich), which were used, if not farther specified, without further purification.

Nuclear magnetic resonance spectroscopy (NMR-Spectroscopy)

[1]H- and two dimensional DOSY-NMR measurements were performed at AVANCE 400- and 700-Spectrometers by Bruker at 298 K in deuterated solvents. Deuterated solvents $CDCl_3$ (δ= 7.26 ppm) and D_2O (δ= 4.80 ppm) were used as calibration standard and Tetramethylsilane (TMS) was chosen as intramolecular standard. The data was evaluated with the software *MestReNova x64.*

Gel permeation chromatography (GPC)

GPC measurements were performed on a PSS SECurity instrument, which consist out of an auto sampler, a column with three GRAM columns (103 and 102 Å, 300 × 8 mm, 10 µm particle size) and two detectors (RI and UV) (Agilent Technologies 1260 Infinity). The polymer samples were filtered (0.4µm) before the injection. DMF (1 g/L lithium bromide) was used as the eluent with a flowrate of 1 mL/min. Molecular weight determination was performed with Poly(methyl methacrylate) (1600 kDa–800 Da) as the calibration standard. The data were fitted with *Excel 2016.*

Transmission electron microscopy (TEM)

TEM images of DNA origami were taken on a JEOL 1400 transmission electron microscope at a voltage of 120 kV. 5 µl of 10-30 nM solution were prepared on Formavar/carbon-film coated copper grids (300 mesh) by Plano GmbH. The samples were incubated for 5 min on the grid. Then the solution was absorbed with a filter paper, followed by 2 ½ min staining with uranyl acetate (4 %). The grid was washed three times with MilliQ water and the remaining solution was removed.

Atomic Force Microscopy (AFM)

40 µl of origami samples in origami buffer (0.5-2 nM, 1 mM Na_2EDTA, 5 mM NaCl, 5 mM TRIS, 12 mM $MgCl_2$, pH=8) were incubated for 10 min on a circular mica substrate (20 mm). The excess solution was removed with a Kimwibe® disposable paper and further 300 µl origami buffer was added on the mica.

The samples were measured in liquid state with Bruker Dimension FastScan BioTM atomic force microscope, which was operated in PeakForce mode. FastScan-D tips from Burker with a nominal spring constant of 0.25 N/m were used.

The DNA origami images were analysed with NanoScope Analysis 1.9.

Agarose Gel

DNA origami samples were analysed via 1% Agarose Gel electrophoresis. To prepare the gel, 0.5 g Agarose und 50 ml TBE buffer (10x tris/borate/EDTA) were mixed in a vile and heated to boil in a microwave until the Agarose was dissolved. After cooling down to around 40 $^\circ$C, the solution was filled in a mould of the electrophoresis unit.

To prepare the samples, 1 µl of the origami solution (10 fmol), 1 µl loading dye (6x Thermo Fisher) and 4 µl 1x origami buffer (1 mM Na_2EDTA, 5 mM NaCl, 5 mM TRIS, 12 mM $MgCl_2$, pH=8) with a total volume of 6 µL were loaded on the gel. The electrophoresis was conducted at 50 V for 4 h at 4 °C and stained with SYBR Gold for 1 h. The gel images were taken with G:BOX Chemi Gel Doc System from Syngene.

PAGE gel

15 % PAGE gel was prepared by mixing 5.63 ml TBE buffer (40 % acrylamide/bis-acrylamide solution 37.5:1, 1.5 ml 10x tris/borate/EDTA), 7.9 ml water, 7.5 µl tetramethylethylenediamine (TEMED) and 75 µL 10% ammonium persulfate (APS).

To calculate the conversion of DNA-polymer conjugate synthesis, 1 µL (10 pmol) of diluted DNA-polymer conjugate solution was hybridized with the complementary Rh6G-DNA sequence (100 µM, 20 pmol, 2 eq.) in 10x origami buffer (0.5 µl) and nuclease-free water (1.5 µl). The solution was mixed with 1.7 µl loading dye (6x Thermo Fisher) and 3.3 µl nuclease-free water to a total volume of 10 µl. To calculate the conversion, 1 µl of StA DNA (100 µM, 10 pmol) was applied as a reference.

All samples and the DNA ladder (Generuler^{TM} ultra low range DNA ladder (Thermo Fisher)) were applied on the gel. The PAGE gel was performed on a Cell SureLockTM mini-cell electrophoresis system from Thermo Fisher using 0.5 × TBE (44.5 mM Tris-Borate, 1 mM EDTA) as the running buffer.

First, the electrophoresis voltage was set to 100 V for 15 min, followed by further 50 min at 150 V. The gel was stained with 50 mL SYBR Gold (1x) for 1 h at room temperature. The images were taken with G:BOX Chemi Gel Doc System from Syngene.

Attenuated total reflection-infrared spectroscopy (ATR-IR)

IR measurement of polymers and ADH were performed on a Bruker Platinum ATR-IR using the software OPUS 7.5 .

5.2 General procedures

General principles, experimental conditions and results of the analytical measurements are listed below.

5.2.1 Polymer synthesis

To synthesize NHS-p(DAAM)-, NHS-p(NIPAM)-, NHS-p(HEA)-, NHS-p(OEGMA)-homo polymers, CTA and AIBN were dissolved in the respective solvent (**Table 4**), purged with argon for one hour and heated to the reaction temperature. The CTA 1 designated in **Table 4** is 4-Cyano-4-(phenylcarbonothioylthio)pentanoic acid N-succinimidyl ester, which was used for the polymerisation of the methacrylates. The polymerisation of the acrylamides and acrylates was carried out using 2-(Dodecylthiocarbonothioylthio)-2-methylpropionic acid N-succinimidyl este (CTA 2). CTAs were used in the ratio of CTA : AIBN was 10:1. The reaction was terminated by fast cooling in liquid nitrogen. After the solution has thawed, the polymer was purified from remains of monomer and CTA by precipitating in ether. The centrifugation (3700 rpm for 20 min) of the solution at room temperature enabled the removal of the supernatant by decanting. The polymeric residue was again dissolved in the reaction solvent. This procedure was repeated two more times. Remains of solvent were removed under vacuum.

The monomer to raft-agent concentration ratio determines the repeat unit ($\overline{X_n}$). Following equation was used to calculate the amount of monomer (M), raft-agent (CTA) and initiator (I).

$$\overline{X_n} = \frac{[M]_0}{[CTA]_0 + 2\,[I]_0} \tag{1}$$

Because the raft-agent (CTA) was used in 10 molar access ($[I]_0 = \frac{[CTA]_0}{10}$), the equation could be transformed to:

$$\overline{X_n} = \frac{[M]_0}{[CTA]_0 + \dfrac{2\,[CTA]_0}{10}} = \frac{[M]_0}{1.2\,[CTA]_0} \tag{2}$$

CTA removal

The obtained polymer was dissolved in its respective reaction solvent and an excess of AIBN (50 eq) was added. The reaction solutions were heated to 80 °C for two days.

Polymer	CTA	solvent	Precipitation solvent	Reaction temperature (T)	Reaction time (t)
NHS-p(OEGMA) (**P1**)	CTA 1	1,4-Dioxane	Diethyl ether	70 °C	16 h
NHS-p(HEA) (**P3**)	CTA 2	DMF	Diethyl ether	65 °C	14 h
NHS-p(NIPAM) (**P4, P5**)	CTA 2	1,4-Dioxane	Diethyl ether	65 °C	16 ½ h
NHS-p(DAAM-*b*-DMA) (**P6**)	CTA 2	1,4-Dioxane	1.block: Petrol ether	65 °C	16 h
			2.block: Diethyl ether	55 °C	20 h

A) N-Hydroxysuccinimide poly-Ethylene glycol methyl ether methacrylate (NHS-p(OEGMA)/ P1)

Ethylene glycol methyl ether methacrylate (OEGMA) (1.5 ml, 5.63 mmol, 0.01 eq), 4-Cyano-4-(phenylcarbonothioylthio)pentanoic acid N-succinimidyl ester (CTA 1) (20 mg, 0.05 mmol, 1 eq) and Azobisisobutyronitrile (AIBN) (0.43 mg, 0.002 mmol, 25 eq) were mixed in 5 ml 1,4-Dioxane. After this, the reaction was carried out under the reaction conditions listed in **Table 4**. The product was obtained as a colourless solid (0.80 g, 0.0428 mmol, 86 %).
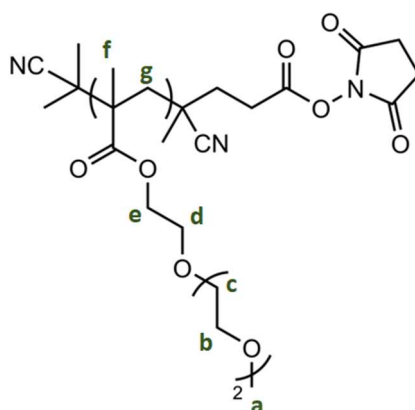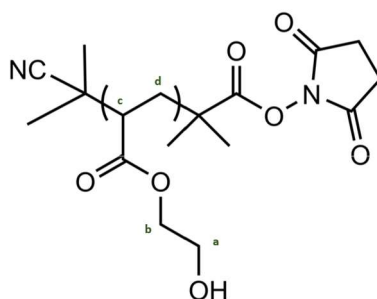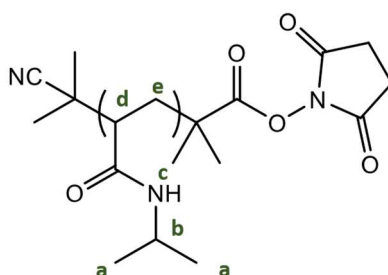

Figure 33: Numbered structural formula of p(OEGMA) (P1) for ^{1}H-NMR evaluation.

Analytic results

GPC (DMF, PMMA-standard) (**Figure 12**): M_w(theor.) = 20000 g/mol, M_w=18696 g/mol, $\overline{X_n}$= 61, Đ= 1.10

^{1}H-NMR (700 Hz, CDCl$_3$) δ [ppm] (cf. Appendix A): 4.08 (m, 2H, **e**), 3.66-3.65 (m, 13 H, **b,c**), 3.55 (s, 2H, **d**), 3.38 (s, 3H, **a**), 1.88-1.80 (m, 2H, **g**), 1.03-0.88 (m, 3H, **f**)

B) N-Hydroxysuccinimide poly-2-Hydroxy-ethylacrylat (NHS-p(HEA)/ P3)

2-Hydroxy-ethylacrylat (0.95 ml, 5.71 mmol, 95 eq), Dodecylthiocarbonothioylthio)-2-methylpropionic acid N-succinimidyl ester (CTA 2) (28.35 mg, 0.06 mmol, 1 eq) and AIBN (0.25 mg, 1.54 mmol, 26 eq) were mixed in 5 ml DMF. The reaction was carried out under the reaction conditions listed in **Table 4**. The product was obtained as a light-yellow solid (1.20 g, 0542 mmol, 90 %).

Figure 34: Numbered structural formula of NHS-p(HEA) (P3) for ^{1}H-NMR evaluation.

Analytic results

GPC (DMF, PMMA-standard) (**Figure 12**): M_w(theor.) =M_w(theor.)= 15000 g/mol, M_w=22149 g/mol, $\overline{X_n}$=130 Đ= 1.32

^{1}H-NMR (700 Hz, D$_2$O) δ [ppm] (cf. Appendix A): 4,22 (m, 2H, **b**), 3.83 (m, 2H, **a**), 2,55-2.47 (m, 1H, **c**), 2.05-1.68 (m, 2H, **d**)

C) N-Hydroxysuccinimide poly-N-Isopropylacrylamide (NHS-p(NIPAM)/ P4)

N-Isopropylacrylamide (0.5 g, 4.4185 mmol, 203 eq), Dodecylthiocarbonothioylthio)-2-methylpropionic acid N-succinimidyl ester (CTA 2) (10.1 mg, 0.0218 mmol, 1 eq) and AIBN (0.177 mg, 0.0011 mmol, 20 eq) were dissolved in 5 ml dioxane. The reaction was performed under the reaction conditions listed in **Table 4**. The product was obtained as a colourless solid (0.37 g, 0.0144 mmol, 66 %).
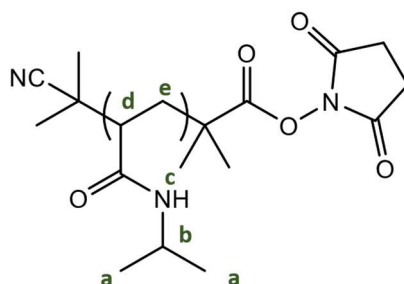

Figure 35: Numbered structural formula of NHS-p(NIPAM) (P4) for ^{1}H-NMR evaluation.

Analytic results

GPC (DMF, PMMA-standard) (**Figure 12**): M_w(theor.)= 20000 g/mol, M_w=25745 g/mol, $\overline{X_n}$=225 Đ= 1.12

^{1}**H-NMR** (700 Hz, CDCl$_3$) δ [ppm] (cf. Appendix A): 7.02-5.81 (m, 1H, **c**), 3.99 (m,1H, **b**), 2.83-1.61 (m, 3 H, **d+e**), 1.13 (s, 6H, **a**)

D) N-Hydroxysuccinimide poly-N-Isopropylacrylamide (NHS-p(NIPAM)/ P5)

N-Isopropylacrylamide (0.5 g, 4.4185 mmol, 313 eq), Dodecylthiocarbonothioylthio)-2-methylpropionic acid N-succinimidyl ester (CTA 2) (6.5 mg, 0.0141 mmol, 1 eq) and AIBN (0.114 mg, 0.0007 mmol, 20 eq) were dissolved in 5 ml dioxane. The reaction was performed under the conditions listed in **Table 4**. The product was obtained as a colourless solid (0.339 g, 0.0110 mmol, 78 %).
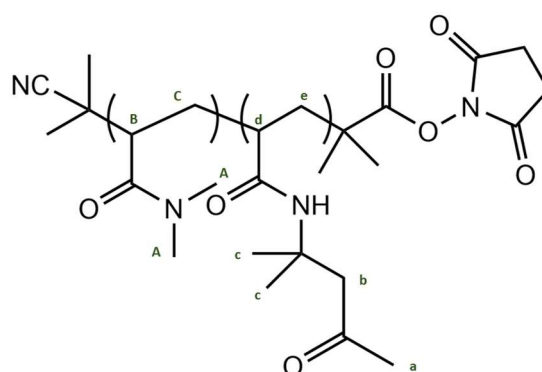
Figure 36: Numbered structural formula of NHS-p(NIPAM) (P5) for ^{1}H-NMR evaluation.

Analytic results

GPC (DMF, PMMA-standard) (**Figure 12**): M_w(theor.)= 30000 g/mol, M_w=30840 g/mol, $\overline{X_n}$=270 Đ= 1.25

^{1}H-NMR (700 Hz, CDCl$_3$) δ [ppm] (cf. Appendix A): 6.87-5.90 (m, 1H, **c**), 3.99 (m,1H, **b**), 2.66-1.61 (m, 3 H, **d+e**), 1.13 (s, 6H, **a**)

E) N-Hydroxysuccinimide poly-diacetone acrylamide (NHS-p(DAAM), 1. Block P6)

Diacetone acrylamide (0.5 g, 2.95 mmol, 32 eq), Dodecylthiocarbonothioylthio)-2-methylpropionic acid N-succinimidyl ester (CTA 2) (47.75 mg, 0.091 mmol, 1 eq) and AIBN (0.8111 mg, 0.0050 mmol, 18 eq) were dissolved in 5 ml dioxane and the reaction solution was heated to 65 °C for 16 h. The reaction was terminated by freezing in liquid nitrogen. The reaction was performed under the conditions listed in **Table 4**. 30 µl of reaction solution was precipitated in petrol ether for NMR and GPC measurement.
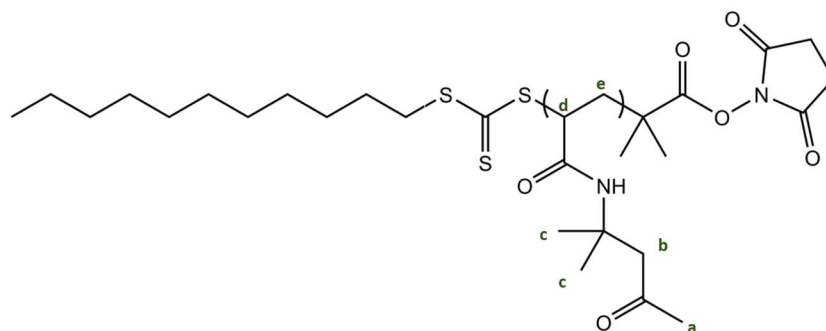
Figure 37: Numbered structural formula of NHS-p(DAAM) (1. block of P6) for ¹H-NMR evaluation.

Analytic results

GPC (DMF, PMMA-standard): M_w(theor.)= 4500 g/mol, M_w=5470 g/mol, $\overline{X_n}$=30 Đ= 1.15

¹H-NMR (700 Hz, CDCl₃) δ [ppm] (cf. Appendix A): 3.31-2.66 (m, 3H, **d+b**), 2.12 (s, 4H, **a**), 1.92-1.65 (m, 2H, **e**), 1.36 (m, 10H, **c**)

F) N-Hydroxysuccinimide poly-diacetone acrylamide-block-poly-dimethylacrylamide (NHS-p(DAAM-*b*-DMA)/ P6)

The second block of NHS-p(DAAM-b-DMA) polymer was calculated on the assumption of 90 % conversion. Dimethylacrylamide (0.894 ml, 8,45 mmol, 103 eq), AIBN (0.6651 mg, 0.0041 mmol, 20 eq) and further 2 ml dry dioxane were added to the frozen solution and purged with argon for one hour. The reaction was performed under the conditions listed in **Table 4**. After precipitation, a colourless solid was obtained (1.1436 g, 0.0634 mmol, 70 %).

Figure 38: Numbered structural formula of NHS-p(DAAM-*b*-DMA) (P6) for ¹H-NMR evaluation.

Analytic results

GPC (DMF, PMMA-standard) (Figure 16): M_w(theor.)= 1500 g/mol, M_w=17917 g/mol, $\overline{X_n}$=127 Đ= 1.13

¹H-NMR (700 Hz, CDCl₃) δ [ppm] (cf. Appendix A): 3.13 (m, **B**), 2.96-2.89 (m, **A+b**), 2.60-2.38 (m, **d**), 2.12 (s, **a**), 1.76-1.62 (m, **e+C**), 1.35 (s, **c**)

5.2.2 DNA-polymer conjugates

A) Synthesis of DNA-polymer conjugates

The synthesis of the DNA-polymer conjugates was performed using NHS-modified polymers (2.5 µmol, 50 eq), which were dissolved in 300 µl dimethylformamide (DMF). Afterwards, 5'amino-oligonucleotide (StA^c: NH$_2$-TTTTCTCTACCACCTACTA or 5'amino-oligonucleotide (StA: 5'-NH$_2$-TTTTAGTAGGTGGTAGAG-3') (50 nmol, 1 eq) was added and the reaction solution was mixed by pipetting up and down. Nuclease free water was added so that the resulting solution contains 33 % water, followed by the addition of N,N'-Diisopropylethylamine (DIPEA) (10 µmol, 50 eq). The reaction was shaken for two days in the absence of light.

Via 15 % PAGE gel the conversion of the conjugation reaction was calculated using the software *ImageJ*. Respective results are summarized in **Table 5**.

Table 5: **Calculated conversions of conjugation reaction**. Ratio of ssDNA-integrals from lane 2 to remaining ssDNA after conjugation. The evaluation of PAGE gel was performed using *ImageJ*. C1^c: DNA-p(OEGMA), C2^c: DNA-p(DMA), C3^c: DNA-p(HEA), C6^c: DNA-p(DAAM-b-DMA) (P6: 17917 g/mol), C7^c:DNA-p(DAAM-b-DMA) (P7: 26014 g/mol), (C8^c:DNA-p(DAAM-b-DMA) (P8: 40704 g/mol)

Conjugate	C1^c	C2^c	C3^c	C6^c	C7^c	C8^c
Conversion [%]	86	78	94	91	93	65

B) ÄKTA^{Pure} purification of DNA-polymer conjugates

Prior to the ÄKTA^{Pure} purification, DMF was removed by spin filtration (20k MWCO spin filter). Therefore, the reaction solution was spin filtered with nuclease free water twice (30 min, 4000 rpm, 5 ml H$_2$O).

Purification of DNA-polymer conjugates from remains of polymer and ssDNA was done via *Fast Protein Liquid Chromatography* (FPLC), which was performed with ÄKTA^{pure} using UNICORN^{TM} software with anion exchange column Capto™ HiRes Q 5/50 (column volume 1 ml). Milli Q water was applied as the mobile phase. 2 M NaCl solution with different gradients were used to elute the bound DNA from the stationary phase.

Before the sample application, the solutions were diluted to 2.4 ml. Thus, the purification program was run four times with 600 µl (500 µl loop). The respective flow rate and the individual number of column volumes (CV) of the purification phases are shown in **Table 6**. The equilibration was performed with 5 CV.
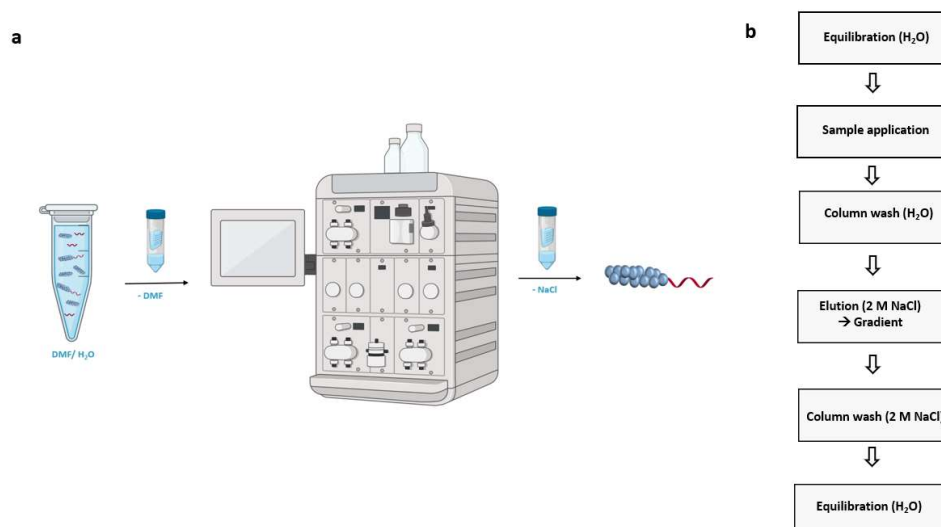
Figure 39: ÄKTA^{pure} purification. (A) Illustration of the DNA-polymer conjugate purification by spin filtration, ÄKTA^{pure} purification and renewed spin filtration. B) Established method with respective phases.

After the chromatographic purification, the combined conjugation fractions were spin filtered again (20k MWCO spin filter, 30 min, 4000 rpm, 5 ml H$_2$O, 3 x) to remove salt from the solution. If the determined concentration was low, the solution was concentrated by freeze drying before it was used for further experiments.

Table 6 summarizes the different gradients, which were used to eluate the respective conjugates.

Table 6: Summarized methods for ÄKTA^{Pure} purification of DNA-polymer conjugates.

DNA-polymer conjugates		Flow rate [ml/min]	Wash 1 [CV]	Elution/ Gradient 2M NaCl [%] : CV
P(OEGMA)^c	C1^c	1.0	10	20 :4, 20 :15, 100 :10
P(DMA)^c	C2^c	0.7	10	20 :5, 20 :15, 100 :5, 100 :5
P(HEA)^c	C3	0.7	5	20 :4, 20 :7, 100 :6
P(NIPAM)	C4	0.7	5	20 :4, 20 :7, 100 :6
P(DAAM-b-DMA)	C6	1	5	50 :2, 50 :100, 100 :8
P(DMA)^c, EtOH	C2^c	0.7	15 (EtOH) 10 (H$_2$O)	20:5, 20:20, 100:10, 100:2
P(DAAM-b-DMA)^c	C7^c	0.7	5	20:4, 20:7, 100:6
P(DAAM-b-DMA)^c, EtOH	C7^c	0.7	15 (EtOH), 10(H$_2$O)	20:5, 20:20, 100:10, 100:2
P(DMA)^c, lower elution conc.	C2^c	0.7	15	2:5, 2:20, 20:5, 100:1

To determine the effectiveness of this purification method, **Table 7** shows the calculated yields. The synthesis of conjugates labeled with a "c "was performed with the complementary StA (StA^c: NH$_2$-TTTTCTCTACCACCTACTA or 5'amino-oligonucleotide). while the unmarked conjugates were synthesized with the corresponding StA (5'-NH$_2$-TTTTAGTAGGTGGTAGAG-3'). The yields were determined considering the 50 nmol used for the conjugation reaction.

Table 7: Summarized results of ÄKTA^{Pure} purification of polymer-conjugates. DF: dilution factor, A^{260}= Absorption at 260 nm, determined yield [%] calculated in relation to the amount of used ssDNA (n= 50 nmol, n= 100 nmol (2x)). Conjugates labelled with a "c" contain complementary StA.

DNA-polymer conjugates		DF	A^{260}	C [µM]	V [µl]	n [nmol]	Yield [%]
P(OEGMA)$^{c\ (2x)}$	C1^c	10	0.3525	236.56	160	55.45	55
P(DMA)^c	C2^c	5	0.0775	41.29	520	21.47	43
P(HEA)^c	C3	-	0.4099	436.76	90	39.31	39
P(NIPAM)	C4	-	0.3580	145.08	145	20.98	42
P(DAAM-b-DMA)	C6	10	0.0603	64.25	710	45.61	91
P(DAAM-b-DMA)^c	C7^c	-	0.1556	165.90	50	8.30	16
P(DAAM-b-DMA)^c, EtOH	C7^c	10	0.0598	63.72	170	10.83	22

Collected and combined fractions of the respective conjugates, which were purified via the ethanol-washing method were analyzed via GPC.

GPC-measurement of purified conjugates

DNA-p(DMA) conjugate (C2^c), EtOH :

GPC (DMF, PMMA-standard): M_w= 26378 g/mol M_w(theor.): 28673 g/mol, Đ= 1.08

DNA-p(DAAM-b-DMA) conjugate (C7^c), EtOH :

GPC (DMF, PMMA-standard): M_w= 2101 g/mol, (M_w (theor.) = 32926 g/mol), Đ= 1.73

5.2.3 DNA multiblock copolymer synthesis
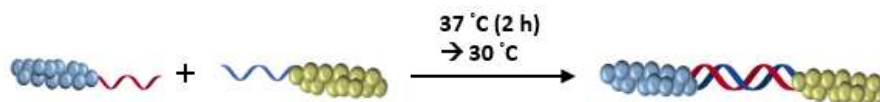
Figure 40: Synthesis of multiblock copolymers through sequence-hybridization.

StA-polymer conjugates (5'-NH_2-TTTTAGTAGGTGGTAGAG-3') and StA^c-polymer conjugates (NH_2-TTTTCTCTACCACCTACTA) were mixed in an equimolar ratio. The concentration of the conjugates should be minimal 100 µM, for which some of the conjugates listed in table **Table 7** were further concentrated. The reaction solution was then filled up to a total volume of 100 µl (or 20 µl for lower approach) with nuclease free water. To hybridize the complementary ssDNA sequences, a temperature program was used (37 °C for 2 h and cooled to 30 °C, which was hold overnight). The successful synthesis of the multiblock copolymers was verified via 10 % PAGE gel. The respective approaches are summarized in **Table 8**.

Table 8: Reaction approaches of multiblock copolymer synthesis.

Multiblock copolymers	Reagents	c [µM]	n [nmol]	V [µl]
p(DMA)^c-p(DMA)	p(DMA)^c	105.27	5	47.5
	p(DMA)	107.03	5	46.7
	Nuclease free water			5.8
p(DMA)^c-p(NIPAM)	p(DMA)^c	105.27	5	47.5
	p(NIPAM)	154.08	5	32.5
	Nuclease free water			20.0
p(DAAM-*b*-DMA)^c-p(DAAM-*b*-DMA)	p(DAAM-*b*-DMA)^c	165.90	1	6.0
	p(NIPAM)	194.99	1	5.1
	Nuclease free water			8.9

5.2.4 DNA origami synthesis

The preparation of the DNA origami nanostructures was carried out by mixing the respective staple strands (8 eq), folding stands (16 eq) and scaffold DNA (M13mp18) in origami buffer (1 mM Na_2EDTA, 5 mM NaCl, 5 mM TRIS, 12 mM $MgCl_2$, pH=8). The use of a temperature program, which starts at 70°C and cools down to 20°C within two hours (0.5 °C/min to 35 °C, 1 °C/min to 20 °C) enables the correct folding of DNA origami.

The purification of generated nanostructure was enabled by precipitation in the same volume of PEG solution (15% PEG8000, 5 mM TRIS buffer, 1 mM Na_2EDTA buffer, 0.505 M NaCl) as the used DNA origami solution. The solution was centrifuged at 12000 x g for 25 min. After this, the supernatant was removed, and the remaining pellet was dissolved in 1x origami buffer. Therefore, the solution was shaked over a period of one hour. Meanwhile the solution was mixed every 10 min with a pipette. This procedure of precipitation and dissolving was repeated two more times. In this work different origami (O1-O4) were synthesized. The deviating sequences from staple strands are summarized in **Table 9**.

Table 9: Overview of deviating sequences from staple stands. StA: extended staple strands with respective StA sequence. StE: extended staple strands with respective StE sequence. Folding strands: replace staple strands and enable folding of DNA origami tube.

Origami	Deviating sequences from staple strands
O$_1$ (tube)	**StA:** 53-60; 63-74; 77-98; 158-179; 182-203 **Folding strand (for tube):** 1, 25, 27, 28, 51, 52, 75, 76, 99, 100, 111, 132, 133, 156, 157, 180, 181, 204, 205, 216
O$_2$ (two triangles on a rectangle)	**StA**: 13-15, 17, 19, 37-44, 46, 59-70, 72, 81, 83, 85, 87, 89, 91, 93, 95, 119-122, 124, 140-147, 148, 162-173, 175, 184, 186-188, 190, 192, 194, 196, 198
O$_3$ (cell uptake tube)	**StA:** 2-24, 26, 29-50, 75, 76, 99, 100, 112-131, 134-155, 158-179, 191-203 **StE:** 56, 58, 60, 72, 74, 77, 79, 81-98 **Folding strand (for tube):** 1, 25, 27, 28, 51, 52, 75, 76, 99, 100, 111, 132, 133, 156, 157, 180, 181, 204, 205, 216
O$_4$ (cell uptake tube, control)	**StE:** 56, 58, 60, 72, 74, 77, 79, 81-98 **Folding strand (for tube):** 1, 25, 27, 28, 51, 52, 75, 76, 99, 100, 111, 132, 133, 156, 157, 180, 181, 204, 205, 216

TECAN DNA Quantification

The quantification of ssDNA and dsDNA (DNA origami) was carried out by absorption measurement at 260 nm. The measurement was performed with Spark® 20M with Nanoquant plate™. To calculate the baselines and measure the samples, 2 µl of the solution were placed on the Nanoquant plate. The Baseline-measurement of DNA-polymer conjugates was done using nuclease free water. To calculate the concentration of origami samples, the baseline was calibrated with 1X OB. The Lambert-Beer law was used to calculate the concentration auf the DNA solutions.

$$c = \frac{A^{260}}{\varepsilon \cdot d}$$

$$\varepsilon(\text{ssDNA}) = 187700 \ \frac{1}{M \cdot cm}$$

$$\varepsilon(\text{dsDNA}) = 119119009 \ \frac{1}{M \cdot cm}$$

With the absorption of DNA at 260 nm (A^{260}), the molar extinction coefficient ε, d= 0.05 cm and the concentration of the solution (c) was determined.

5.2.5 Annealing of DNA-polymer conjugates to DNA origami
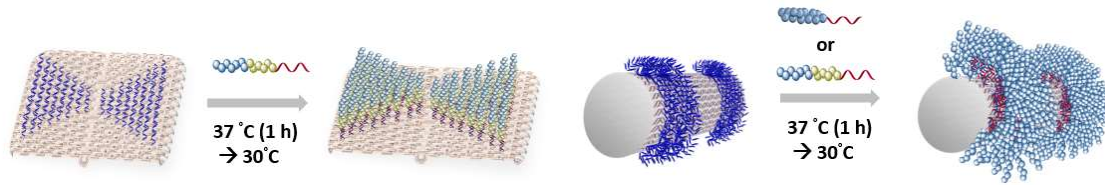
Figure 41: Schematic illustration of homopolymer-or block copolymer-DNA conjugate annealing to DNA origami surface.

To anneal the DNA-polymer conjugates to the DNA origami, the DNA origami (n= 0.4 pmol, c(final)= 8 nM, 1 eq) and purified DNA polymer conjugates (50 eq) were mixed. Additionally, origami buffer (1 mM Na_2EDTA, 5 mM NaCl, 5 mM TRIS, 12 mM $MgCl_2$, pH=8) was added to a total volume of 50 µl. To calculate the necessary amount of DNA-polymer conjugates, the number of sticky sequences on used DNA origami was considered:

DNA origami tubes (O1): 86 StA, 4300 eq, n=1.72 nmol, c(final)=34.4 µM

DNA origami rectangles (O2): 70 StA, n=1.4 nmol, c(final)=28.0 µM, 3500 eq

cell-uptake origami (O3): 123 StA, n=2.46 nmol, c(final)=49.2 µM, 6150 eq

The samples were heated to 37 °C for 1 h and cooled to 30 °C after this, which was held overnight. Via spin filtration (Amicon Ultra-0.5 mL Centrifugal Filters MWCO 100K), remains of DNA-polymer conjugates were removed. Therefore, the samples were centrifugated (5000 x g, 5 min) three times with 300 µL origami buffer (1 mM Na_2EDTA, 5 mM NaCl, 5 mM TRIS, 12 mM $MgCl_2$, pH=8). The inverted column was placed in a new vessel and was centrifugated for further 2 min at 2 g. The concentration was determined at Spark® 20M with Nanoquant plate^TM.

5.2.6 Crosslinking of p(DAAM-*b*-DMA) coated DNA origami
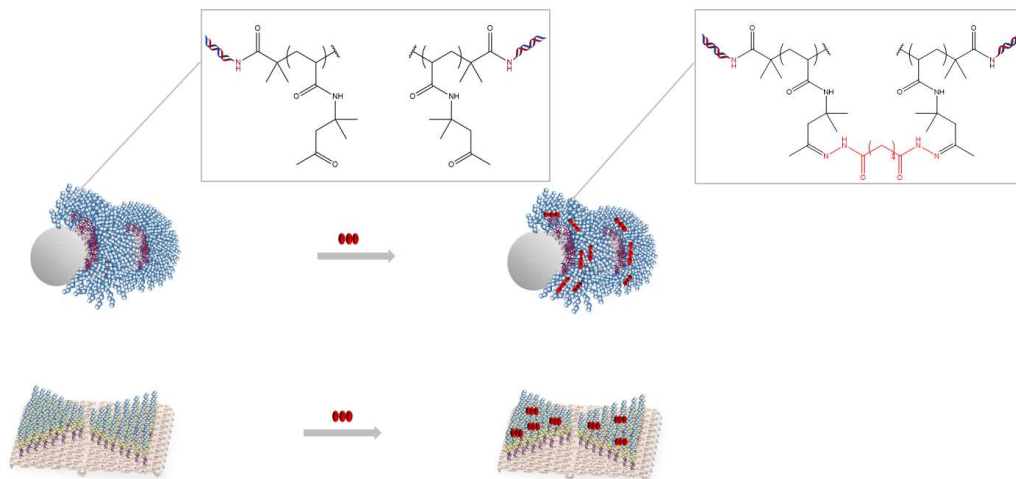
Figure 42*: Crosslinking of p(DAAM-*b*-DMA) coated DNA origami tube and DNA origami rectangles.

In consideration of the number of repeat units of the p(DAAM) block and the number of StA on the DNA origami surface, the amount of crosslinker Adipic acid dihydrazide (ADH) was calculated. To 50-70 µl of coated DNA origami (5- 10 nM), the respective amount from a serial dilution of ADH in origami buffer was added. The pH was adjusted to pH=5 through the addition of CH_3COOH/CH_3COONa- buffer (1M, pH=4.7). The reaction was carried out at room temperature overnight.

The purification was performed analogously to the annealing of the DNA-polymer conjugates to the origami surface via spin filtration (Amicon Ultra-0.5 mL Centrifugal Filters MWCO 100K). The structures were monitored by AFM measurement using the liquid modus.

5.2.7 Template-guided synthesis of polymer nanoparticles
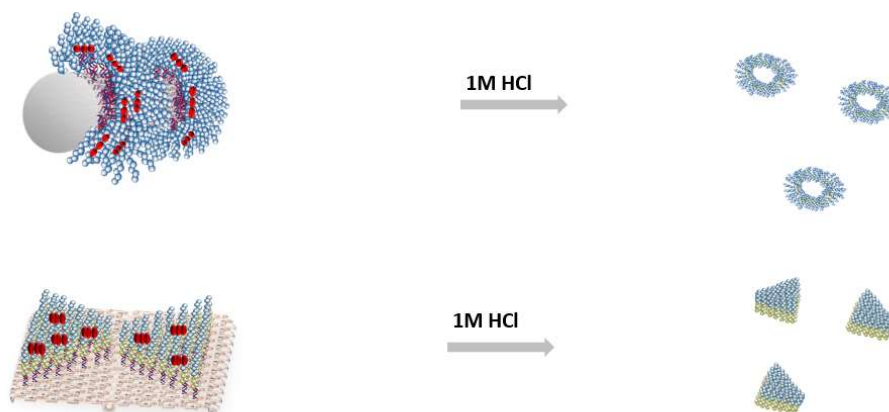
Figure 43: Degradation of ADH-crosslinked p(DAAM-*b*-DMA) coated DNA origami structures.

To degrade the DNA origami template, 30 µl of 1 M HCl was incubated with crosslinked p(DAAM-*b*-DMA)-origami sample on the mica surface for 5 min. The measurement was performed in liquid state on FastScan BioTM atomic force microscope.

5.2.8 Cell uptake experiments of homopolymer coated DNA origami structures
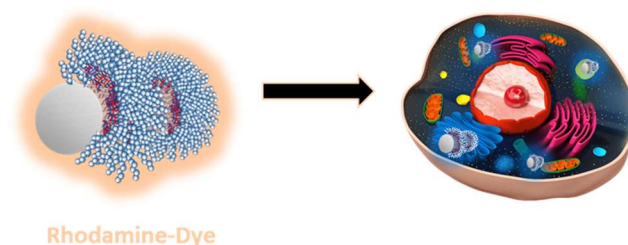
Figure 44: Cellular internalization of three different homopolymer (p(OEGMA), p(DMA), p(HEA)) coated DNA origami tubes. All samples were labelled with a rhodamine dye.

The used cell uptake origami (O3, cf. **Table 9**) contained two StA areas to anneal different DNA-polymer conjugates and one StE area to attach a fluorescent dye labelled DNA. The coating of the DNA origami tube (O3) was carried out using three different homopolymer conjugates (DNA-p(OEGMA), -p(DMA), -p(HEA). To calculate the required amount of conjugates (50 eq) and dyes, the respective sticky sequences on the origami surface were considered In addition, all samples were labelled with rhodamine-DNA. To the negative control origami (O4, cf. **Table 9**) only complementary Rhodamine-DNA was annealed.

MDA-MB-231 cells were precultured in DMEM-Dulbecco's Modified Eagle Medium, which was supplemented with 10% FBS and 1% penicillin/streptomycin. The cells were seeded in a 10-well confocal plate with a respective density of 5.000 cells/well and adhered there overnight.

The origami samples were dissolved in 1x OB-buffer (35 nM) before being diluted with DMEM to 7 nM. After that, the cells were treated with the three different homopolymer-coated origami and then incubated for 24 h at 37 °C (5% CO_2). The cells were washed with DMEM and stained with NucBlue™ for 10 mins, followed by further washing. Cellular uptake was conducted live by confocal laser scanning microscopy (Leica Stellaris 8). To visualize NucBlue™ stained nuclei, a 405 nm diode laser was used (DAPI channel). The rhodamine labelled origami samples were visualized using a white light laser at 550 nm.

6 Bibliography

[1]   V. Kumar, *Theranostics* **2016**, *6*, 710–725.

[2]   N. C. Seeman, *Theor. Biol* **1982**, *99*, 237–247.

[3]   R. A. Hughes, A. D. Ellington, *Cold Spring Harb. Perspect. Biol.* **2017**, *9*, 1–17.

[4]   Y. Li, Y. D. Tseng, S. Y. Kwon, L. D'Espaux, J. S. Bunch, P. L. McEuen, D. Luo, *Nat. Mater.* **2004**, *3*, 38–42.

[5]   D. R. Duckett, A. I. H. Murchie, S. Diekmann, E. von Kitzing, B. Kemper, D. M. J. Lilley, *Cell* **1988**, *55*, 79–89.

[6]   J. D. Tanima Bhattacharyya, Deepanjan Panda, *Org. Lett.* **2021**, *23*, 3004–3009.

[7]   P. W. K. Rothemund, *Nature* **2006**, *440*, 297–302.

[8]   F. A. Hays, J. Watson, P. S. Ho, *J. Biol. Chem.* **2003**, *278*, 49663–49666.

[9]   S. M. Douglas, H. Dietz, T. Liedl, B. Högberg, F. Graf, W. M. Shih, *Nature* **2009**, *459*, 414–418.

[10]   N. C. Seeman, *Mol. Biotechnol* **2007**, *37*.

[11]   H. Yan, T. H. LaBean, L. Feng, J. H. Reif, *Proc. Natl. Acad. Sci. USA* **2003**, *100*, 8103–8109.

[12]   F. Schneider, N. Möritz, H. Dietz, *Seq. events Dur. Fold. a DNA origami* **2019**, *5*, 1–10.

[13]   P. W. K. Rothemund, *Nature* **2006**, *440*, 297–302.

[14]   F. Benn, N. E. C. Haley, A. E. Lucas, E. Silvester, S. Helmi, R. Schreiber, J. Bath, A. J. Turberfield, *Angew. Chem. Int.* **2018**, *57*, 7687–7690.

[15]   K. Tapio, I. Bald, *Multifunct. Mater.* **2020**, *3*.

[16]   M. Langecker, V. Arnaut, T. G. Martin, J. List, S. Renner, M. Mayer, H. Dietz, F. . Simmel, *Science.* **2012**, *338*, 932–936.

[17]   C. Zhou, X. Duan, N. Liu, *Nat. Commun.* **2015**, *6*, 1–6.

[18]   H. Gu, J. Chao, S. J. Xiao, N. C. Seeman, *Nature* **2010**, *465*, 181–202.

[19]   Y. N. Zhang, et al. Int., *Angew. Chem.* **2016**, *55*, 8036–8040.

[20]   S.-T. Wang, M. A. Gray, S. Xuan, M. M. Stevens, C. R. Bertozzi, O. Gang, *PNAS* **2020**, *117*, 6339–6348.

[21]   S. D. Perrault, W. M. Shih, *ACS Nano* **2014**, *8*, 5132–5140.

[22]   A. L. Roodhuizen, P. J. T. M. Hendrikx, P. A. J. Hilbers, T. F. A. de Greef, A. J. Markvoort, *ACS Nano* **2019**, *13*, 10898–10809.

[23]   J. Hahn, S. F. J. Wickham, W. M. Shih, S. D. Perrault, *ACS Nano* **2014**, *8*, 8765–75.

[24]   M. Guéroult, D. Picot, J. Abi-Ghanem, B. Hartmann, M. Baaden, *PLoS Comput. Biol.* **2010**, *6*.

[25]   P. Winterwerber, C. J. Whitfield, D. Y. W. Ng, T. Weil, *Angew. Chemie - Int. Ed.* **2022**, *61*, 1–9.

[26] Q. Shen, M. W. Grome, Y. Yang, C. Lin, *Adv Biosyst.* **2020**, *4*.

[27] N. Stephanopoulos, *Chem-Cell Press* **2020**, *6*, 364–405.

[28] Y. Tokura, Y. Y. Jiang, A. . Welle, M. H. Stenzel, K. M. Krzemien, J. Michaelis, R. . Berger, C. Barner-Kowollik, Y. Z. Wu, T. Weil, *Angew. Chem., Int. Ed.* **2016**, *55*, 5692–5697.

[29] D. Colombani, **1997**, *22*, 1649–1720.

[30] N. Hadjichristidis, H. Iatrou, S. Pispas, M. Pitsikalis, *J. Polym. Sci. Pol. Chem* **2000**, *38*, 3211–3234.

[31] C. L. Moad, G. Moad, *Chem. Teach. Int.* **2021**, *3*, 3–17.

[32] S. Perrier, *Macromolecules* **2017**, *50*, 7433–7447.

[33] E. R. Graeme Moad, *RAFT Polymerization: Methods, Synthesis and Applications*, WILEY-VCH GmbH, Weinheim, **2022**.

[34] D. G. Moad, D. E. Rizzardo, D. S. H. Thang, *Chem. – An Asian J.* **2013**, *8*, 1634–1644.

[35] G. Gody, T. Maschmeyer, P. B. Zetterlund, S. Perrier, *Macromolecules* **2014**, *47*, 3451–3460.

[36] H. Willcock, R. K. O'Reilly, *Polym. Chem.* **2010**, *1*, 149–157.

[37] H. Sun, L. Yang, M. P. Thompson, S. Schara, W. Cao, W. Choi, Z. Hu, N. Zang, W. Tan, N. C. Gianneschi, *Bioconjug. Chem.* **2019**, *30*, 1889–1904.

[38] N. Stephanopoulos, *Bioconjugate Chem.* **2019**, *30*, 1915–1922.

[39] S.-I. Nakano, N. Sugimoto, *Biophys. Rev.* **2016**, *8*, 11–23.

[40] N. C. Seeman, H. F. Sleiman, *Nat. Rev. Mater.* **2017**, *3*.

[41] W. Shao, S. Khin, W. C. Kopp, *Biopreserv. Biobank.* **2012**, *10*, 4–11.

[42] Y. Tokura, Y. Jiang, A. Welle, M. H. Stenzel, K. M. Krzemien, J. Michaelis, R. Berger, C. Barner-Kowollik, Y. Wu, T. Weil, *Angew. Chem* **2016**, *55*, 5692–5697.

[43] L. Peng, C. S. Wu, M. You, D. Han, Y. Chen, T. Fu, M. Ye, W. Tan, *Chem. Sci.* **2013**, *4*, 1928–1938.

[44] C. J. Whitfield, M. Zhang, P. Winterwerber, Y. Wu, D. Y. W. Ng, T. Weil, *Chem. Rev.* **2021**, *121*, 11030–11084.

[45] M. Kwaka, A. Herrmann, *Chem. Soc. Rev.* **2011**, *40*, 5745–5755.

[46] J. Jeong, H. Park, *Bioconjugate Chem* **2001**, *12*, 917–923.

[47] R. B. Fong, Z. L. Ding, C. J. Long, A. S. Hoffman, P. Stayton, *Bioconjugate Chem.* **1999**, *10*, 720–725.

[48] Kwak M and Herrmann A, *Angew. Chem* **2010**, *49*, 8574–8587.

[49] P. Datta, J. Genzer, *J. Polym. Sci. Part A Polym. Chem.* **2016**, *54*, 263–274.

[50] J. Gačanin, C. V. Synatschke, T. Weil, *Adv. Funct. Mater* **2020**, *30*.

[51] A. D. Keefe, S. Pai, A. Ellington, *Nat. Rev. Drug Discov.* **2010**, *9*, 537–550.

[52] T. R. Wilks, R. K. O'Reilly, *Sci. Rep.* **2016**, *6*, 1–11.

[53] J. Zimmermann, M. Kwak, A. J. Musser, A. Herrmann, in *Bioconjugation Protoc. Methods Mol. Biol.* (Ed.: S. Mark), Humana Press, Totowa, USA, **2011**, 239–266.

[54] T. Lückerath, K. Koynov, S. Loescher, C. J. Whitfield, L. Nuhn, A. Walther, C. Barner-Kowollik, D. Y. W. Ng, T. Weil, *Angew. Chem.* **2020**, *59*, 15474–15479.

[55] C. Zhang, L. Hao, C. M. Calabrese, Y. Zhou, C. H. Choi, H. Xing, C. Mirkin, *Small* **2015**, *11*, 5360–5368.

[56] F. Ding, Q. Mou, Y. Ma, G. Pan, Y. Guo, G. Tong, C. H. J. Choi, X. Zhu, C. Zhang, *Angew. Chem* **2018**, *57*, 3064–3068.

[57] W. P. Klein, R. P. Thomsen, K. B. Turner, S. A. Walper, J. Vranish, J. Kjems, M. G. Ancona, I. L. Medintz*, *ACS Nano* **2019**, *13*, 13677–13689.

[58] K. Bartnik, A. Barth, M. Pilo-Pais, A. H. Crevenna, T. Liedl, D. C. Lamb*, *J. Am. Chem. Soc* **2020**, *142*, 815–825.

[59] N. Alleva, P. Winterwerber, C. J. Whitfield, D. Y. W. Ng, T. Weil, *ChemRxiv* **2022**.

[60] P. Winterwerber, S. Harvey, D. Y. W. Ng, T. Weil, *Angew Chem Int Ed Engl.* **2020**, *59*, 6144–6149.

[61] Y. Tokura, S. Harvey, X. Xu, C. Chen, S. Morsbach, K. Wunderlich, G. Fytas, Y. Wu, D. Y. W. Ng, T. Weil, *Chem. Commun.* **2018**, *54*, 2808–2811.

[62] C. E. Castro, F. Kilchherr, D.-N. Kim, E. L. Shiao, T. Wauer, P. Wortmann, M. Bathe, H. Dietz, *Nat. Methods* **2011**, *8*, 221–229.

[63] L. C. Bock, L. C. Griffin, J. A. Latham, E. H. Vermaas, J. J. Toole, *Nature* **1992**, *355*, 564–566.

[64] D. Sen, W. Gilbert, *Nature* **1998**, *334*, 364–366.

[65] O. Mendoza, A. Bourdoncle, J.-B. Boulé, R. . Brosh, J.-L. Mergny, *Nucleic Acids Res.* **2016**, *44*, 1989–2006.

[66] Y. Tokura, Design of Polymer Nanoarchitectures by DNA Origami Technology, Ulm univeristy, **2018**.

[67] N. Hannewald, P. Winterwerber, S. Zechel, D. Y. W. Ng, M. D. Hager, T. Weil, U. S. Schubert, *Angew. Chemie - Int. Ed.* **2021**, *60*, 6218–6229.

[68] S. Hansson, V. Trouillet, T. Tischer, A. S. Goldmann, A. Carlmark, C. Barner-Kowollik, E. Malmström, *Biomacromolecules* **2013**, *14*, 64–74.

[69] A. Krissanaprasit, M. Madsen, J. B. Knudsen, D. Gudnason, W. Surareungchai, V. Birkedal, K. V. Gothelf, *ACS Nano* **2016**, *10*, 2243–2250.

[70] D. K. R. Falatach, C. McGlone, M.S.Al-Abdul-Wahid, S. Averick, R. C. Page, J.A.Berberich, D.Konkolewicz, R. Falatach, C. McGlone, M.S.Al-Abdul-Wahid, S. Averick, R. C. Page, J.A.Berberich, *Chem. Commun.* **2015**, *51*, 5343–5346.

[71] S. M. Ryan, G. Mantovani, X. Wang, D. M. Haddleton, D. J. Brayden, *Expert Opin. Drug Deliv.*

2008, *5*, 371–383.

[72]   Z. G. Wang, P. Zhan, B. Ding, *ACS Nano* **2013**, *7*, 1591–1598.

[73]   T. Yu, H. Sean, C. Chen, Y. Wu, D. Y. W. Ng, T. Weil, *Angew.Chem.Int.Ed* **2018**, *57*, 1603–1607.

[74]   S. Kotta, H. M. Aldawsari, S. M. Badr-Eldin, A. B. Nair, K. YT, *Pharmaceutics* **2022**, *14*, 1636.

[75]   Q. Zhang, Q. Jiang, N. Li, L. Dai, Q. Liu, L. Song, J. Wang, Y. Li, J. Tian, B. Ding, Y. Du, *ACS Nano* **2014**, *8*, 6633–6643.

[76]   G. Pan, X. Jin, Q. Mou, C. Zhang, *Chinese Chem. Lett.* **2017**, *28*, 1822–1828.

[77]   M. I. F. Daniela de Morais Zanata, *Polym. Chem.* **2021**, *12*, 4668–4679.

[78]   O. V. Khutoryanskaya, Z. A. Mayeva, G. A. Mun, V. V. Khutoryanskiy, *Biomacromolecules* **2008**, *9*, 3353–3361.

[79]   S. Dai, P. Ravib, K. C. Tam, *Soft Matter* **2008**, *4*, 435–449.

[80]   M. M. Rana, H. D. la Hoz, Siegler, *Polymers (Basel).* **2021**, *13*, 3154.

[81]   Y. Li, E. Gabriele, F. Samain, N. Favalli, F. Sladojevich, J. Scheuermann, D. Neri, *ACS Comb. Sci.* **2016**, *18*, 438–443.

[82]   N. Kessel, D. R. Illsley, J. L. Keddie, *oatings Technol. Res.* **2008**, *5*, 285–297.

[83]   B. Wei, M. Dai, P. Yin, *Nature* **2019**, *485*, 9–25.

[84]   A. H. El-Sagheer, T. Brown, *Chem. Soc. Rev.* **2010**, *39*, 1388–1405.

Appendix A
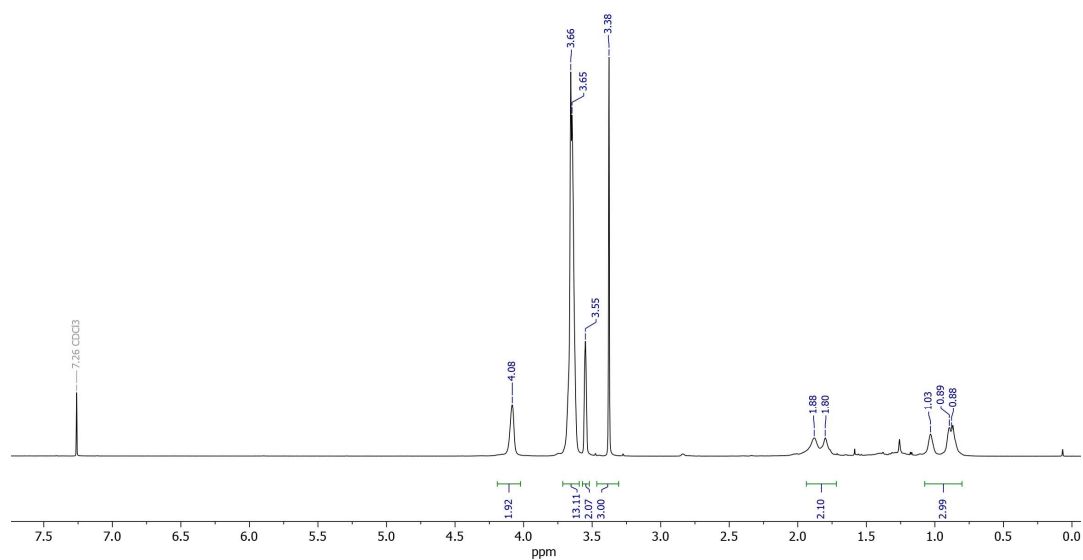
Figure 45: ^{1}H-NMR (700 Hz, CDCl$_3$) of NHS-p(OEGMA) (P1).
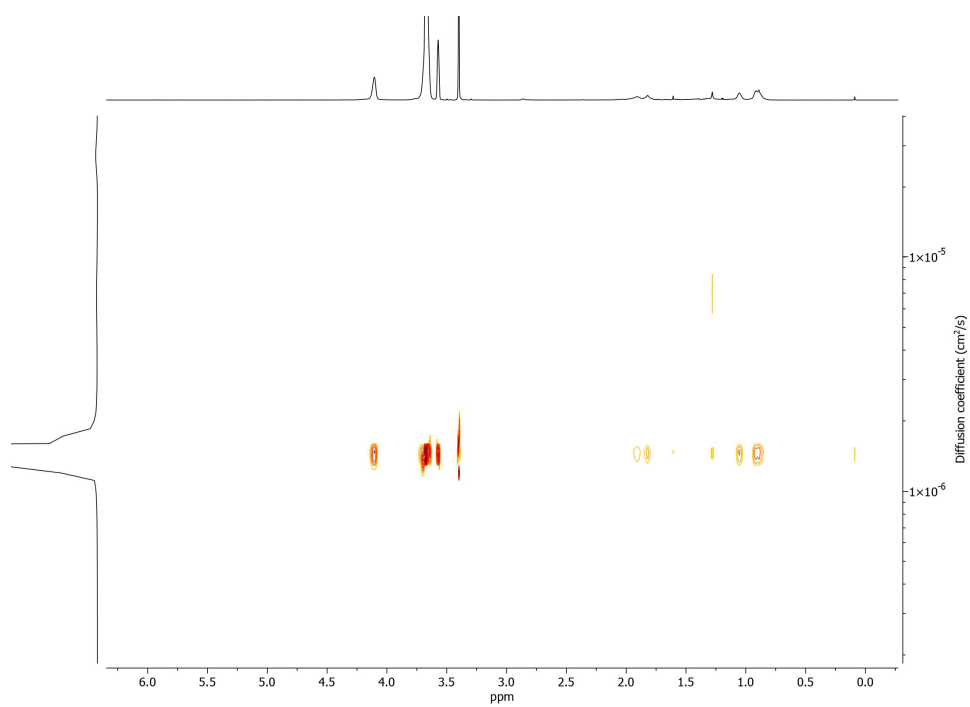
Figure 46: ^{1}H-DOSY NMR (700 Hz, CDCl$_3$) of NHS-p(OEGMA(P1).
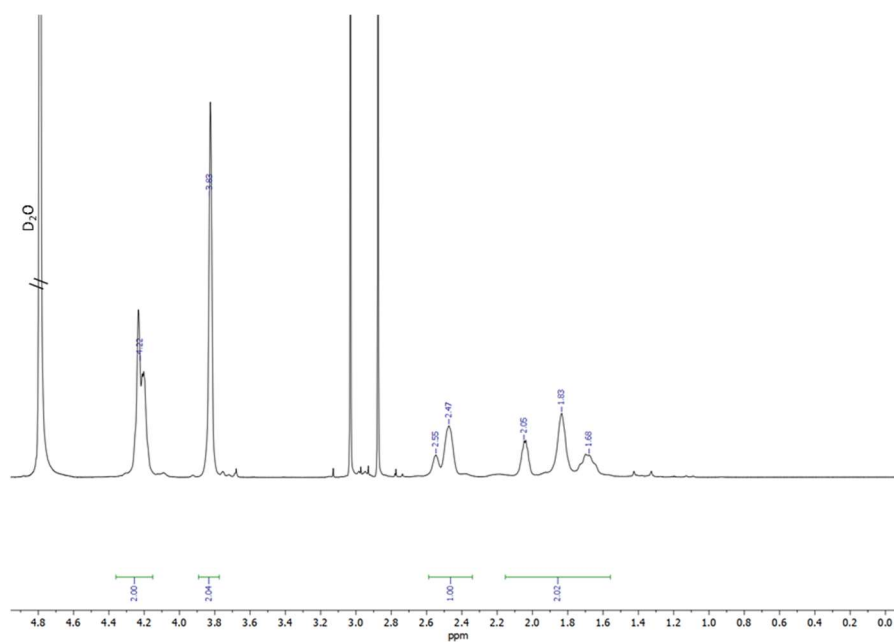
Figure 47: ^{1}H-NMR (700 Hz, D$_2$O) of NHS-p(HEA) (P3).
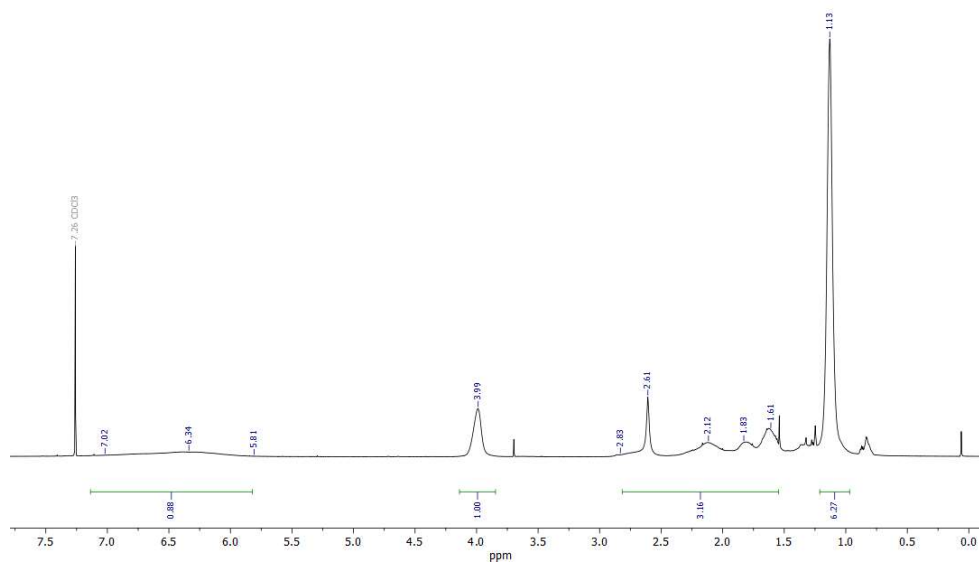
Figure 48: ^{1}H-NMR (700 Hz, CDCl$_3$) of NHS-p(NIPAM) (P4).

Figure 49: ^{1}H-DOSY NMR (700 Hz, CDCl$_3$) of NHS-p(NIPAM) (P4).

Figure 50: 1H-NMR (700 Hz, CDCl3) of NHS-p(NIPAM) (P5).
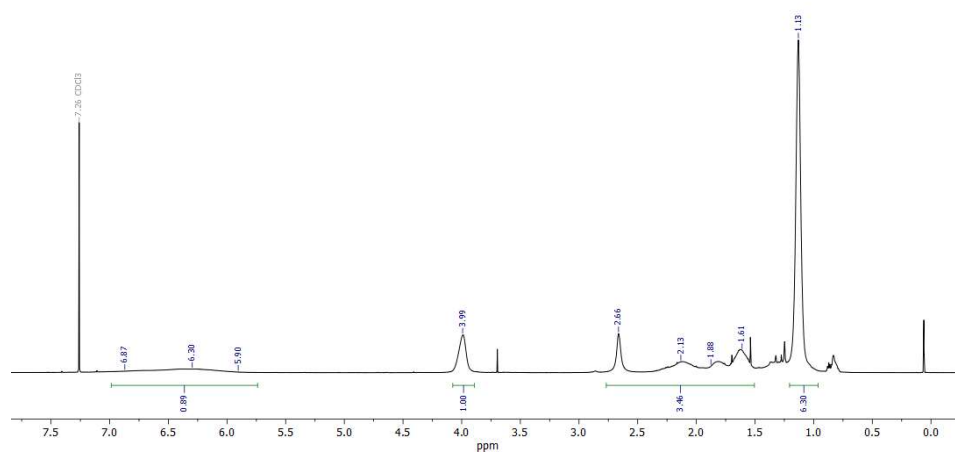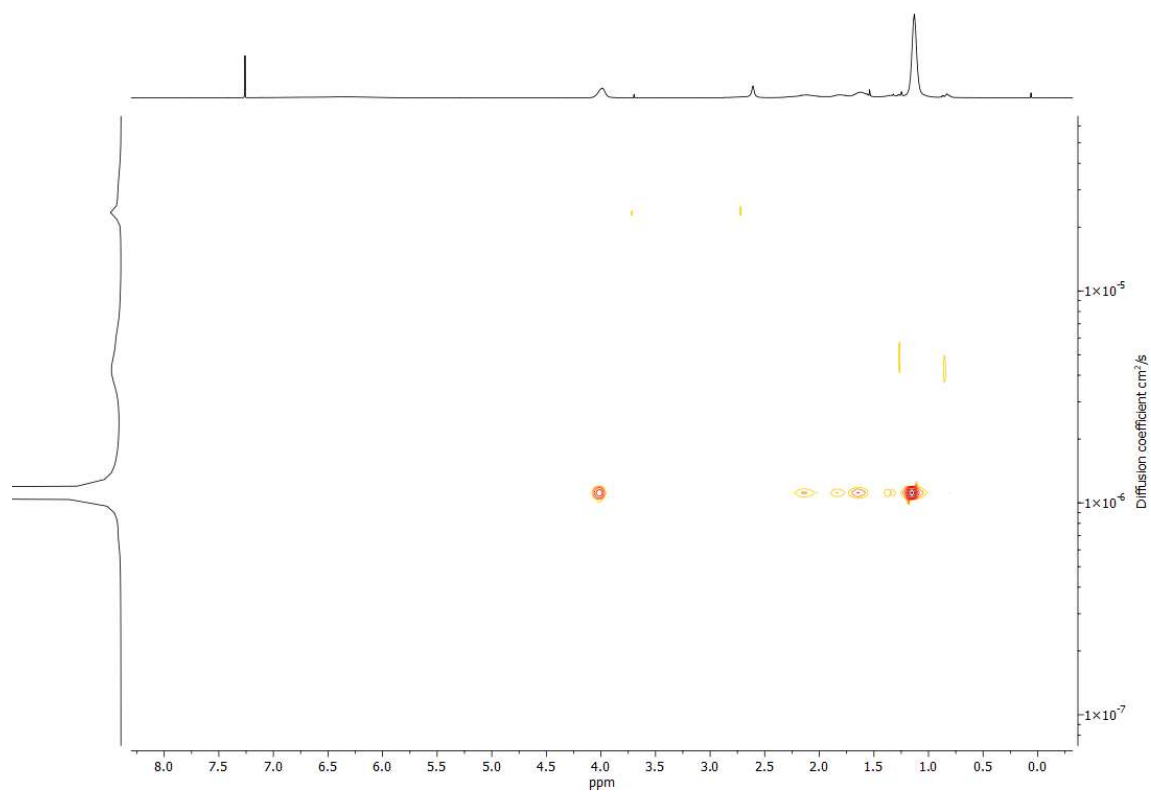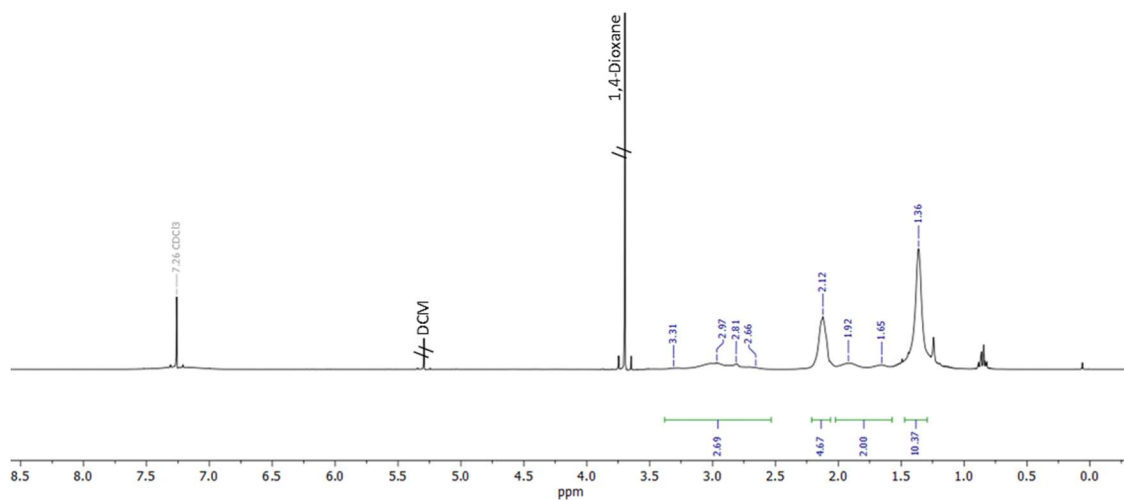
Figure 51: ¹H-NMR (400 Hz, CDCl₃) of NHS-p(DAAM) (1. Block P6).
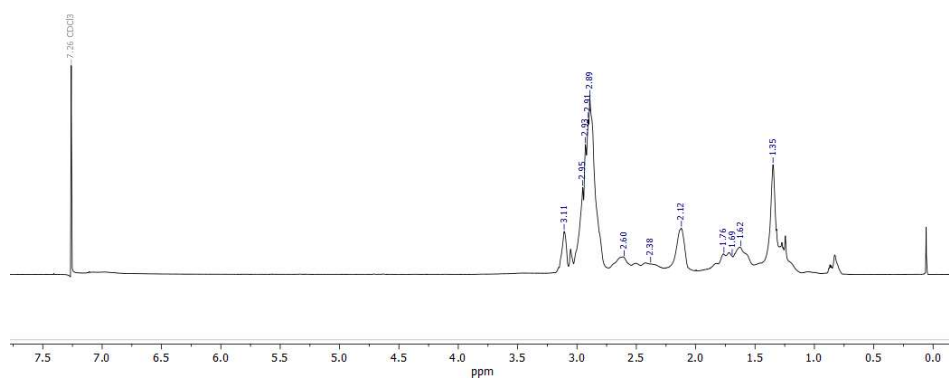
Figure 52: ¹H-NMR (700 Hz, CDCl₃) of NHS-p(DAAM-*b*-DMA) (P6).
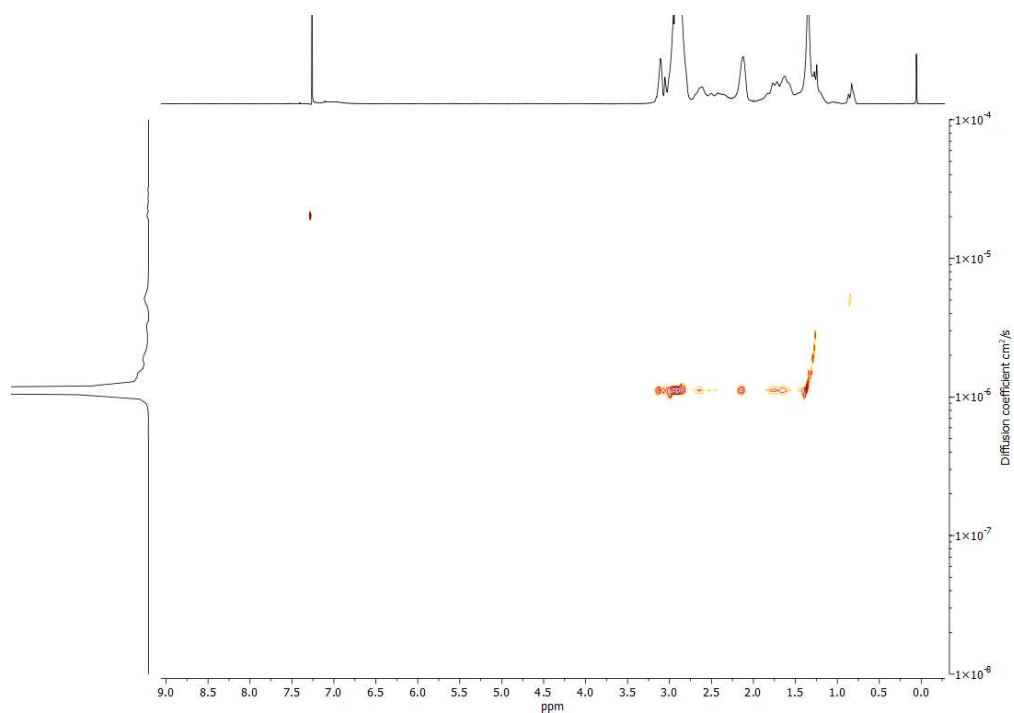
Figure 53: 1H-DOSY NMR (700 Hz, CDCl3) of NHS-p(DAAM-*b*-DMA) (P6).

Appendix B
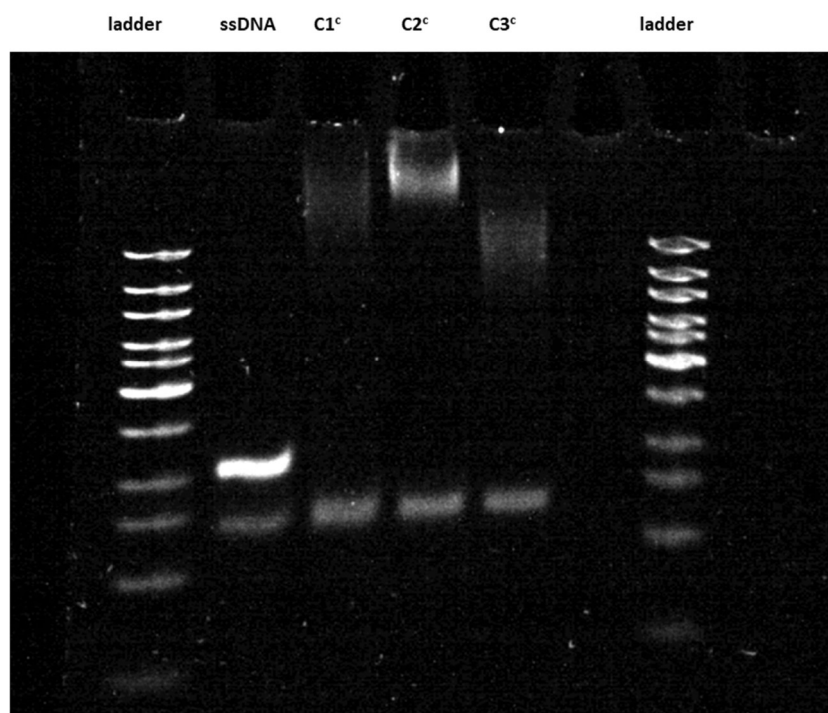
Figure 54: 15 % PAGE gel of purified DNA-homopolymer conjugates. L1: marker (GeneRuler™ Ultra Low Range DNA Ladder (Thermofisher), L2: stAᶜ, L3: C1ᶜ p(OEGMA), L4: C2ᶜ p(DMA)), L5: C3 p(HEA).
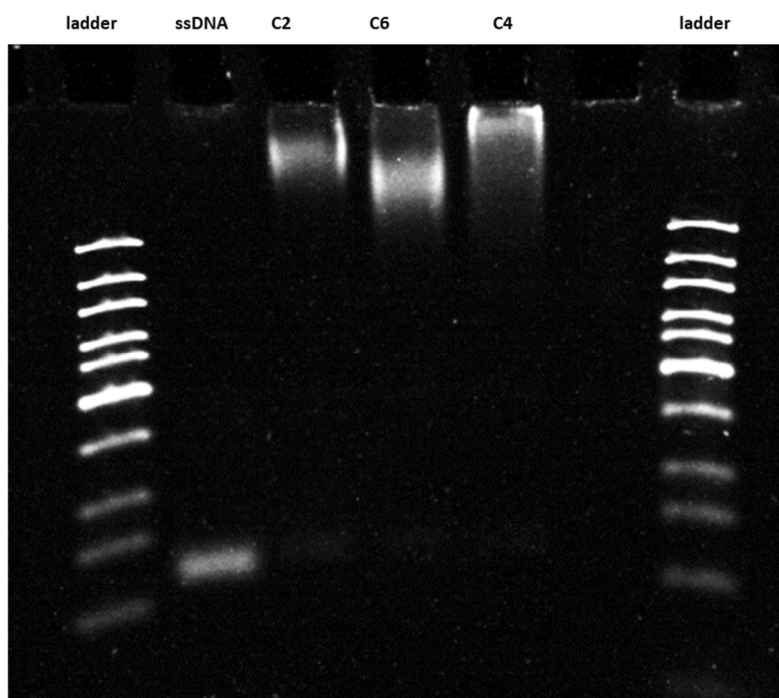
Figure 55: **15 % PAGE gel of purified DNA-homopolymer conjugates.** L1: marker (GeneRuler™ Ultra Low Range DNA Ladder (Thermofisher), L2: stA, L3: C2 p(DMA) L4: C6 p(DAAM-b-DMA)), L5: C4 p(NIPAM).
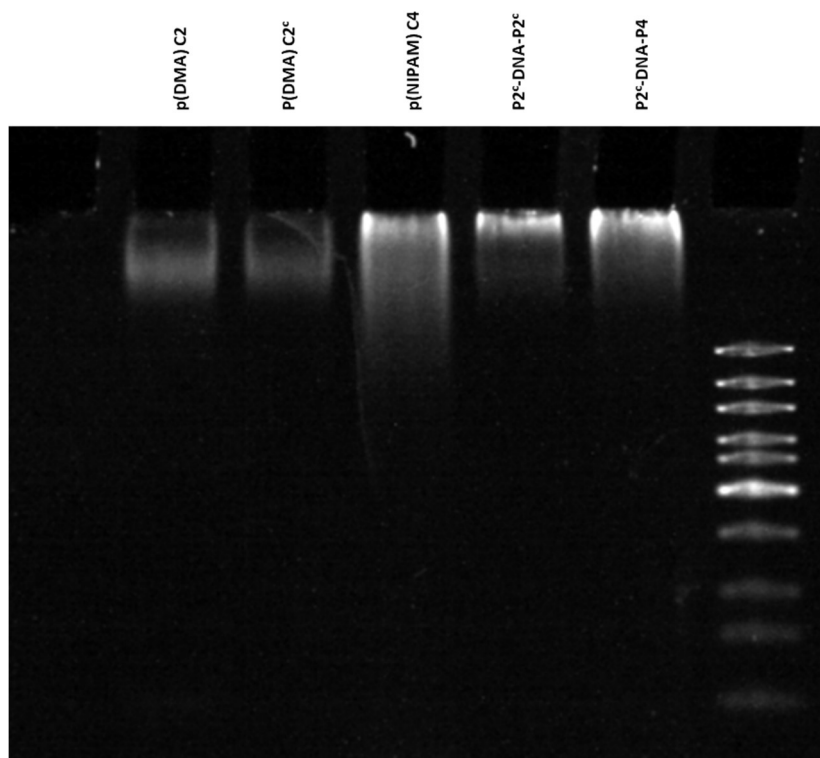
Figure 56: Multiblock copolymer synthesis of C2ᶜ-DNA-C2 and C2ᶜ-DNA-C4.
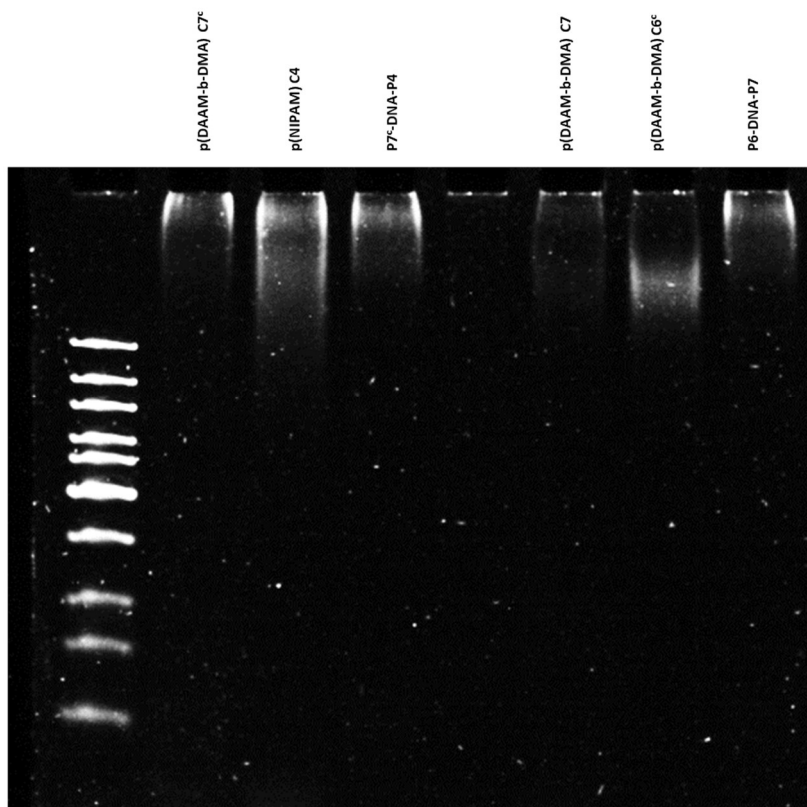
Figure 57: Multiblock copolymer synthesis of P7ᶜ-DNA-P4 and P6ᶜ-DNA-P7.
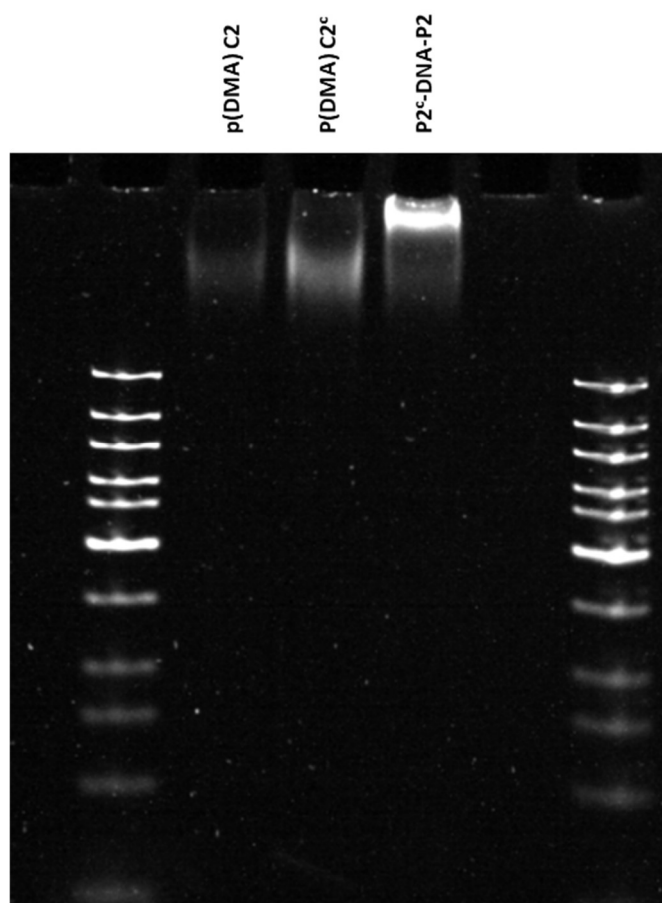
Figure 58: Multiblock copolymer synthesis of C2ᶜ-DNA-C2.

Appendix C
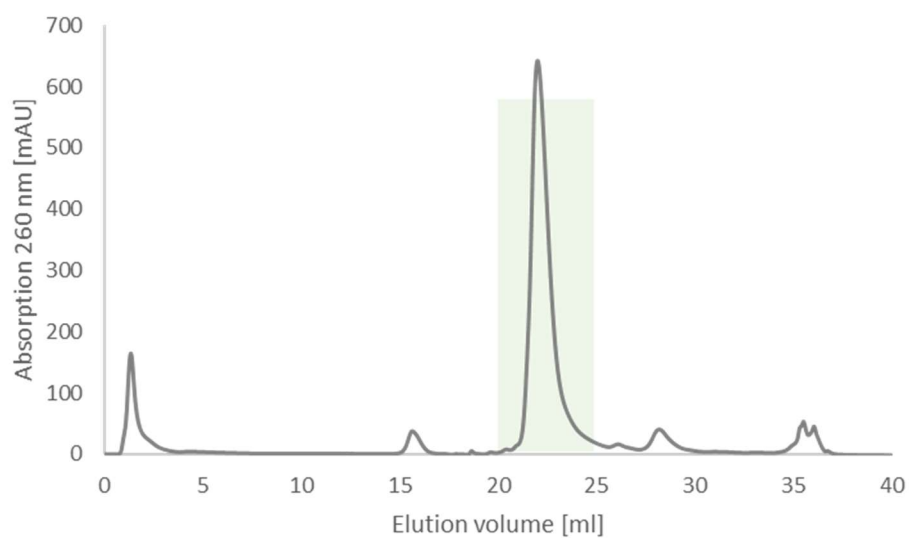
Figure 59: Elution diagram of DNA-p(OEGMA) conjugate (C1^c).
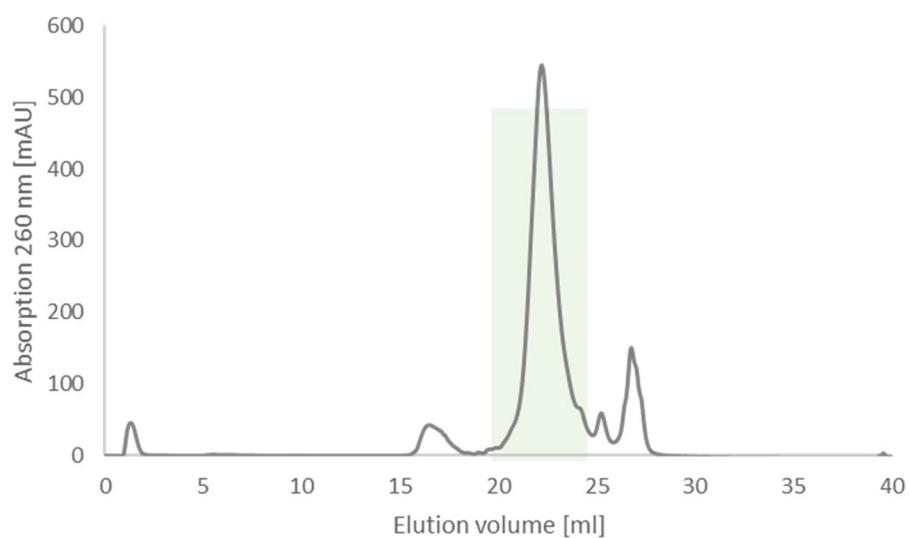
Figure 60: Elution diagram of DNA-p(HEA) conjugate (C3^c).
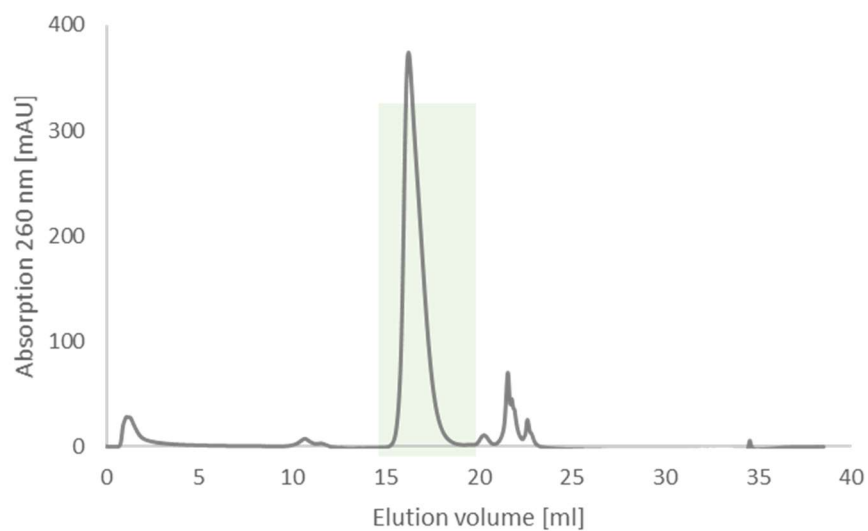
Figure 61: Elution diagram of DNA-p(NIPAM) conjugate (C4).
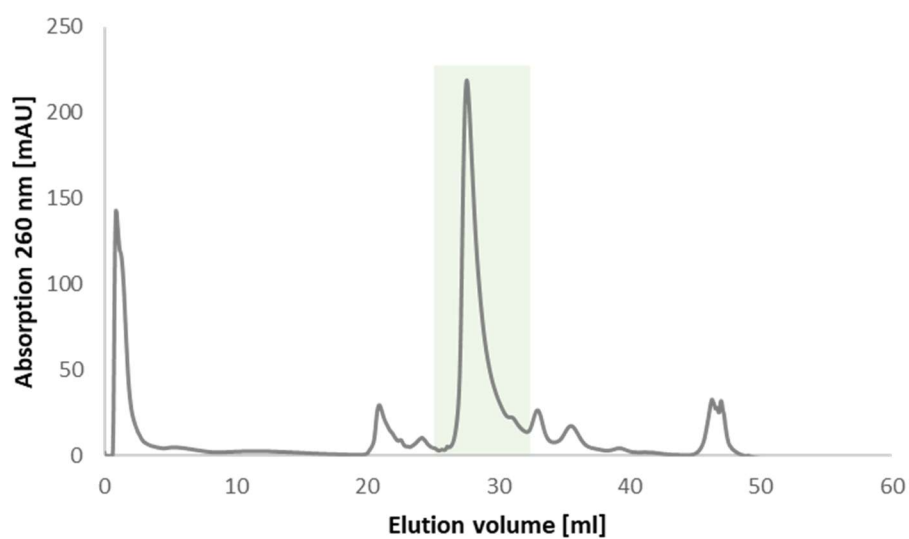
Figure 62: **Elution diagram of DNA-p(DAAM-*b*-DMA) conjugate (C7^c).** Column wash was conducted with 10 CV Ethanol and 10 CV H_2O.
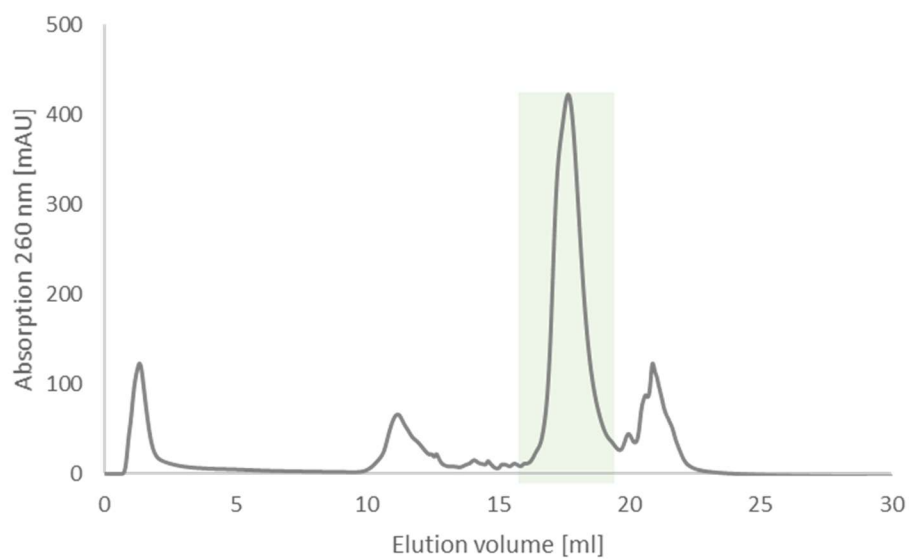
Figure 63: Elution diagram of DNA-p(DAAM-*b*-DMA) conjugate (C7).
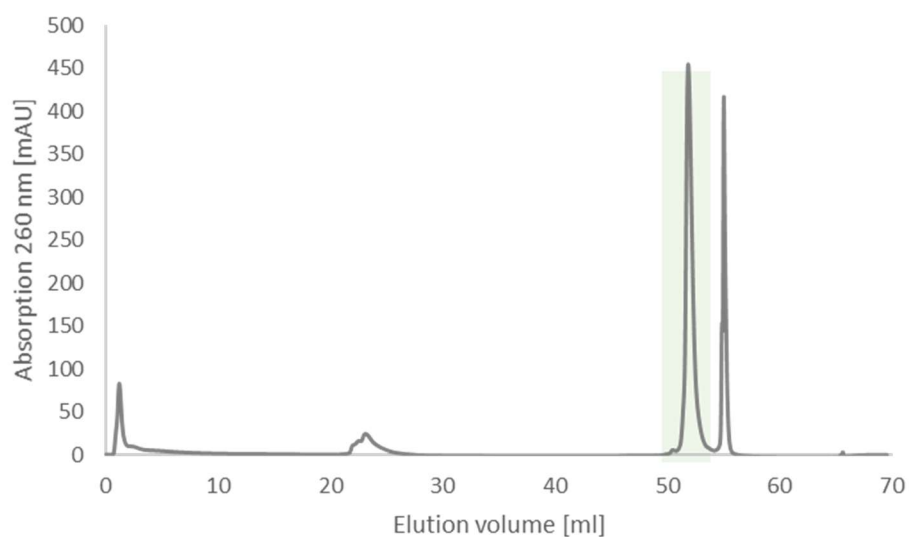
Figure 64: Elution diagram of DNA-p(DMA) conjugate (C1) eluted with lower elution concentration.
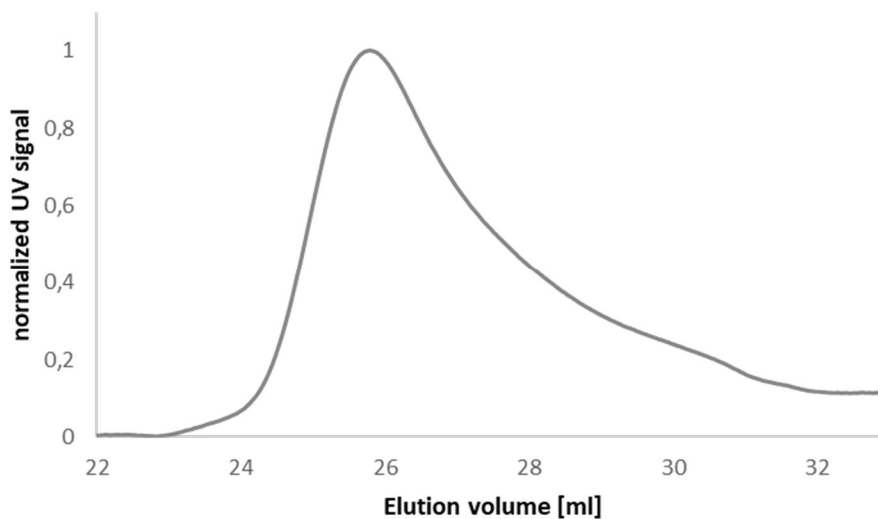
Figure 65: DMF-GPC of ÄKTA[pure] isolated DNA-p(DAAM-b-DMA) conjugate (C7[c]). Column wash was conducted with 10 CV Ethanol and 10 CV H_2O.
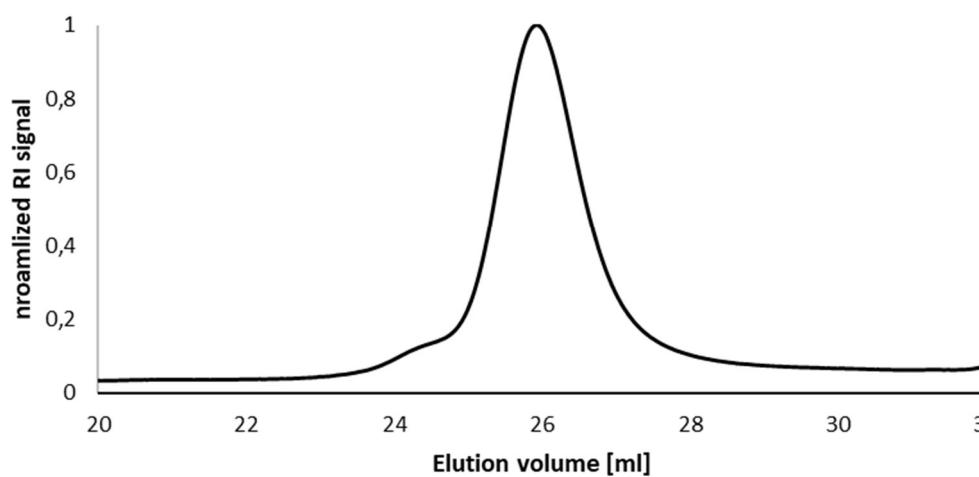
Figure 66: DMF-GPC of ÄKTA[pure] isolated DNA-p(DMA) conjugate. Column wash was performed with water.

Appendix D
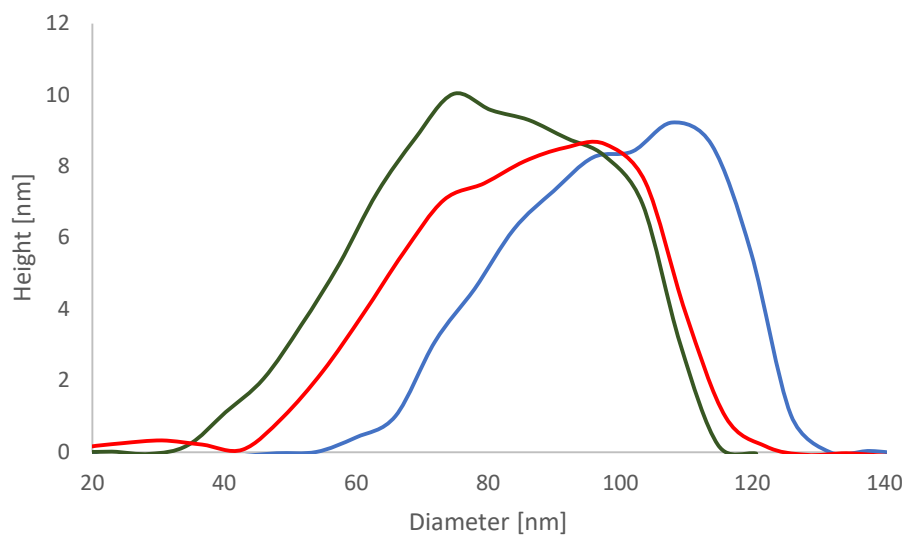
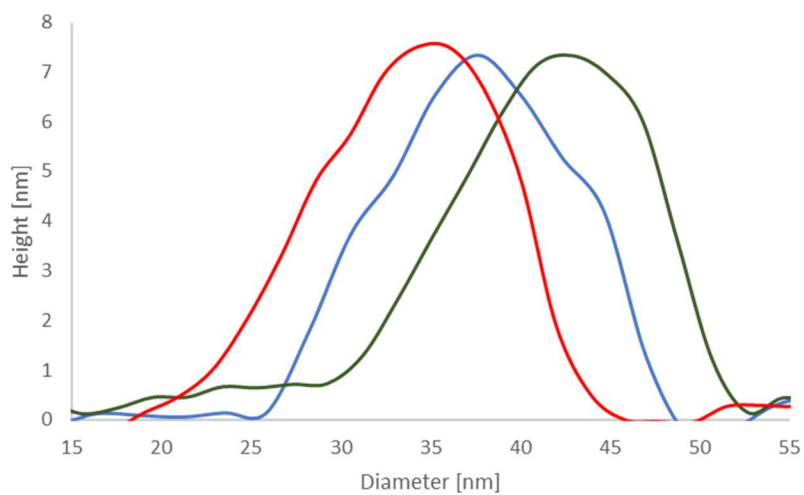**Figure 67: Height profiles of crosslinked DNA origami tubes**.

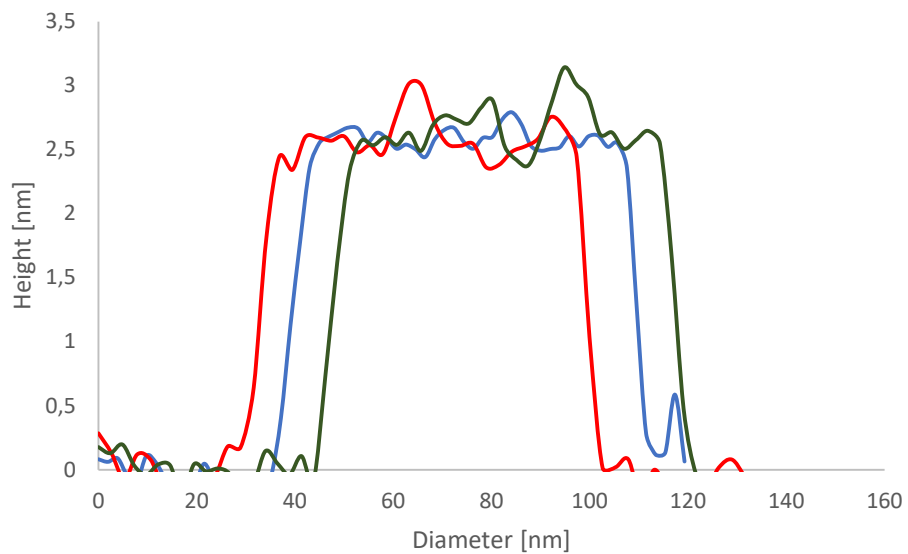**Figure 68: Height profiles of formed nanostructures after decomposition of DNA origami tube.**

Figure 69: Height profiles of three uncoated DNA origami rectangles.
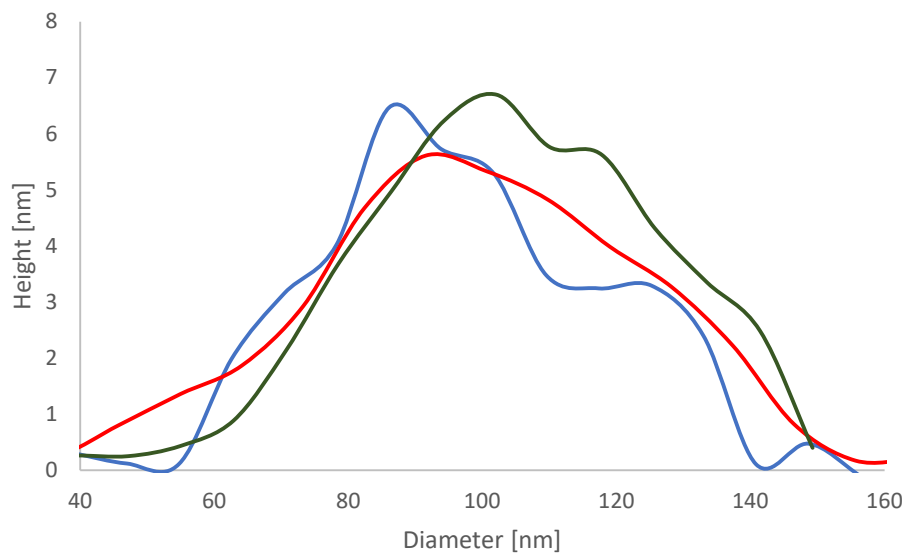

Figure 70: Height profiles of three crosslinked rectangles.
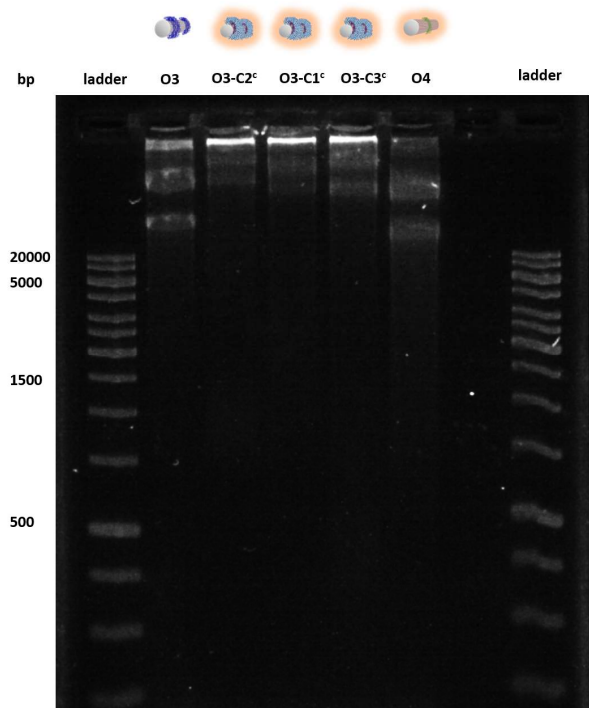
Figure 71: Full image of monitoring of the uncoated, the coated DNA origami tubes (O3-C1^c/C2^c/C3^c) and the control by 1% agarose gel, stained with SYBR Gold. Ladder: GeneRuler^{TM} 1kb DNA ladder (Thermofisher), O3: tube with two StA areas, O3-C2^c: rhodamine dye and p(DMA) coated tube, O3-C1^c: rhodamine dye and p(OEGMA) coated tube, O3-C3^c: rhodamine dye and p(HEA) coated tube, O4: tube only StE and rhodamine dye coated.